LAWRENCE
LIVERMORE
NATIONAL
LABORATORY

LLNL-TR-662055

National Ignition Facility Laser Design and Cost Basis Part I August 1993

J. Paisner

October 6, 2014

Disclaimer

This work performed under the auspices of the U.S. Department of Energy by Lawrence Livermore National Laboratory under Contract DE-AC52-07NA27344.

NIF-93-030
L-15864-1

National Ignition Facility
Laser Design and Cost Basis

July 1993

NIF

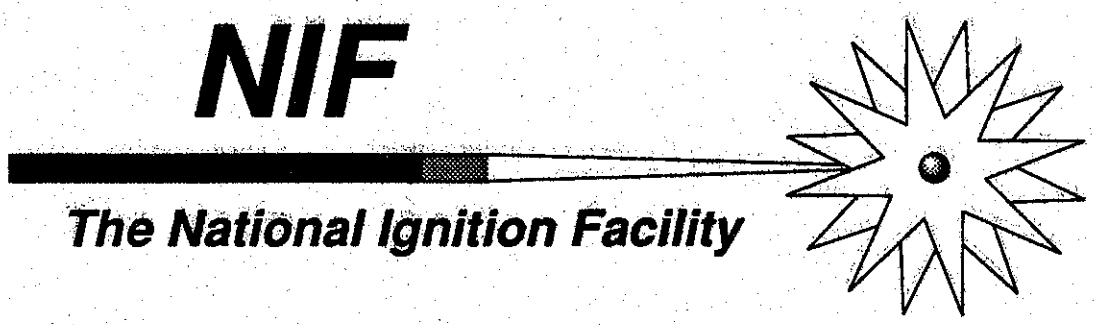

The National Ignition Facility

University of California
Lawrence Livermore
National Laboratory

NIF-93-020
L-15594-1
DRAFT Rev. 2

National Ignition Facility
Laser Design and Cost Basis

July 1993

NIF

The National Ignition Facility

Lawrence Livermore
National Laboratory

National Ignition Facility
Laser Design and Cost Basis

August 1993

J.A. Paisner
National Ignition Facility
Project Manager

LAWRENCE LIVERMORE NATIONAL LABORATORY
University of California • Livermore, California • 94550

DISCLAIMER

CONTENTS

APPENDICES

List of Figures

List of Tables

Chapter 1

INTRODUCTION

Key Decision-0 for a National Ignition Facility (NIF) sponsored by LLNL's Inertial Confinement Fusion Program (ICF) was signed in January, 1993. Supported by twenty years of experimental and theoretical research, and as established architects of several successful large-scale solid state laser drivers, LLNL must now prepare a formal Conceptual Design Report for NIF. Aside from engineering specifications for building NIF, we must provide cost estimates for the technology and a provable rationale for both design rigor and the price tag for this project.

LLNL has a long history of developing laser drivers for specific goals. Nova and the more recent effort, Beamlet Demonstration Project, will contribute to the ongoing technological demonstration for NIF. Careful theoretical predictions buoyed by experimental results continue to mark our progress towards a laser facility that is designed in response to fusion target requirements.

Engineering costs from Beamlet provide a current basis-of-estimate for NIF, which must then benefit from the historical data we can gather from Nova. Our design efforts for NIF involve elaborate, automated optimization procedures coupled with computer simulation of laser performance that direct our attention to capable, flexible, and cost effective laser drivers. In the past, we have used programmatic funds or special appropriation to pay for prototype development and vendor facilitation—items that reduce the final cost of large engineering projects.

Barring any major political or ecological event that may redirect public thinking, or any successful alternative to the fusion process, we believe that the commitment to NIF will be based mainly on economic criteria. Can we afford it? So that an affirmative answer may be given, we believe that the ICF program at LLNL must once again aggressively pursue laser system cost engineering.

In the chapters that follow, we present a brief history of solid state laser costs at LLNL, a design rationale for NIF based on fusion target requirements, and a cost basis for the various subsystems anticipated for NIF. In this last, we pay particular attention to deriving costs from Beamlet, elucidate the facilitation efforts that have reduced costs in past laser engineering efforts, and make specific proposals that will reduce the cost of NIF without affecting its performance.

Chapter 2

HISTORICAL PERSPECTIVE

Inertial confinement fusion research at LLNL has concentrated on X-ray driven or indirect drive capsules for over two decades. Figure 2-1 shows that Nova and its predecessors have worked up from barely detectable yields to ICF target gains near 10^{-2}.

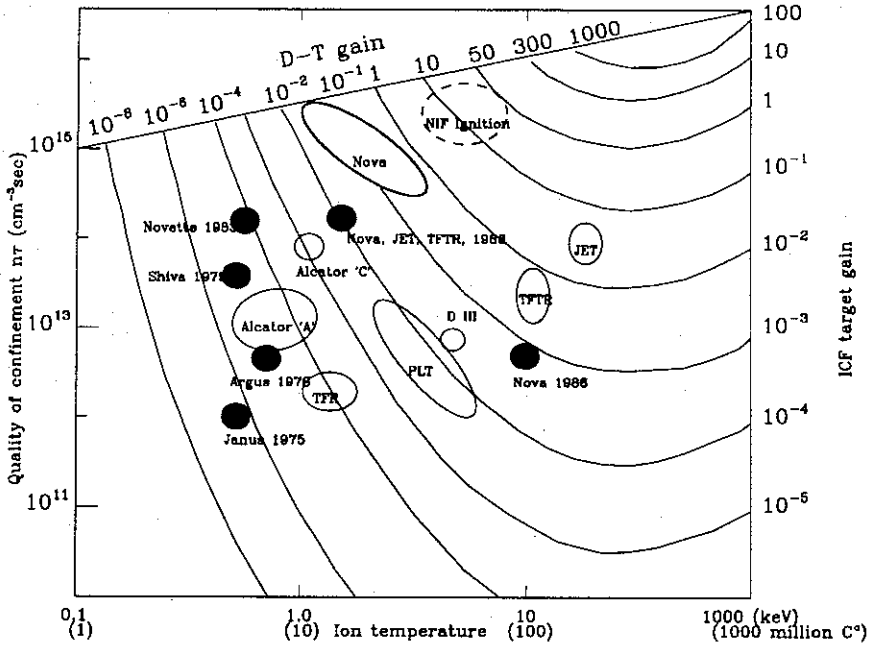

Figure 2-1 Thermonuclear conditions achieved in fusion experiments

Since most ICF ignition-relevant experimental and simulation results concern an X-ray driven, indirect drive design, the NIF baseline laser system is chosen to support this type of device. However, we do *not* preclude direct drive or other advanced concept fusion devices (fast igniter, etc.) for incremental funding. The procedure we have devised to determine the NIF laser primary criteria from target experimental requirements is described in detail below. It emerges that the NIF laser must meet the following criteria for indirect drive:

- $E_{3\omega} \sim 1.8\,\mathrm{MJ}$ at 3ω
- $E_{1\omega} \sim 3.25$ to $4.5\,\mathrm{MJ}$
- $\tau_{\mathrm{eff}}(1\omega) \sim 3.6$ to $4.8\,\mathrm{nsec}$
- two cones on either side
- ≥ 8 fold azimuthal symmetry
- beam smoothing

Laser system hardware costs have been assembled for each line-item project at LLNL, and are often used to project the cost of newly proposed lasers. This material has been published in several forms. Some accounts list total cost including facilities and overhead. Others list only the cost of the laser system.[1] Adjustment for inflation is sometimes included. The following table summarizes the laser hardware cost per red optical joule for each project in year-spent dollars. The final entry projects NIF costs *after* any cost reduction program.

[1] J. T. Hunt, *High Peak Power Nd:Glass Laser Facilities for End Users*, SPIE Vol. 1410 Solid State Lasers II (1991).

Laser System Costs [2,3,4]

System	Year	Chains	Aperture	Material	Laser Cost	Energy (3 nsec)	$/J
Argus[2]	1976	2	20 cm	ED-2	\$3.5 to 6.6M	2.2 to 4 kJ	~ 200
Shiva[2,3]	1977	20	20 cm	ED-2	\$29M	20 kJ	1450
Nova[4]	1984	10	46 cm	LG-750&LHG-8	\$54M	120 kJ	447
NIF	1996	205	35 cm	Phosphate	\$282M	3140 kJ	89

Of all these project costs, the Argus data is least reliable because the programmatic contribution is uncertain. Figure 2-2 presents this same data graphically.

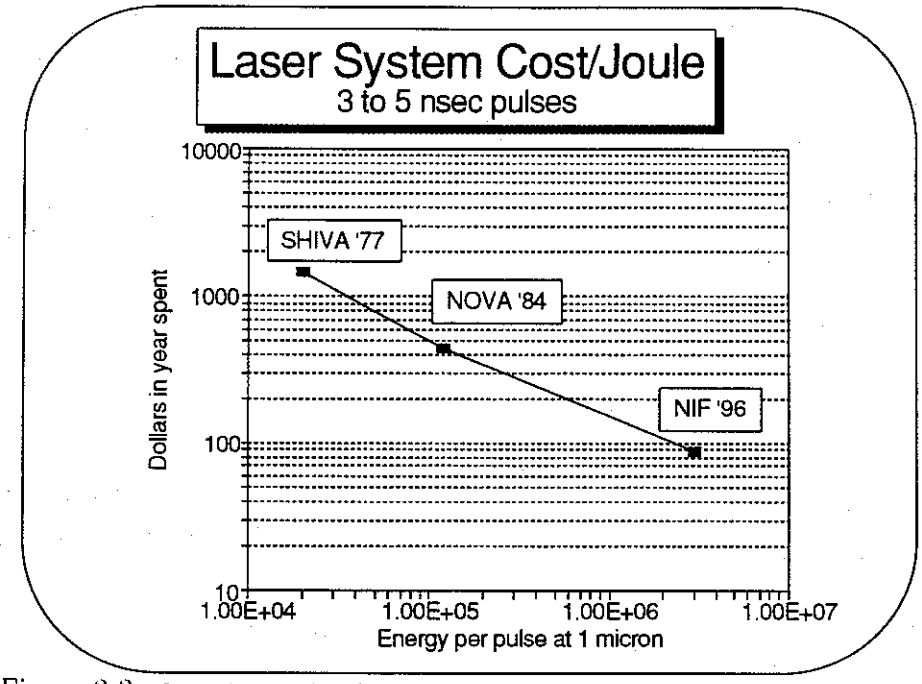

Figure 2-2 Laser System Cost/Joule

The projected NIF cost is at the minimum of the expected range in current dollars and is predicated on the success of a component development/cost reduction/optics manufacturing program. Accepting the table values without adjustment for inflation, the effective learning is:

Comparison	Learning
Shiva - Nova	$S = 0.63$
Nova - NIF	$S = 0.67$
Shiva - NIF	$S = 0.68$

where

$$\frac{(\text{Cost/Joule})_1}{(\text{Cost/Joule})_0} = \left(\frac{\text{Energy}_1}{\text{Energy}_0}\right)^{\ln S/\ln 2}$$

Effective learning with $S < 0.80$ is aggressive, and depends on technological innovations or entirely new ICF concepts along the way. Significant reductions in Cost/Joule beyond those achievable for NIF are somewhat speculative without identifying the pathway, though the learning curve treatment shows no obvious saturation.

[2] R. J. Gilmartin, *Cost and performance of upgrades,*, LLNL ICF internal memorandum, 3 April 1979

[3] H. J. Rien, *Shiva hardware cost analysis,*, LLNL ICF internal memorandum, 16 December 1977.

[4] G. J. Suski, *Nova as-built cost analysis,* LLNL ICF internal memorandum, 31 July 1985.

In hindsight, given the way Nova has actually been used, there are several cost savings that might have reduced Nova's price. Optical isolation in Nova is excessive for a 3ω machine with unopposed beams because Nova was designed to be a 1, 2, or 3ω target shooting facility tolerant of opposed beams. Elaborate and expensive N_2 gas flow and clean filtered air flow systems have given way to local clean areas in post Nova projects like Phebus. Also, the Nova project supported a very expensive controls software and hardware development project. Today, such tasks are much less expensive and easier, and these factor into reductions in NIF projected costs.

The principal cost centers in all these lasers are their amplifiers, and the heart of these devices are the glass slabs. The cost per cubic centimeter of laser glass has responded to past cost reduction programs and economies of scale. Some of this material has also found its way into the literature and is documented in memoranda. [5,6,7]

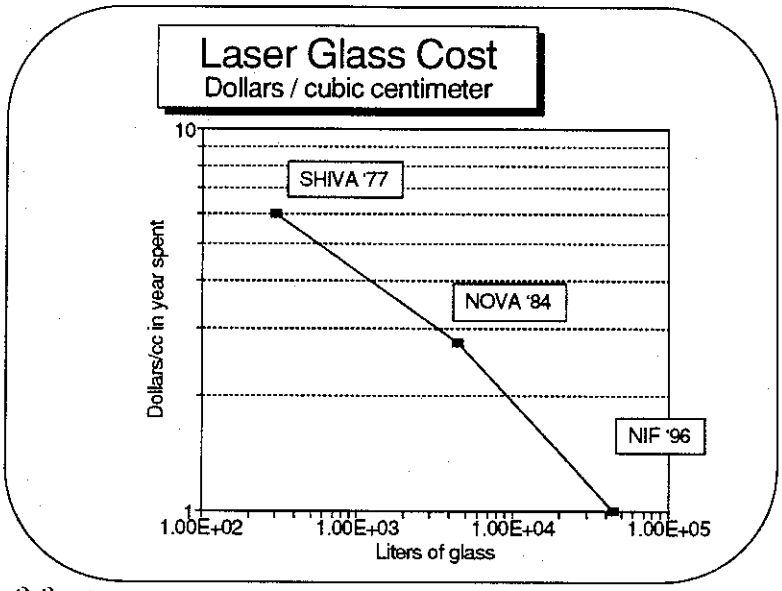

Figure 2-3 Laser Glass Cost

Given that the NIF laser is optimized to support an indirect drive experimental program, it is worth noting that this same baseline laser system will meet or exceed the direct drive ignition energy levels specified by our sister laboratories. To conduct direct drive experiments with NIF, building space is left to install an array of turning mirrors to redirect the laser beams. At the output relay plane an array of converters could be located, arranged to mimic the architecture selected for LLE's Ω-Upgrade. Sixty $f/8$ irradiation directions can be constructed using 240 beamlets in 2×2 clusters similar to those employed for indirect drive studies. The currently published direct drive ignition requirements can be met:

- $E_{3\omega} = 1.5 - 2.0\,\mathrm{MJ}$ [8]
- $E_{1\omega} \sim 2.9\,\mathrm{MJ} \Rightarrow 906\,\mathrm{TW}$ red
- $\tau_{\mathrm{equiv}}(1\omega) \sim 3.2\,\mathrm{nsec}$
- 60 beam directions in 2×2 clusters (240 beamlets)
- Beam smoothing using broadband (≈ 11Å) SSD.
- Power balance $< 8\%$

[5] K. R. Manes, *Multi-megajoule ND:Glass fusion laser designs,* Laser Interaction and Related Plasma Phenomena, Vol. 7, Edited by H. Hora and G. Miley, Plenum (1986).

[6] K. R. Manes, *Glass production costs,* ICF internal memorandum, 29 May 1985.

[7] J. Atherton, *Input for development paths of NIF laser components,* ICF internal memorandum, 20 February 1993.

[8] J. M. Soures, private correspondence to M. Sluyter, OIF, 8 June 1993.

Even with today's low conversion, inefficient beam smoothing techniques and low UV transport efficiencies, the NIF baseline laser system should be able to deliver more than 600 kJ shaped and conditioned pulses to direct drive targets, being principally limited by UV transport optics damage. Beam expansion similar to that employed by the Ω Upgrade and Nova could raise NIF UV transport capacity to levels required for LLE's direct drive chamber architecture.

We suggest that little effort be expended on the direct drive alternative in the NIF CDR. By adopting LLE's 60-beam architecture in 2×2 clusters, we believe that further design effort for the baseline CDR is not needed. It is reasonably certain that such an architecture can be routed to the target since LLE has already overcome all geometrical obstacles in this design. It is difficult to plan for advanced fusion driver concepts like fast igniter precisely because they are uncertain. Several—perhaps as many as 12 beamlets—would have to be retrofitted with grating compressors and reflective focusing optics. These might be located on an inner cluster. The chosen NIF baseline does not preclude eventual installation of such hardware at some future time.

Chapter 3

LASER DESIGN BASIS STUDY

After the NIF Key Decision-0 had been signed in January 1993, the LLNL NIF project office chartered a group of scientists, engineers and designers to establish a design/cost basis for the NIF laser system. Previous design studies rarely linked performance with cost. Though many laser configurations satisfy target requirements for ignition, the optimum from a cost/performance perspective had not been studied in detail. A preliminary effort for this study was to quantify the relationships among laser design, laser cost, and laser performance. The current effort is to establish a data base of consistent technical and cost information for the NIF project so a single point design can be defined.

This report summarizes the work performed during the Laser Design Basis (LDB) study effort. Chapter 4 discusses the flowdown of requirements from the target requirements to the laser functional and subsystem requirements. These form the basis for the design and cost information that follow. Chapter 5 summarizes the system optimization studies. The performance/cost model is described along with sensitivity results that characterize different laser system configurations. Chapter 6 lists general cost control methodologies. The chapters following discuss each major laser subsystem. In these sections subsystem design descriptions, cost summaries and cost reduction strategies are detailed. Chapter 16 summarizes top level NIF construction costs and provides an integrated schedule of the NIF construction project and the component development program. The final chapter summarizes key findings established during the LDB study.

3.1 *LDB Objectives*

The primary objectives of the LDB study are five-fold:

- Establish a comprehensive and consistent cost data base for the NIF laser system
- Develop cost sensitivity relationships for critical components of the NIF laser subsystems
- Optimize the laser system configuration for maximum performance at minimum cost and risk
- Parameterize performance and cost as a function of critical design variables
- Define component development activities required to achieve cost goals

To achieve these objectives an entry point design configuration was defined. Based on that design a bottom-up cost estimate was assembled. For each subsystem labor and material cost estimates were compiled into a single comprehensive data base. These costs are categorized as either fixed or marginal. Fixed costs are costs that are independent of the laser configuration. Scaling relationships were developed for all marginal costs whose value depended on any of the basic design parameters, such as number of beamlets, aperture size, spatial filter length, laser glass volume, and laser glass area. These parameters were then input into the CHAINOP optimization code discussed in Chapter 5. This code determines minimum cost laser designs that satisfy defined performance requirements. CHAINOP can also be used to determine sensitivity to different input assumptions. The results of these analyses are discussed in Chapter 5 and in summary Chapter 17. All costs used in this analysis are dependent on a development program for the high efficiency, low cost, production components needed for NIF. For each subsystem these activities and their costs are discussed in Chapters 7–15.

The cost/performance optimization method instituted for the LDB is an iterative process. Costs are dependent on the specifics of a design and the optimum design point can not be determined until the cost sensitivities are understood. To enable the process, an entry point design has been chosen to establish initial costs and cost scaling parameters. The scaling rules permit the process to consider a wide range of configurations with reasonable accuracy. When a new point design is established the scaling parameters may be updated to improve the accuracy of the analysis about the new baseline point.

The system layout selected as the entry point into the design optimization process is shown in Figures 3.1 and 3.2. A detailed parametric description is provided in the NIF Configuration Summary in the Appendix. The laser configuration is a four pass architecture with the laser pulse input into the output spatial filter. The beamlets are arranged in units (beamlines) of 16, packed in an array that is 4 beams wide by 4 beams high. Configurations with more beams in a single beamline array have cost advantages that merit further evaluation. This important design issue will be resolved before the end of the CDR and will require engineering assessments beyond the scope of the LDB study. A total of 192 NIF beamlets is contained in the entry point design. This corresponds to the minimum number of beams required for target symmetry. The laser performance improvement that can be achieved by adding beamlets and associated costs are discussed in Chapter 5.

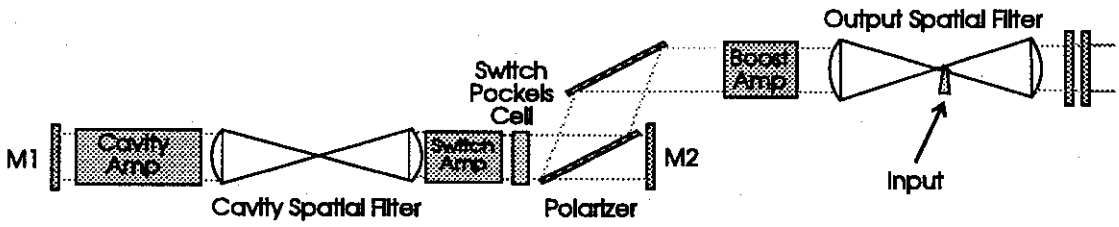

Figure 3-1 Schematic for a beamlet of the NIF entry point design.

The input laser pulse is provided by the pulse generation system. The system is envisioned to be a compact stand-alone optical package located near the output spatial filter where the beam is injected into the boost amplifier. Each beamlet will have its own dedicated package to provide the formatted pulse at the proper wavelength. It is expected that four wavelengths will be required to satisfy beam smoothing requirements. In addition, two different pulse shapes must be provided by the pulse generator, one for the inner and one for the outer cone of beams in the target area. The energy required for the entry point design input pulse is 0.5 J. Costing analyses completed during the LDB study show that energies up to about 3.0 J can be accommodated without cost increase.

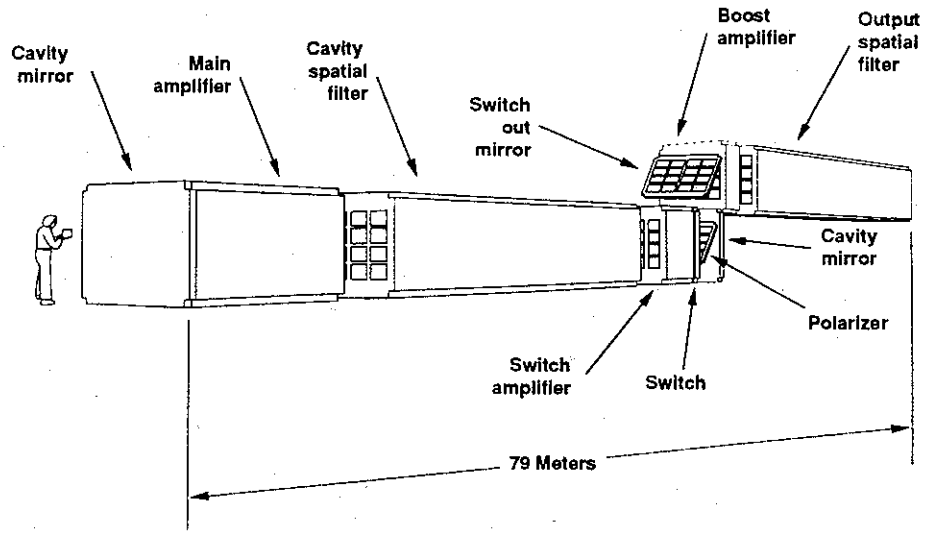

Figure 3-2 NIF beamline conceptual drawing.

After injection into the output spatial filter the laser beam passes through three amplifier stages: 1) main amplifier, 2) switch amplifier, and 3) boost amplifier. The number of laser slabs in each of these stages is variable in the optimization analysis. The entry point design assumes 11, 5, and 3 slabs/beam in each stage. Nominal hard aperture size is 35 cm—a reasonable compromise between minimizing optic manufacturing risk and system cost. Amplifier flashlamps, optimally packed to provide high transfer efficiency and uniform pump deposition, are driven with 248 MJ of electrical energy. The power conditioning system providing this power is based on metalized dielectric capacitors whose design and performance parameters will be validated during its component development program. Switch-out of the pulse from the amplifier cavity is accomplished with a Plasma Electrode Pockels Cell (PEPC) switch operating at better than 99% switching efficiency. U-turn optics, an alternative proposal to the PEPC suggested by C. Vann and others, was not considered during the LDB study but should be evaluated by experiments on the Beamlet Demonstration Project.

After passing through the booster amplifier and output spatial filter, the 1ω beams are transported directly to the target chamber with a minimum number of high reflectivity mirrors. Beam transport designs lacking a second target chamber were not considered. At the chamber the beams are directed to either inner or outer cone arrays. Figure 3-3 shows that space for at least 192 beams can be accommodated with a 5 m radius target chamber. Clustered into groups of 4, the beams are directed through the final optic systems. Within each final optic system the frequency of the beam is tripled using a KDP doubling crystal followed by a KD*P mixing crystal, and then phase modulated using a kinoform phase plate. Other converter configurations were not evaluated during the LDB study but should be considered during the remainder of the CDR.

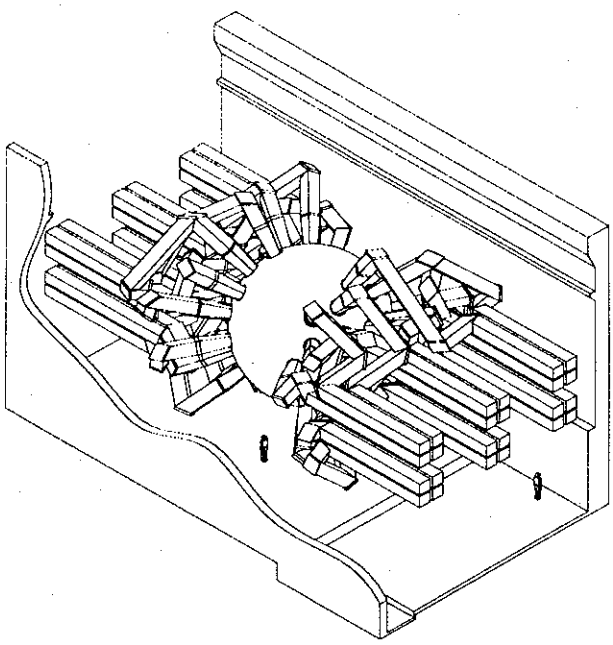

Figure 3-3 NIF conceptual drawing showing beam transport to the spherical target chamber.

During the transport of each laser beam from the master oscillator to the target, precision systems provide for the alignment, diagnostics and control required for efficient system operation at high power. The basic alignment requirements for the entry point design are that the centering accuracy of the laser beam inside the power amplifier cavity should be less than 1% of the aperture, that the pointing accuracy of the 1ω beam on the converter shall be less than ± 35 micro radians and that the pointing accuracy and stability of the 3ω beam at the target shall be greater than 50 microns.

Chapter 4

REQUIREMENTS

To understand the process of estimating costs of a large laser system like NIF, it is worth reviewing how we produce a conceptual design for the facility. From target ignition requirements we design a laser driver, matching requisite energy and peak power. Damage thresholds and parasitic behavior in large aperture optics lead us to consider a system composed of several identical beamlines or beamlets. A single beamline is optimized to produce the most energy and power for the least cost. Geometric considerations like how large a building is required for housing the facility are peripherally considered. Much of this process can be computerized so that designs failing to meet target requirements, or exceeding our technological grasp are quickly eliminated from contention. Candidate designs are subjected to increasing numbers of experimental and theoretical tests of robustness. This chapter provides insight into how the energy and peak power requirements can be met by LLNL's NIF design.

4.1 *Target requirements*

The process for sizing NIF must be simple, easy to communicate, logically defensible and adaptive to technological break throughs. Post Nova ICF laser design has become a mature engineering sub-specialty. A laser system of the NIF class is no longer an object of research in itself, and its performance should not be in doubt. Ignition targets trace from Nova experiments on the low energy side and forty years of nuclear weapons testing on the high energy side. Fundamentally an exercise in interpolation, they are the researched items. Target requirements and relative confidence of achieving ignition conditions must be the dominant factors used to establish the laser requirements for NIF. Because the data base is so extensive, indirect drive targets are the designs that must determine NIF's laser architecture. Care must be taken not to preclude direct drive designs, but very advanced designs, such as the fast igniter concepts, can have little influence at this stage owing to their speculative character.

Plasma energy transport and capsule hydrodynamics in indirect drive hohlraums similar to those tested with Nova have been used to derive the top level laser system requirements that must be met to achieve thermonuclear ignition. LASNEX simulations suggest that target ignition will require:

- An optimum laser spot size and intensity distribution at the laser entrance hole (plasma energy transport)
- A symmetrical implosion of the capsule (hydrodynamics)
- A carefully shaped laser temporal pulse
- Sufficient energy in the pulse to give a high probability of ignition

These criteria are outlined by the chart in Figure 4-1.

The focal spot dimension is determined by the focal length of the final optic, the feature size imprinted on the near field beam by a phase plate, and phase errors put on the beam by the laser system. Our scheme for producing a focal spot with the requisite smoothness is to do temporal and spatial smoothing in the plane of the target's laser entrance hole. Temporal smoothing is achieved by irradiating the LEH plane with four wavelengths separated by 7 angstroms; a total wavelength spread of 20 angstroms. The beams are clustered into groups of four and each beam in a cluster is a different wavelength. Thus the total number of beamlines used to irradiate the target must be evenly divisible by four.

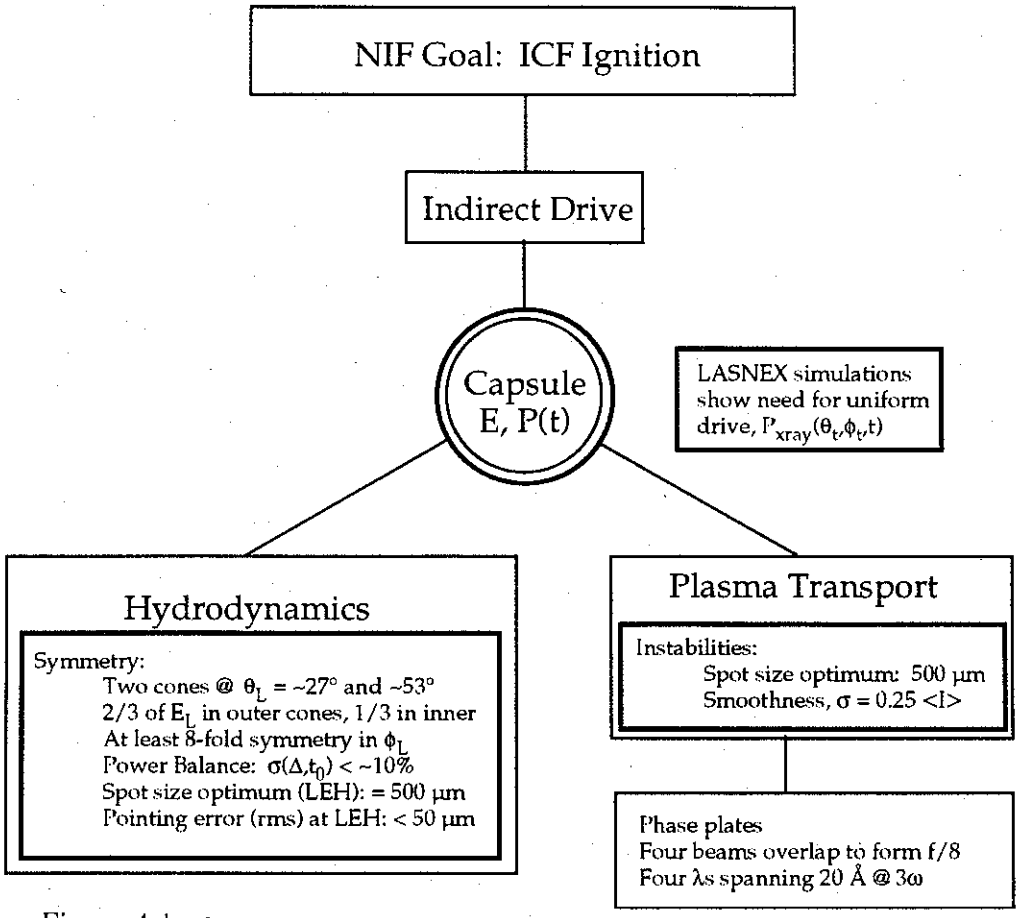

Figure 4-1 Ignition requirement for indirect drive targets.

Symmetrical implosion of the capsule requires that the target be irradiated with the correct beam geometry. LLNL target designers have chosen a two-sided target irradiation geometry whereby each side of the target is irradiated with two well defined cones of beams. These cones lie at elevation half-angles, θ, of approximately 27 and 53 degrees with a nominal split in laser energy of 1/3 to 2/3. Thus, the side to side requirement for a symmetrical capsule implosion implies that the total number of beams be evenly divisible by six. Additionally, at least an eight-fold rotation symmetry in the azimuth angle, ϕ, is required to smooth the lower order P_n terms in the drive pressure and thus insure a symmetrical implosion. Azimuthal symmetry requires that the number of beams be evenly divisible by an integer equal to or greater than eight.

The relationship between the target irradiation geometry and the beamlet count is explored in Table 4-1. The first row in this table arrives at the minimum number of beamlets, 192, which meets symmetry and smoothing criteria. Increasing the azimuthal symmetry increases the number of beamlets. We've thus established a minimum number of beamlets in NIF without ever discussing an energy requirement!

Table 4-1 Target irradiation symmetry and smoothing requirements influence the beamlet count.

Order of azimuthal symmetry	Beamlet cluster size for focal spot smoothing	Beamlet multiplier for side to side uniformity	Resultant beamlet count
8	4	6	192
9	4	6	216
10	4	6	240
11	4	6	264
12	4	6	288
13	4	6	312
14	4	6	336
15	4	6	360
16	4	6	384
17	4	6	408
18	4	6	432

In addition to these symmetry considerations, NIF must deliver its laser drive pulses according to stringent requirements in time and space. Targets respond to input power, and after they have imploded no additional energy is of use. Notions of beam-to-beam energy balance and simultaneity must give way to beam power balance in NIF. Ideas about beam profiles, power densities and pointing, so familiar in Nova experiments, take on new meaning when continuous contour random phase plates condition each beamlet on its way to the target. Each modern beamlet has a beam area of $\sim 0.1\,\mathrm{m}^2$, depending on the details of its design, so the systems outlined in Table 4-1 range in total beam area from about $19\,\mathrm{m}^2$ to over $40\,\mathrm{m}^2$.

4.2 *Laser Requirements*

A formula exists for estimating the "safety factor" or "target margin" for a given NIF indirect drive ignition target.[1,2,3] This figure of merit is parameterized by a scaled capsule radius, R, and hohlraum temperature, T. Each ignition experiment (i.e., each point in RT space) presumes a unique two-step temporal shape for the incident 0.351 micron laser drive pulse. The formula may be used to construct a contour plot showing the expected target margin as a function of the peak UV power and total UV energy incident on each optimized target's laser entrance hole (LEH).

---

[1] Steve Haan, *Pulse shapes for the Nova Upgrade*, LLNL ICF internal memorandum, July 28, 1992.

[2] Steve Haan, *Figure-of-merit for upgrade target systematics*, LLNL ICF internal memorandum, October 4, 1992, rev. October 9,1992.

[3] Steve Haan, *Revised figure of merit for NIF target systematics*, LLNL ICF internal memorandum, July 29, 1993.

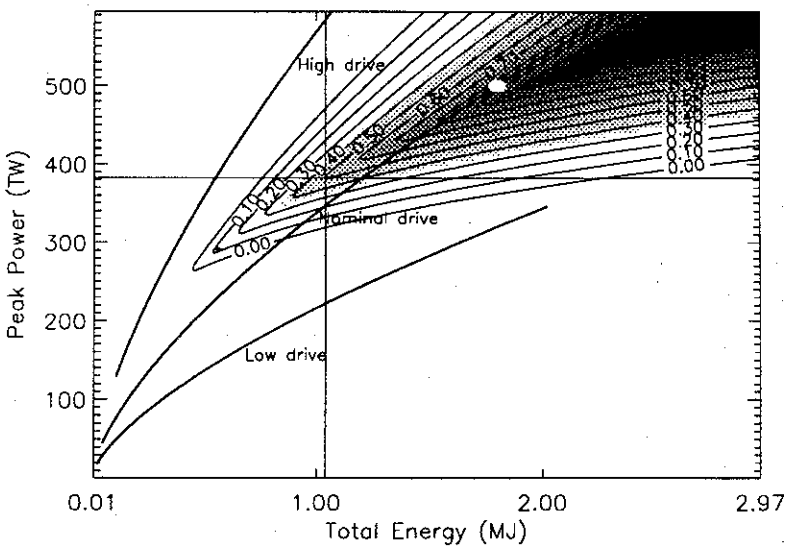

Figure 4-2 **The target margin or safety factor is represented by a contour. The total UV energy and peak power incident on the laser entrance hole to the target are provided as axes values. Each point on the plane corresponds to a unique two-step temporal pulse. The baseline design is marked by a white dot.**

Figure 4-2 maps some 10,000 target point designs in peak UV laser power versus UV energy space. Contours of equal figure of merit above 30% have been shaded. Prudence demands that the NIF baseline target design lie above the 50% contour, a condition first achieved when the laser's peak power exceeds 380 TW and its energy exceeds 1.1 MJ. Each target simulation employs a unique pulse shape and the baseline design target indicated in Figure 4-2 supposes NIF will deliver the pulse shown in Figure 4-3 (a). The corresponding, simplified, two step pulse shape is shown in Figure 4-3 (b).

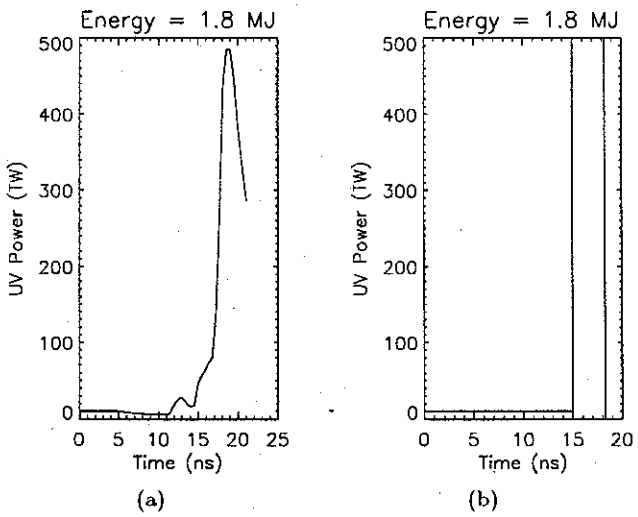

Figure 4-3 **Temporal pulses used in calculations**

The one micron laser pulse that is needed to generate the UV pulse may be found by working backward from the LEH through the target irradiating optical components, UV beam transport optics, random phase plates, and the frequency conversion crystals.

Figure 4-4 plots the power dependence of the frequency conversion efficiencies used for simulation. The baseline case peak efficiency for our idealized converter is 70%—reached only during the high drive portion of the one micron laser pulse. Untested tripling schemes with improved dynamic range and peak efficiency have been proposed. These schemes are capable of producing 75% tripling efficiencies for both power and energy. We will adopt this figure as the best achievable by any combination of pulse stacking or converter design. The standard IL^2 rule provides an optimum thickness for these converter crystals at the peak power.

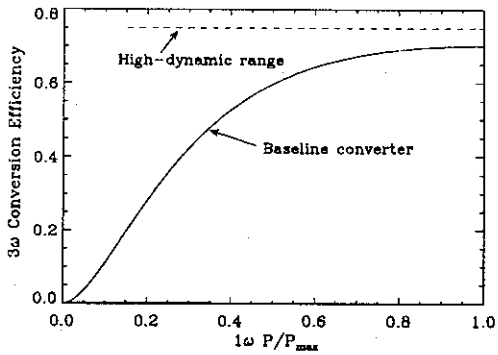

Figure 4-4 3ω conversion efficiency curve used in the pulse shaping analysis. This is the Type II-Type II tripling efficiency curve presented in the 1985 Laser Annual Report (p. 6-45)

Figure 4-5 outlines the calculation for the baseline pulse shape in Figure 4-3 . A 933 TW-4.5 MJ, one micron, pulse is required for generating the 500 TW-1.8 MJ, UV pulse. Conservative losses are used to provide for laser design margin. Assuming the shaped, one micron, pulse is well behaved (i.e., its power increases monotonically with time), then a 4.8 nsec, temporally *uniform* one micron pulse will have the same peak power, total energy, damage threshold, gain saturation characteristics, and last photon B-integral as the shaped pulse.

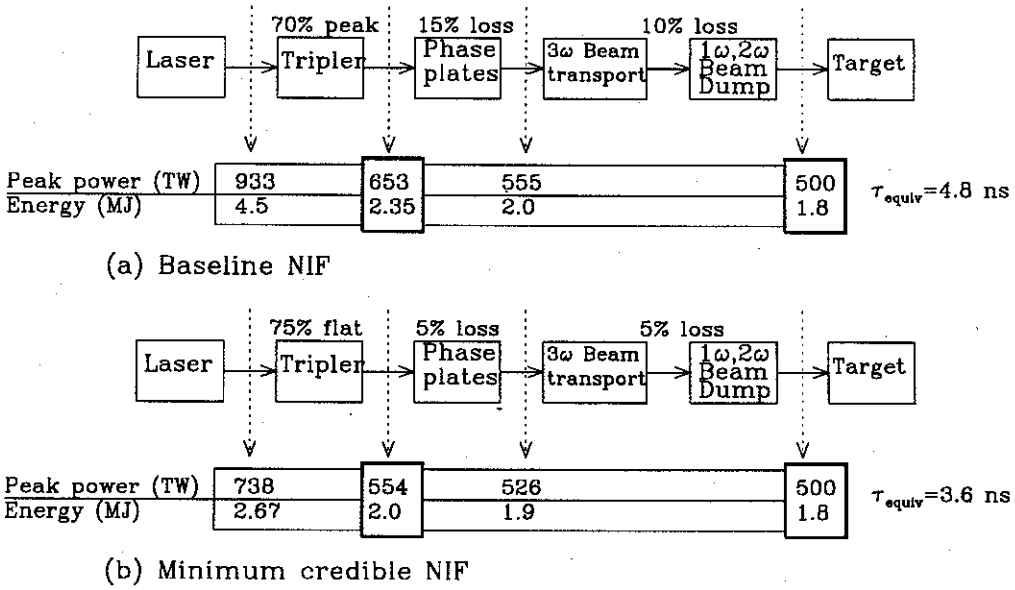

Figure 4-5 The relationship between the UV pulse and the one micron pulse required. The pulse lengths are those effective pulse lengths for the one micron pulse, i.e. a square pulse with the same energy and peak power.

This last is the *equivalent* one micron pulse length—merely the peak one micron energy divided by the total power. The computer program, CHAINOP (See Chapter 5), can be used to maximize the *bang-per-buck*, J/$, at this equivalent pulse length, while varying other optical parameters.

In addition to the baseline laser, Figure 4-5 also outlines the calculation for a minimum credible NIF laser. The ~20% design margin built into the NIF baseline is removed by assuming that a new converter achieves an efficiency of 75% at any intensity (high dynamic range), that the phase plate beam smoothing system is 95% efficient rather than only 85%, that the UV transport efficiency rises from 90% to 95%, and the UV damage threshold improves by 10%. This minimum credible NIF represents a far more aggressive design that exposes the project to significant risks; however, it represents the extremum on the low side in cost.

4.3 *Beamlet count*

We've used CHAINOP to estimate the energy and peak power for optimized NIF beamlets. Figure 4-6 shows an iso-cost contour as a function of optimized beamlet energy and peak one micron power. The beam area used in these calculations was about 940 cm^2, corresponding to 35 cm hard aperture optics with vignette and fill factors amounting to 77%. The cost of hardware for a single beamline is nearly the same for all designs along this curve. The effective one micron pulse length is represented on this plot by a straight line emanating from the origin and intersecting the isocost curve at that peak power and energy available from the optimized beamlet.

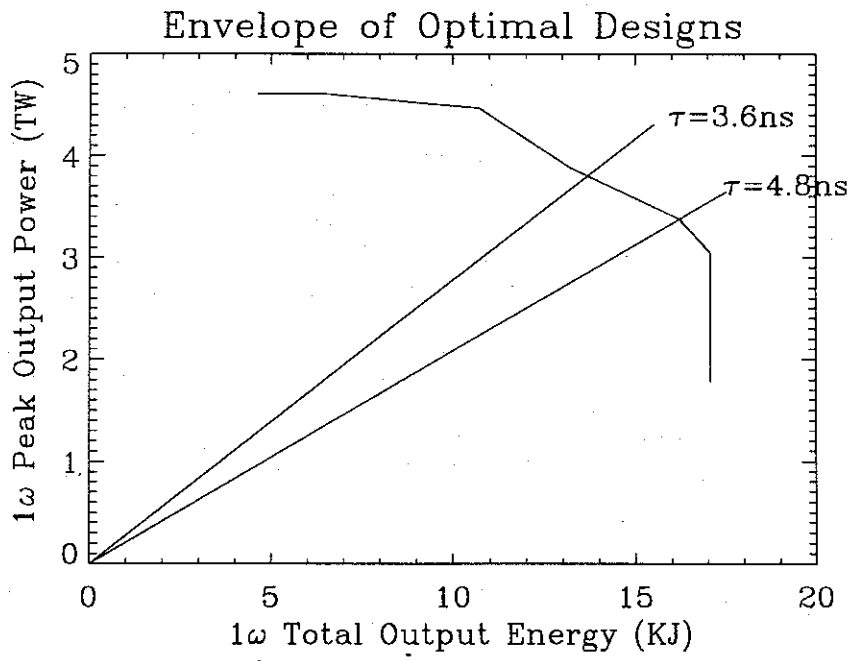

Figure 4-6 Isocost beamlet curve parameterized by one micron energy and peak power at the tripler. The equivalent 4.8 nsec one micron pulse will produce a peak power of 3.3 TW and energy of 16.1 kJ

From Figure 4-6 we see that the 4.8 nsec optimized 35 cm beamlet can produce peak power of ~3.25 TW. Thus, the number of beamlets, N, required to generate a 933 TW-4.5 MJ, one micron pulse is

$$N = \frac{933\,\mathrm{TW}}{3.25\,\mathrm{TW}} \approx 288$$

Equivalently, we can divide the total energy required by the energy per beamlet—4.5 MJ/16 kJ—to arrive at the same figure.

For the minimum credible case where the tripling efficiency is independent of power, the effective pulse length is given by

$$t = \frac{2.67\,\mathrm{MJ}}{738\,\mathrm{TW}} = \frac{1.8\,\mathrm{MJ}}{500\,\mathrm{TW}} = 3.6\,\mathrm{nsec.}$$

Using Figure 4-6 we discover that the power per NIF beamlet is 3.85 TW. The number of beamlines for this case is then

$$N = \frac{738\,\mathrm{TW}}{3.85\,\mathrm{TW}} \approx 192,$$

This type of analysis shows that wide dynamic range conversion could produce a 15% reduction in number of beamlets, while improvements in UV transmission, peak conversion efficiency, and phase plate efficiency contribute 6%, 7%, and 12% reductions respectively. To make full use of such improvements, UV optics damage thresholds would also have to increase; however, the product of the latter three figures, 25% to 27%, represents the baseline NIF laser design margin.

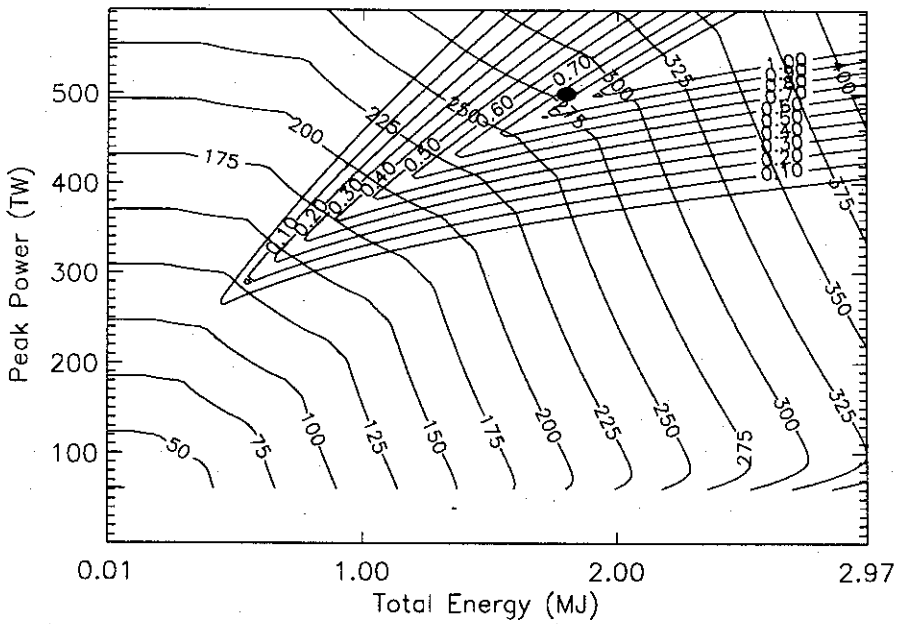

Figure 4-7 Target margin versus number of isocost beamlets. The baseline case is indicated by the dark spot.

A computational procedure has been developed to combine the target margin figure of merit with the CHAINOP results. The algorithm was used to generate Figure 4-7 , showing contours of constant target margin plotted atop contours of number of optimized isocost 35 × 35 cm^2 beamlets.

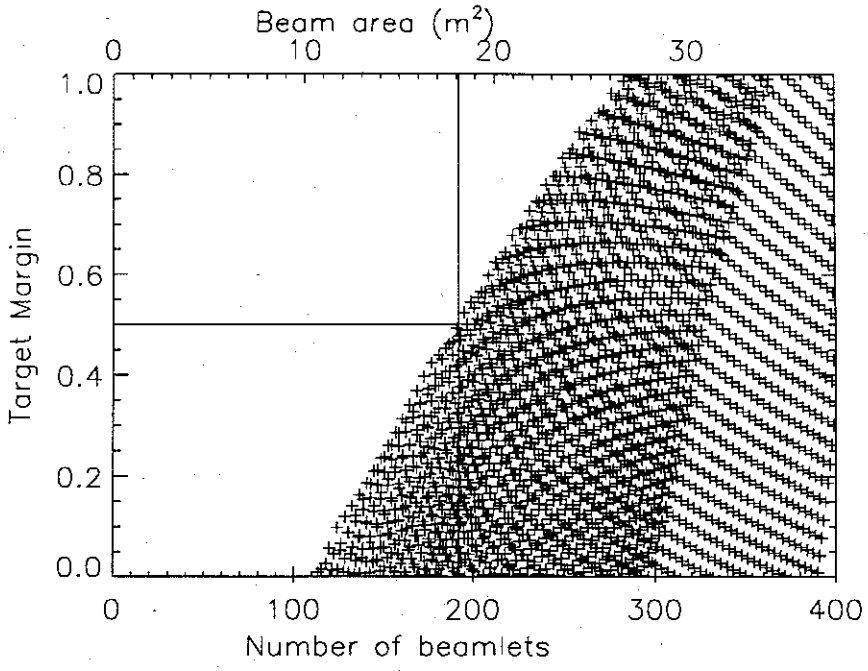

Figure 4-8 Target margin versus number of optimized isocost beamlets. Target margin first exceeds 50% for NIF designs with >192 beamlets.

Figure 4-8 also plots beamlet count, but in a slightly different format. Figure 4-8 shows that the target margin first exceeds 50% for NIF designs with >192 beamlets. The 500 TW-1.8 MJ point design requires the construction of a laser system having a $\sim 27\,\mathrm{m}^2$ beam aperture and reaches a target margin of almost one. Many target designs with figures of merit over 80% should be accessible. The ridge line apparent in the contour plot shows up as a characteristic line with most of the 10,000 cases clearly suboptimal for a given number of beamlets or beam area. Since laser system cost scales almost linearly with beam area or number of beamlets, Figure 4-8 is a risk vs. cost plot.

Starting from theoretical results substantiated by experimental work, and following logic similar to that above, we conclude that a reasonable set of NIF baseline laser system requirements is

- Irradiating wavelength: 0.351 micrometers
- UV energy incident on the LEH: 1.8 MJ
- UV peak power incident on the LEH: 500 TW
- UV pulse length: 20 nsec
- Contrast ratio of the irradiating UV pulse: up to 50:1
- Beam smoothing requirements at LEH
- Little of the fundamental or frequency doubled light can reach the target

Given these top level target requirements, we can derive specific laser system requirements.

4.3.1 *Power Balance*

NIF ignition targets simulated with LASNEX call for detailed laser pulse shapes in time that differ for inner and outer cones. If we designate an *ideal* temporal pulse shape by $P(t)$ and require that the NIF laser reproduce it, we expect to find some deviation between $P(t)$ and the actual average NIF pulse shape, $P_0(t)$. Given adequate warning, the target design group can cope with as much as a 10% deviation between $P(t)$ and any $P_0(t)$ that delivers the same energy as $P(t)$, without unduly compromising the ignition experiment.

There is an equally tight specification on the variation between NIF beamlet powers during a shot. We can express this beam power balance requirement at any time into the pulse, t_0 in terms of a boxcar averaged rms deviation between every beamlet's power history, $P_i(t)$, and $P_0(t)$:

$$\sigma(\Delta, t_0) = \frac{\sqrt{\frac{1}{N}\sum_{i=1}^{N}\{\int_{t_0-\Delta/2}^{t_0+\Delta/2}[P_i(\tau) - P_0(\tau)]\,d\tau\}^2}}{\int_{t_0-\Delta/2}^{t_0+\Delta/2} P_0(\tau)d\tau}.$$

The deviation, $\sigma(\Delta, t_0)$, is specified in terms of a maximum allowed value given Δ for any time t_0 into the pulse:

1. For $0 < t_0 < 10$nsec during the *foot* of the pulse, $\sigma(30\text{ psec}, t_0) < 0.5$ and $\sigma(6\text{ nsec}, t_0) < 0.2$

2. For $10 < t_0 < 15$nsec, $\sigma(30\text{ psec}, t_0) < 0.3$ and $\sigma(3\text{ nsec}, t_0) < 0.1$

3. For $t_0 > 15$nsec during the peak of the *drive* pulse, $\sigma(30\text{ psec}, t_0) < 0.2$ and $\sigma(2\text{ nsec}, t_0) < 0.1$ (the comparable requirement for direct drive is 0.08)

4. Deviations larger than the above can be tolerated only if they are confined to an interval less than 30 psec long. This 30 psec limit, when applied to identical pulse shapes from every beamlet, constitutes a *simultaneity* requirement.

Figure 4-9 (a) shows the baseline pulse shape with acceptable levels of noise for the $27\,\text{m}^2$, 288 beamlet baseline case. Backing up through the transport optics, phase plate and nominally 70% peak conversion efficiency tripler leads to the pulses displayed in Figure 4-9 (b). Power balance error allowances have yet to be allocated for each subsystem.

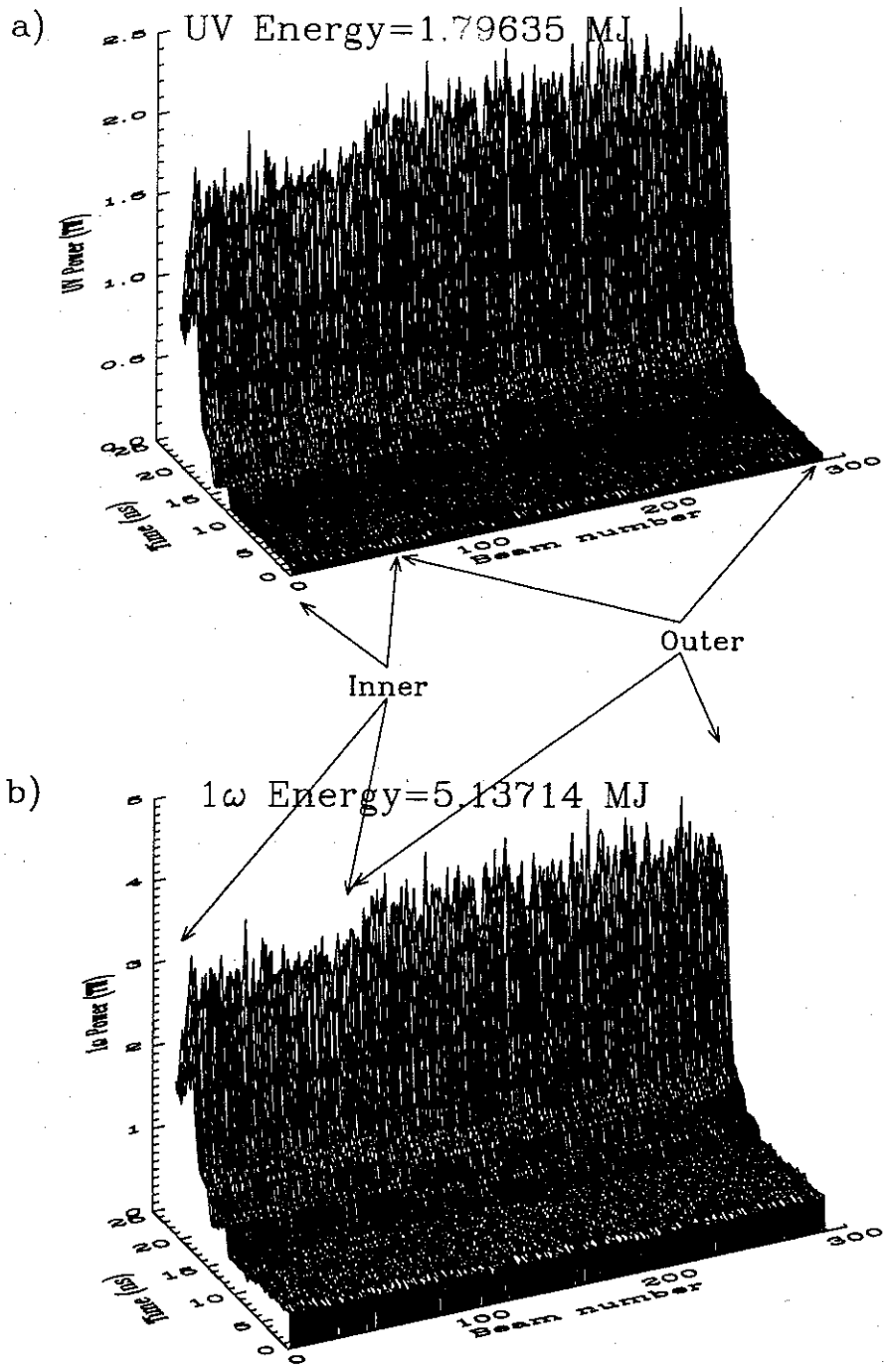

Figure 4-9 Baseline pulse shapes with acceptable noise added. a) UV energy at the LEH. b) 1ω energy just before tripler.

4.3.2 *Pointing*

NIF ignition targets simulated with LASNEX are sensitive to the precise location of the laser beams as they approach and enter the LEH. An rms deviation over 50 μm between the centroid of the individual four beamlet clusters and the pre-selected aim points could reduce the target's performance. The NIF beam pointing specification with respect to a reference point in the target chamber's center derives from this observation.

Near the chamber center—a volume of $6^3\,\mathrm{cm}^3$, and (x, y, z) ranging over $(\pm 3, \pm 3, \pm 3)$—every four beamlet cluster should be a speckle pattern within an approximately 500 μm diameter super-gaussian envelope whose axis is well defined. The NIF pointing specification is met when Δ_i, the vector distances from the nominal aim point for the i^{th} beamlet cluster to that beamlet cluster's measured centroid axis, obeys

$$\sqrt{\frac{1}{N}\sum_{i}^{N}\Delta_i^2} \leq 50\mu\mathrm{m}.$$

4.3.3 *Beam Conditioning*

NIF focal spot smoothness criteria should be divorced from specific beam smoothing methods. Even today there appear to be several ways to effect beam "smoothing" adequate to suppress some of the known plasma instabilities anticipated in a NIF ignition target. Several new methods will almost certainly emerge given the active research going on in this area. We offer the following specification and outline one method for achieving it.

The baseline indirect drive NIF target demands that each individual 0.351 μm beamlet be focused to a 500 μm diameter spot using a 700 cm focal length lens. The spot size specification comes from LASNEX simulation of NIF targets and the lens focal length requirement emerges from a combination of geometric considerations driven by target irradiation symmetry, mechanical interference and the damaging effects of ignition target emanations on focusing optics. The spot size specification reduces to:

> *All* of the 1.8 MJ/ 500 TW ultraviolet laser pulse must pass through 500 μm diameter circles normal to each beamlet axis.

Consequently, 1.8 MJ is the energy delivered through the central regions of target entrance hole(s). Any energy that is scattered outside the hole(s) provides no useful function, though the laser must still be designed to produce it.

Beam smoothness in indirect drive target plasmas must be adequate to hold plasma instability growth within tolerable levels. We expect that instantaneously each beamlet focal distribution will be speckle like; i.e., Rayleigh or exponentially distributed. The smoothness specification reduces to a requirement on the standard deviation of the irradiance anywhere within the specified 500 μm circles. In particular, the standard deviation of the irradiance within any region of the beam several speckles across, about 30 μm in diameter, averaged over a time short compared to the hydrodynamics or thermal self-focusing time-scale, ~ 100 psec, should be $\sigma \leq 0.25\langle I \rangle$. This criterion may be met by groups of up to four beamlets treated as a cluster. The smoothness specification is therefore

For any $30\,\mu$m diameter circle, C, located anywhere in all the $500\,\mu$m spots

$$\sigma = 0.25\langle I\rangle = \frac{\left[\int_\tau \int_C (I - \langle I\rangle)^2\, dA dt\right]^{1/2}}{\tau},$$

where $\tau \approx 10$ psec.

To assure that such specifications are not vacuous for NIF, we summarize one method that meets these requirements. Phase plates that take a uniform NIF size beam into a $500\,\mu$m diameter have a translation decorrelation length or speckle radius given by $\delta x = \lambda F_{\text{number}} = 7.7\mu$m. On the average, then, there will be four speckles in every $30\,\mu$m circle. If each beamlet in each four beam cluster has a different wavelength and we average over a time long compared to their beat frequencies, then there should be four independent patterns averaged in time. With our specified averaging time of 10 psec, a wavelength separation of 20 cm^{-1} should suffice between beamlet center frequencies, since we can expect more than 16 clearly differing patterns leading to $\sim\sqrt{16} = 4$ incoherent independent temporal patterns.

Speckle statistics provides us with a probability density function for such intensity summations of N independent exponentially distributed beams,

$$p(I) = \frac{N^N I^{N-1}}{\Gamma(N)\langle I\rangle^N} \exp\left(-\frac{NI}{\langle I\rangle}\right),$$

where $\Gamma(N)$ is Euler's gamma function making this expression valid for any real, positive N including fractional values. The standard deviation of the laser irradiance is thus

$$\sigma = \frac{\langle I\rangle}{\sqrt{\left(\begin{array}{c}\text{number of speckles}\\ \text{in circle}\end{array}\right)\left(\begin{array}{c}\text{number of independent patterns}\\ \text{averaged in time}\end{array}\right)}}.$$

$$= \frac{\langle I\rangle}{\sqrt{4\times 4}}$$

Only 1% of the energy in the four overlapped focal spots will be delivered at an irradiance greater than $1.7 \times \langle I\rangle$ in this case.

Given a *perfect* input ultraviolet laser beam, then, random phase plates having a lateral coherence length or characteristic structure radius of about 0.6 cm can produce the required spot size. The center wavelengths of each of the four overlapping beamlets would be 3508 Å, 3511 Å, 3514 Å, and 3517 Å. Within a given 10 psec integration time, about 20 beats should be realized due to the $60\,\text{cm}^{-1}$ bandwidth specified. We require $\sqrt{20} \approx 4$ distinct patterns in time within our averaging temporal window and a like number, 4, spatial speckles within our spatial averaging area. As an added measure of conservatism, we have approximately doubled the separation between wavelengths to span ~ 20 Å in the ultraviolet and set the baseline center frequencies to 3503 Å, 3510 Å, 3517 Å, and 3524 Å. Preliminary plasma simulations suggest that this strategy will suppress the worst instabilities. It remains for further plasma simulation calculations and yet to be conducted Nova experiments to test the validity of this method.

4.3.4 *NIF Laser Beam Quality*

A beamlet of the NIF laser must meet two beam quality requirements:

- The beam quality must be consistent with a spot size on target of 500μm diameter.
- The beam quality must be consistent with high-efficiency frequency tripling.

The final target focus lens in the baseline design has focal length 7 m, so the spot size requirement means that the laser energy be contained within ± 35 microradians of the nominal beam axis. The use of kinoform phase plates reduces this figure to ± 25 microradians.

Any beam meeting the target spot size requirement is suitable for high-efficiency frequency tripling with properly-designed KDP or deuterated KDP frequency converters of either the Type I-II or Type II-II designs. Both types have been tested on Nova and have given whole-beam efficiency exceeding 70%. The baseline converter for the Beamlet Demonstration Project and NIF is a Type I-II converter, since that design is less sensitive to beam depolarization and requires smaller crystal boules. This design has given whole-beam efficiency exceeding 70% in small-scale experiments at typical NIF design fluences and intensities. The Type II-II converter allows somewhat looser pointing specifications on the crystals, but otherwise has similar tolerances.

Figure errors on optical components deflect rays from the desired direction and contribute to beam divergence. Opticians measure and quote figure errors using computer-interpreted interferograms which report peak-to-valley figure error at a test wavelength of 633 nm. We are interested in the contribution of that error to the angular distribution of rays in the far-field, which is what we mean by "beam quality" or "beam divergence".

We estimate the effect of figure errors using a model developed for the Nova laser[3] that is suitable for the typical errors we see on large laser components. These are smooth, low-spatial-frequency errors with two cycles or less across the aperture. We assume that the peak-to-valley errors are random and add as the square root of the sum of squares (RSS-Gaussian statistics). Then the model predicts that the focal spot in the far-field has a radius (defined as roughly $1/e^2$ intensity or 90% included energy) that exceeds the diffraction limit by one Airy disk radius for each third of a wave of accumulated RSS peak-to-valley optical figure error. That is:

$$\theta_{\text{far-field}} = \theta_{\text{diffraction limit}} \left(1 + 3 * W_{\text{rss}}\right),$$

where W_{rss} is the accumulated random figure error. The model has been tested on Nova and correctly predicts the effect of accumulated random figure errors on output beam divergence. The central Airy disc of a 35 cm beam at 1 μm has a radius of 3.4 μrad, and we take this as the nominal diffraction-limited spot size for an NIF beamlet.

The model must be modified for a multipass design such as the NIF beamlet, since errors on multipassed components add coherently rather than randomly. We take account of the coherence by linear accumulation of figure error on multipassed components so that the net figure error becomes

$$W_{\text{rss}} = \sqrt{\Sigma n_i (m_i W_i)^2},$$

where n_i is the number of components of type i and m_i is the number of passes.

The most instructive way to organize the components of an NIF beamline is by the weight, nm^2, of their figure error, as shown in Table 4-2. It is clear that the overwhelming contribution to beam divergence is from the laser slabs within the multipass cavity, so those must be finished to tight specifications. The NIF baseline (11-5-3) has more multipassed components than the baseline layout of the Beamlet Demonstration Project (11-0-5), so it has slightly greater sensitivity to figure error.

---

[3] L. G. Seppala and K. Moore, *Wavefront distortion in Nova and Beamlet,* ICF internal memorandum (BLT92-073), April 1992.

Table 4-2 Components organized by weight of their figure error.

COMPONENT	Weight nm^2 of the figure error. Beamlet 11-0-5	NIF 11-5-3
Cavity disk	176	256
Cavity SF Lens	25	32
Switch window	18	32
KDP crystal	11	18
Booster disk	5	12
Transport Mirror	4	7
Transport SF and Focus lens	3	6
Cavity Mirror	5	5
Polarizer transmission	4	4
Polarizer reflection	1	4
Chamber window & Debris sh.	2	2

Table 4-3 gives a suggested set of specifications for optical figure error on the various optical components. Assuming a wavefront error of $3\lambda/4$ on the input beam from the front end, these specifications lead to a projected beam divergence of $\pm 24\,\mu$rad for the 11-0-5 layout of the Beamlet Demonstration Project and $\pm 30\,\mu$rad for the 11-5-3 NIF baseline beamlet. Both meet the spot size requirement of $\pm 35\,\mu$rad, though neither gives much leeway for smoothing the spot using kinoforms. This is not likely to be a problem if the spot has a smooth profile.

Table 4-3 Suggested working specifications for optics figure errors.

	(PV error at 1 μm, similar to Nova specifications and inspections)
Laser disks:	70% of order $< \lambda/10$ in transmission (installed in cavity) remainder of order $< \lambda/5$ (installed in booster)
Lenses:	$< \lambda/10$ in transmission (Cavity SF); lower is acceptable for transport SF and Focus if there is a significant cost impact
Mirrors:	$< \lambda/4$ in reflection ($\lambda/8$ surface flatness)
Windows:	$< \lambda/10$ in transmission switch windows; lower would be acceptable for chamber window if there is a significant cost impact
Switch crystal:	$< \lambda/4$ in transmission
Polarizer:	$< \lambda/10$ transmission, $< \lambda/2$ reflection ($\lambda/4$ surface flatness)
Debris shield:	$< \lambda/2$ in transmission

Brewster's-angle slab amplifiers have pump-induced thermal distortions caused by the spatial variation of heating of the slab by the flashlamps, causing aberrations on the laser beam. These distortions vary somewhat with amplifier design and with the position of a slab within an amplifier, but are roughly proportional to the number of slabs. Current models suggest that the distortion introduced by a single pass through an 11-slab-long amplifier is about $\pm 20\,\mu$rad and consists mostly of negative cylinder (astigmatism) with the axis of the cylinder lying along the short dimension of the slab (that is, perpendicular to the beam polarization). Our ability to measure the very small distortions introduced by a single slab is not good, so there is some uncertainty in the exact magnitude of these distortions for NIF amplifier designs. These uncertainties will be removed and the thermal models verified when measurements are made on the full amplifier array of the Beamlet Demonstration Project.

The accumulated divergence in the NIF beamline is projected to be about $\pm 100\,\mu$rad after four passes through the cavity and two passes through the booster amplifier. This should not have a

serious effect on frequency conversion, but a divergence of this magnitude fails to meet the target spot size requirement. Therefore, it will be necessary to correct for the pump-induced distortion.

Correction of the distortion can take one of several forms:

- Tilt of spatial filter lenses – If the lenses are tilted, astigmatism can be introduced to compensate for the amplifier astigmatism. This requires no special figuring of optics, but may introduce other aberrations and complicate the assembly of the laser.
- Add active adaptive optical correction to the system – Adaptive beam correction can easily remove the amplifier distortion, and may correct other aberrations. This would allow a relaxation of the figure specifications of Table 4-3 , reducing the cost of the optical components. We must trade that against the considerable expense of any adaptive-optical system. The Beamlet Demonstration Project will install adaptive correction to test some of these issues and tradeoffs.
- Figure an optical component to compensate the pump-induced distortion – This solution is much less expensive than adaptive correction, but also less flexible. There is perfect correction only at the design pumping level and progressive deterioration as we move away from that level. The alignment system may be affected.

The final item is the anticipated solution for NIF, but these issues must be explored in more detail in the final design of the system.

Taken together, the foregoing establish laser functional requirements. The expanded flow-down chart in Figure 4-10 carries the target requirements we first encountered in Figure 4-1 down to the subsystem requirements. Detailed subsystem requirement documentation has been finalized for the Beamlet project; and the NIF equivalent, including target area specifications, exists in draft form as of this writing.

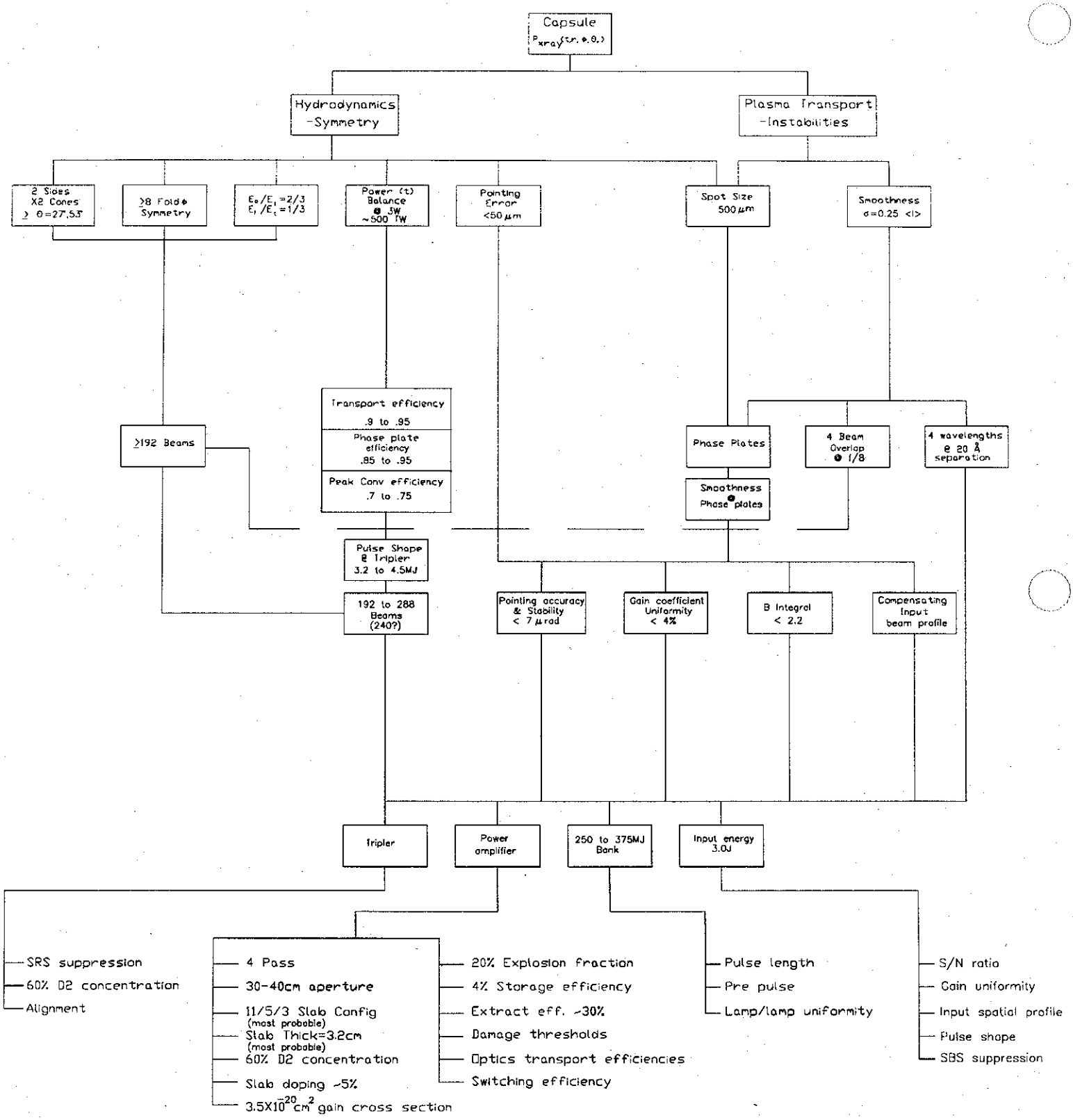

Figure 4-10 Expanded flowdown chart.

4.4 *Operating range*

The current baseline NIF chain design is the one among the family of optimized isocost lasers which matches the 1.8 MJ-500 TW baseline ignition target. As such, it will have a particular frequency converter and is necessarily sub-optimal for all other points in (P_{uv}, E_{uv}) space. Having designed the NIF for optimum performance at one point, we have calculated its access to interesting regions of (P_{uv}, E_{uv}) space; i.e., the NIF operating range in regions of highest ignition probability figure of merit. Figure 4-11 shows the expected performance of 288 baseline (35×35 cm^2) beamlets. The high power performance is artificially clamped by our design choice that the frequency conversion be maximized for the highest drive power of the baseline target. In fact, more infrared power is expected for shorter effective pulse duration, but beam quality and focusing specifications become increasingly problematic beyond the peak of the conversion curve. Useful on-target power is not likely to exceed 500 TW at any energy. Longer effective pulse durations imply lower peak power and correspondingly lower conversion efficiency. This accounts for the roll back in energy predicted for pulse durations well above our design point. A "normal operation" line which intersects the baseline target point has been calculated using the more conservative baseline NIF transfer efficiencies listed in Figure 4-5a). A laser design margin of 20 to 25% separates "normal operation" from "redline" or damage limited performance.

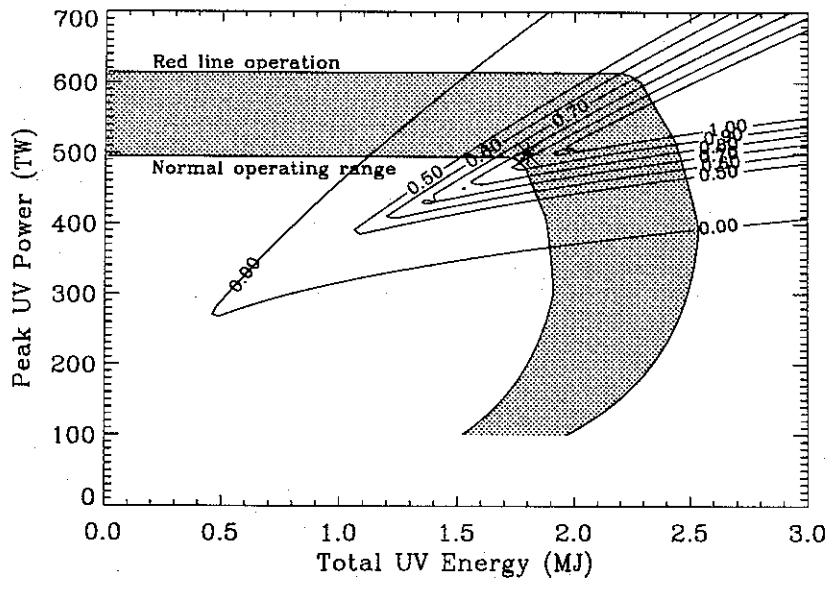

Figure 4-11 Accessible P_{uv}, E_{uv} space.

Since so much seems to depend on frequency conversion efficiency, a second series of calculations optimized the converter for each pulse shape while leaving the laser chain design fixed at the current baseline. Figure 4-12 is the result. Within the region of high target margin figure of merit, say above the 50% contour, there is little additional space accessed for what would certainly be a very large cost.

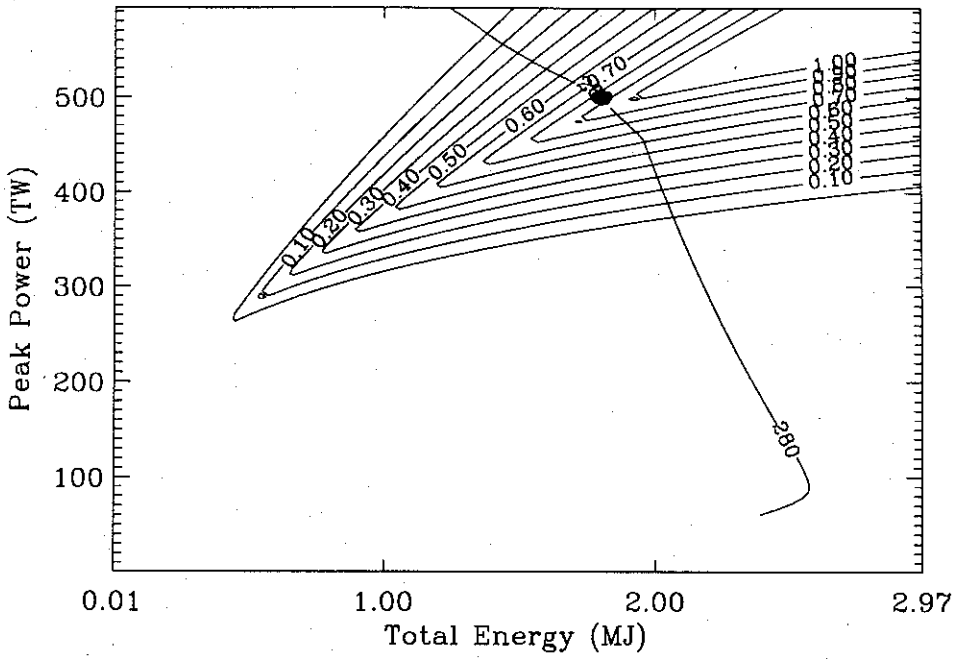

Figure 4-12 Operating range accessible with optimized frequency converters.

The particular choice of target design for which we have optimized the laser has also effectively maximized our access to interesting target irradiation space, within our present understanding of target margin. The 288 beam contour could just as well be achieved with a smaller number of larger aperture beams. For example, 240 beamlets with an aperture of $\sim$38.3 cm would provide identical performance. Additionally, if we are willing to increase laser performance risk (i.e., remove any design margin) then 192 beams with 39.4 cm aperture would do the job. If we assume we can invent a frequency converter with infinite dynamic range and peak efficiency of 75%, the aperture for the 192 beam case could be reduced to 35 cm. This last option constitutes our minimum credible NIF design.

Figure 4-13 explores the operating range of this minimum credible NIF design given four scenarios. If an infinite dynamic range converter becomes available and higher damage threshold optics are produced, the minimum credible NIF could access the same experimental region as the current 27 m^2 baseline design. If, however, it had to be operated with even a 20% laser design margin or engineering safety factor, it would fall well short of the NIF baseline target requirements.

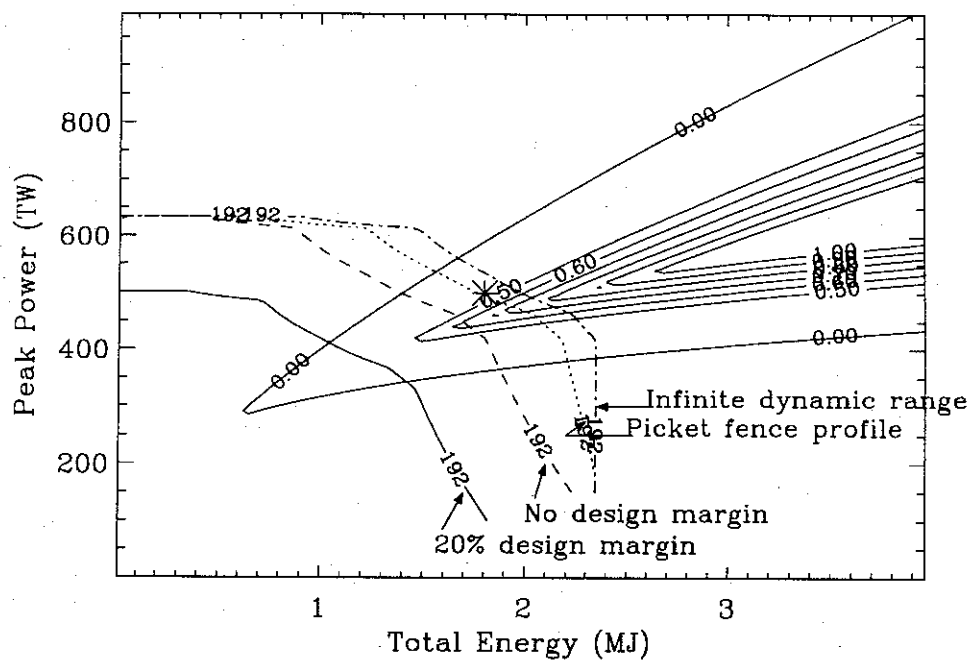

Figure 4-13 Minimum credible NIF laser design.

Chapter 5

SYSTEM DESIGN/COST OPTIMIZATION

5.1 *Laser chain design optimization methodology*

The laser chain designs used in this study were produced by CHAINOP, a computer program that models the performance and cost of a laser system. It adjusts a number of parameters to maximize output per unit cost while remaining within a set of design constraints. The constraints include fluences, nonlinear effects, and pulse distortion. The code was designed for speed at the expense of accuracy, because searching the multidimensional design space for the best chain can require the simulation and cost evaluation of tens of thousands of different designs. Once the best design is approximately determined, it is refined with the use of more accurate, but slower, codes.

Several analytical models have been built into CHAINOP to simulate important optical effects. These include the pumping process that turns capacitor bank energy into inversion in the laser slabs, the propagation of the laser beam through the system (including gain, loss, diffraction, and nonlinear optical effects), frequency conversion of the beam, and cost of the system. We will consider these in turn.

The pump model simulates capacitor bank electrical performance, flashlamp operation, pump cavity performance, and laser glass energy storage. The bank can be modeled with standard pulsed circuit analysis techniques, with the minor complication that the flashlamp load has nonlinear V-I characteristics. On the basis of extensive measurements, we know that the flashlamps take a certain amount of time (about 30 microseconds) to turn input energy into optical radiation from the plasma. They then radiate for 300 μs with a complicated line-and-continuum spectral structure. We have carefully characterized the radiative efficiency and spectral shape as a function of lamp loading, size and fill pressure, and produced a phenomenological model that fits the data over a wide range. We are therefore able to accurately calculate the conversion of bank energy to pump photon energy.

Pump photons propagate through the amplifier cavity until they produce useful inversion or get lost through light leaks or absorbing structures in the cavity. This three-dimensional, multi-wavelength process is so complicated that we can calculate it only approximately, and we rely on the extensive measurements that have been made on the various amplifier test beds at LLNL. Once the pump light reaches the laser glass, it is absorbed and the resulting excitations rapidly decay to the upper laser level with appropriate quantum defects. The upper level decays slowly, at a rate that depends on the doping level and the slab dimensions (due to amplified spontaneous emission and resonance line trapping effects). The inversion also changes its spatial shape when resonance-line decays are reabsorbed by nearby ions. In CHAINOP, we adjust the lamp spacing, lamp loading, pump pulse duration, and doping in order to get the best possible level of inversion.

When the time of peak inversion density is reached, roughly 250 μs into the pumping pulse, the laser beam is injected into the cavity. It is then amplified by the laser slabs, undergoes loss in the slabs and other components, changes spatial shape from diffraction, spatial filtering, and nonlinear optical effects, and changes temporal shape due to gain saturation effects. CHAINOP models the losses as lumped transmissions less than unity. The gain is modeled with a single-saturation-fluence Frantz-Nodvik formalism, but with a saturation fluence value adjusted to fit the experimentally determined effects of inhomogeneous extraction in LG-750 glass. The Frantz-Nodvik equations allow determination of the gains of the first and last photons in the laser pulse, and therefore of the pulse distortion.

Propagation effects are modeled only approximately. Saturation is calculated assuming a flat transverse profile. Edge effects (apodization and alignment) are calculated using the diffraction spreading of an abrupt edge when propagated over the distance from the nearest relay plane. The fill factor due to multi-pass vignette is calculated based on the sizes of the injection mirror and beam dump. The effects of amplitude and phase noise sources, and of the nonlinear growth of the resulting beam's transverse intensity fluctuations, are approximated by using a formula that depends on the accumulated B-integral since the last spatial filter pinhole. This formula was derived based on the observed irregularities on our existing large laser systems. In addition, the fact that beam irregularities rise abruptly to dangerous levels as the B-integral rises above a critical value (typically around 2.0 to 2.5) is approximated by applying a maximum-B-integral constraint. The B-integral is calculated from the average transverse intensity of the last photon in the pulse (the worst case), allowing for beam size changes, intensity changes due to gain and loss, and component tilt.

Frequency conversion is handled by a constant conversion fraction for the peak power (assumed to be at the end of the pulse) times another constant fraction for the energy. The energy fraction depends on the exact output pulse shape, but for NIF baseline fusion pulses it is around 75% of the power conversion fraction. The converter thicknesses needed to get good conversion increase for longer pulses, but the actual values must be found by the user. The code simply uses a conversion value that assumes that the proper thicknesses are being used.

System cost is approximated by fitting linear constant-plus-slope tangent lines to costs that depend on bank energy, glass volume, beam area, slab count times beam area, and cavity length times beam area. The constant portions of these costs are then combined with other constant costs for fixed project costs, vendor facilitization, and so forth. The result is a set of cost coefficients that can be used to calculate laser system cost for the entire NIF laser. Note, however, that if the size of the beams is changed, or the total project size is changed, or the beam grouping is changed, then the constant-plus-slope points of tangency to the actual cost scalings will change. As a result, both the slope and constant values must be recalculated before optimization is carried out. This is readily done with spreadsheets which contain the costing data.

Constraints are applied to the peak fluence at each component (this depends on the average fluence and B-integral since the last pinhole), to the total B-integral between pinholes, and to the ratio of first-photon gain to last-photon gain. This last constraint avoids the situation where the chain distorts the pulse so much that the front end cannot produce a preshaped pulse that will result in the desired pulse at the output.

In order to verify correct operation of the code, a second version was written by a second author, using a different computer language and a different optimization algorithm. The results are substantially identical to those of the original version. Performance/cost data presented in this report are from both these versions. A third author did a translation to a third language; results were exactly the same. The PC version can calculate the performance and cost of more than 25 chains per second.

5.2 *Optimal laser chain results*

The CHAINOP code is supplied with a chain layout (4-bounce multi-pass section followed by a booster amplifier in this case) and a set of laser parameters and cost coefficients. One especially important input parameter is the equivalent square pulse width of the one-micron pulse.

CHAINOP can adjust the input energy, stored energy density (from lamp spacing, lamp loading, pump pulse duration, and slab doping), slab counts, and beam aspect ratio to get the best possible value of laser output energy divided by chain cost. The slab count must be allowed to take on non-integer values to allow rapid optimization. Once an optimum is found, slab counts or other

quantities can be fixed and the chain reoptimized without adjusting those values. The final result is the best possible chain with the specified material properties and chain layout parameters, within the specified constraint values.

The important input parameters and constraints that led to the baseline design are shown in Table 5-1.

Table 5-1 Input parameters and constraints that led to baseline design.

Input Parameters	Value
hard aperture width:	35 cm
laser design pulse width:	4.8 ns
amplifier configuration:	4×4
amplifier explosion fraction:	0.2
amplifier pumping MSA equivalency:	1.0
injection energy @ 4.8 ns limited to:	0.5 J
injection mirror area:	0.5 cm^2
beam dump area:	50 cm^2
crystal deuteration of switch/doubler/tripler:	60% / 0% / 60%
total output energy fixed at:	1.8 MJ
1w/3w peak power conversion efficiency:	70%
1w/3w energy conversion efficiency:	52%
Constraints	
maximum between-pinhole B integral:	2.2
maximum 1st-to-last photon gain ratio:	35

Table 5-2 lists the damage thresholds used in CHAINOP for the NIF components and compares them to Beamlet values.

Table 5-2 Summary of one nanosecond damage thresholds used in CHAINOP calculations

Type of optic	Damage fluence rated at 1 ns NIF (J/cm^2)	Beamlet (J/cm^2)	Value of exponent scaling factor, α
AR	22.0	18.7	0.4
Glass	22.0	18.7	0.4
HR	19.0	13.3	0.3
Pol X	14.0	10.0	0.3
Pol R	16.0	11.5	0.3
KD*P	20.0	14.0	0.5
KDP3	9.0	6.3	0.5
AR 3ω	10.0	8.4	0.4

The value of the damage threshold of an optic at pulse lengths other than one nanosecond is obtained from Table 5-2 using the scaling relationship

$$F(\tau) = \tau^{\alpha} F_{\mathrm{D}}(1\,\mathrm{ns}), \tag{5.1}$$

where τ is the pulse length in nanoseconds, and α is the exponent scaling parameter.

The progress of the non-integer-slab optimization, followed by the closest odd-integer-slab optimization is shown in Table 5-3. The cost quoted here assumes a 288 beamlet, 35 cm aperture, system.

Table 5-3 Cost of choosing a odd-integer design close to the optimized case.

Slabs Count			Cost	
Main Amp	Switch Amp	Boost Amp	($M)*	Comments
10.047	3.438	3.095	532	opt case w/ 0.5 J injection energy limit
11	3	3	540	< 0.5 J injection energy required
9	5	3	536	0.5 J injection energy limit
11	5	3	538	0.5 J injection energy limit

*Material and labor for NIF construction

More details on the cost and performance of the 11-5-3 laser configuration are given in Appendix A. The one micron performance of this chain at other pulse widths is shown in Figure 5-1.

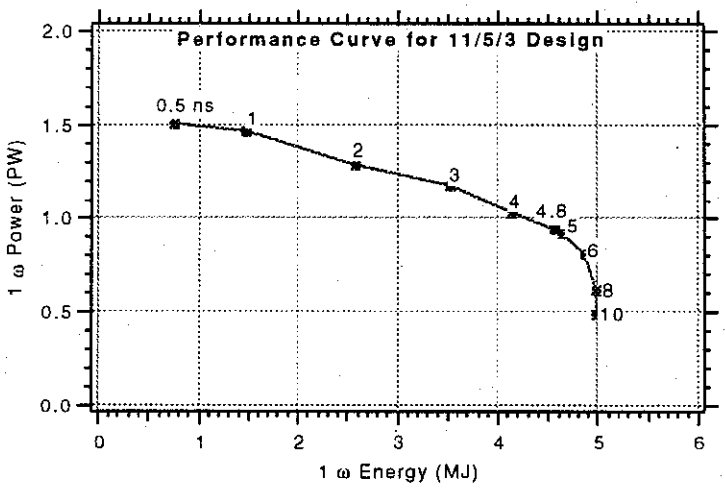

Figure 5-1 Performance curve for the 11/5/3 design shown in the previous tables.

Figure 4-6 in Chapter 4 shows the performance of isocost chains designed for a large variety of different pulse widths. The hard aperture was 35 cm for these calculations.

5.3 *Cost effectiveness sensitivities*

By changing the value of any one of the CHAINOP input parameters, we can find the effect of variations of that parameter on the bang-per-buck of optimized lasers. For example, Figure 5-2 shows the effect of changing the pumping efficacy (by changing lamp output, pump-photon transfer, glass absorption, or glass decay). The equation is written in terms of ratios and difference to minimize the effect of errors in absolute cost and performance parameters. The linear fit to the curve shown in Figure 5-2 is

$$C/C_0 = 1 + 0.6704(p/p_0 - 1), \tag{5.2}$$

where C_0 is the baseline bang-for-buck. This type of information allows us to decide how to most effectively invest in improved technology, since each changed parameter has a corresponding cost.

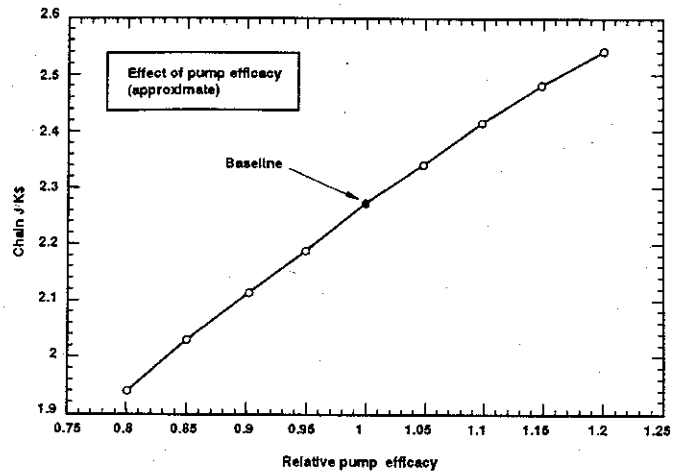

Figure 5-2 Cost effectiveness of a chain vs. the amplifier's relative pump efficacy. The pump efficacy has been normalized to the MSA cavity pumping LG-750. Relative to the MSA, the pump efficacy of Beamlet's amplifier is $0.75p_0$; the NIF amplifier is assumed to be $0.93p_0$

The same analysis has been used to investigate the effect of other critical parameters on the cost effectiveness of the laser design.[1] The results are summarized in Table 5-4. *Italicized entries in the table were calculated after removing damage constraints.*

[1] J. B. Trenholme, *What are the best laser glass parameters*, LLNL ICF internal memorandum June 2, 1993.

Table 5-4 NIF Entry Values

SYSTEM PARAMETER	Value of scaling parameter	NIF entry value	Beamlet value	Extremum Value
Increasing transmission of 3w beam transport	1	0.9	—	0.95
Increasing transmission of phase plate	1	0.85	—	0.95
Increasing peak tripling efficiency	1	0.7	0.7	0.75
Pumping efficacy	0.67	0.91	0.75	1†
Increasing hard aperture of baseline beamlet	0.66	35 cm	39.3 cm	40 cm
Nonlinear optic coefficient, γ, of laser glass	-0.3142	2.90	2.9	TBD
Amount of phase noise in 2 mm to 10 mm sizes	-0.25 – 0.2	—	—	TBD
Stimulated emission cross section	-0.1544	3.5×10^{-20} cm^2	3.5×10^{-20} cm^2	TBD
Cost of bulk laser glass	-0.1088	\$0.88 per cc	\$3.50 per cc	\$0.88 per cc
Per surface loss of laser slabs	-0.0967	0.005	0.0001	0.0001
Increasing dynamic range of tripler‡	0.09	2	2	4
Effective degeneracy effect of inhomogeneity	-0.0790	0.192	0.192	TBD
Bulk loss coefficient of the laser glass	-0.0151	0.05 per m	0.15 per m	TBD
Damage threshold	TBD	see Table 5-2	see Table 5-2	TBD
Grouping	<0.01	4×4	2×2	4×36

† The pumping efficacy parameter was chosen to be unity for the multisegment amplifier (MSA). The other values in this row are relative to the MSA.

‡ The effective one micron pulse length is a function of the tripler's dynamic range; as the dynamic range increases the effective one micron pulse length decreases.

One must remember that the NIF entry values used in Table 5-4 are based on the assumption that a component/technology development program has been successfully completed. Without this investment, the value for C_0 used in Equation (5.2) is approximately two times smaller. That is, the scaling parameters in Table 5-4 are derivative amounts *after* investing in a component development program. In particular, our analysis of the amplifier showed that the continuous pour laser glass technology and the pulse power development programs reduces the cost of the amplifier hardware by a factor of about two.

To combine the effects of several changes in the parameters listed in Figure 5-2 , multiply the individual factors together. Thus, a 40% increase of cross section causes a 6.176% drop in goodness, a 25% decrease in non-linearity causes a 7.855% rise in goodness, and both together cause approximately (1-0.06176) * (1+0.07855) = 1.0119, for a 1.19% net rise.

Chapter 6

COST

In 1982, two years before Nova was completed, we anticipated that a multi-megajoule ICF laser would be required for demonstrating ignition. And we anticipated that commitment to build such a machine would be based to a great extent on its cost. As a result we developed a four-element strategy for reducing NIF project cost—*minimize the project overhead, increase the performance of the laser, decrease the complexity of the system, and reduce the cost of individual components.* We suspect that every component must be at least 2× and more likely 3× cheaper than Beamlet Demonstration Project's costs. Such cost decreases are possible only by large, up-front investments.

6.1 *Reducing the project's overhead*

Historically, only a fraction of the cost of ICF laser systems such as Nova has been associated directly with purchase of the laser hardware. For example, the cost of laser hardware for Nova was about one third of total costs for the Nova Project. Project overhead costs also included research and technology development, system design, capitalization of production facilities, assembly labor, office and laboratory buildings, target facilities, contingency funds, and management. Several years of component development using programmatic operating funds preceded Nova construction.

Compared to Nova, a much higher fraction of the NIF project dollars must be spent on laser hardware. The funds for activities such as engineering design of the facility, design and prototype development of major subsystems, and capitalization of production facilities will have to come from operating funds or from special appropriations, *not* from project moneys.

6.2 *Increasing the performance of the laser*

The cost study reported in the **Laser Program Annual Report–1982** identified the power amplifier as the most expensive component—some 70% of the total laser hardware cost. Responding to that study, our attention has been focused on improving the amplifier's efficiency. Our success is marked by storage efficiency exceeding 3.5% and stored energy density of 250 joules per liter—a threefold improvement in efficiency over Nova. In a similar effort, we set out to improve the damage threshold of the optics, and succeeded by increasing their threshold by a factor of two to three. In 1984, after Nova came on line, we discovered that Nova's tripling efficiency was lower than expected. A year of scientific testing paid off by uncovering the source of the problem—a nonlinear induced rotation of the beam's polarization field. When our suggested solution was incorporated, the peak frequency conversion efficiency improved to some 80%. By such performance improvements, the total output energy has increased, making the overall cost decrease.

6.3 *Decreasing the system's complexity*

Experience with the construction of single pass MOPA system architectures has shown that the cost per unit energy output of the preamplifier portion of the system is disproportionately higher than for the power amplifiers. With multipass architectures, it is possible to eliminate the preamplifier components by using the power amplifiers themselves as a driver. Analysis suggests that multipass systems may be 25% more cost effective than conventional single pass MOPA systems—a result of eliminating preamplifier components (see **Laser Annual Report–1984**, p6-92). The

Beamlet laser will test this concept with a four-pass laser architecture that uses a large aperture (37 cm) high power switch. Despite other system improvements (over Nova) like higher damage thresholds, more efficient frequency conversion, and cost effective pulse generation, Beamlet is still too expensive to provide a cost basis for NIF without further component development. We hope that experience with Beamlet will guide us in steps for reducing system complexity.

6.4 *Reducing the cost of the individual components*

Improving performance and reducing complexity has a significant effect on cost, but the remaining challenge for attaining our cost goals is to reduce the basic cost of materials, fabrication, and assembly of all the separate components comprising the laser system. *More than a twofold reduction in unit costs compared to Beamlet is required to meet the cost goals of NIF.*

As detailed below, we have investigated cost reduction of individual components. But major effort must be exerted in the areas of mechanical, electrical and optical components so that the overall cost of NIF approaches target values.

6.5 *Basis for the cost of NIF's components*

Most of the development work during the last decade was directed towards improving the performance of the laser components. Although many performance improvements have been realized, the components are still too expensive. Today, the cost of laser hardware is the issue, not its performance. The basis for our costs lies in what technological improvements we can foster in manufacturing, finishing, and assembly. Credibility for our final cost projections will be based on how well we can trace the figures to actual Beamlet and Nova purchases.

LLNL laser systems have always been cost optimized to meet energy and power goals. Nova was optimized with technology available in the early 80's for pulses shorter than about 2 nsec. As Figure 6-1 shows, the Beamlet is designed to perform well at 3 nsec. Present day target designs call for a longer ignition target pulse so the NIF baseline laser system is optimized for 4.8 nsec pulses. Consequently, NIF should be capable of higher fluences than Beamlet at the longer pulse lengths.

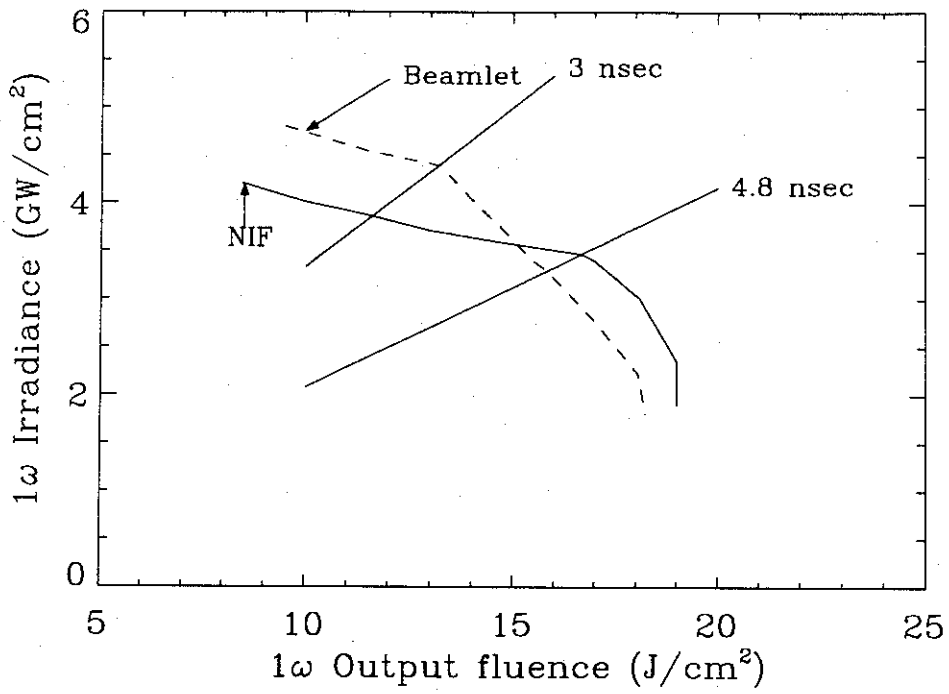

Figure 6-1 Irradiance versus fluence for Beamlet and NIF.

Figure 6-2 compares the one micron power versus energy available at the tripler from a single Nova beamline to Beamlet and the 35 cm hard aperture NIF baseline. The calculation used to generate this figure used a $39 \times 39\,\mathrm{cm}^2$ aperture for the Pockels cell switch—somewhat larger than the actual Beamlet PEPC switch installed initially. There is significant difference in cost of the laser hardware for each of these systems. In particular, compared to Beamlet, we'll need more than a twofold reduction in cost of the NIF laser hardware; compared to Nova, we'll need more than a six-fold reduction. Thus, we must identify a cost reduction path for each component, and then trace the cost to Nova and Beamlet. Our current understanding is that most of this cost reduction will follow from the use of new technologies in optical manufacturing.

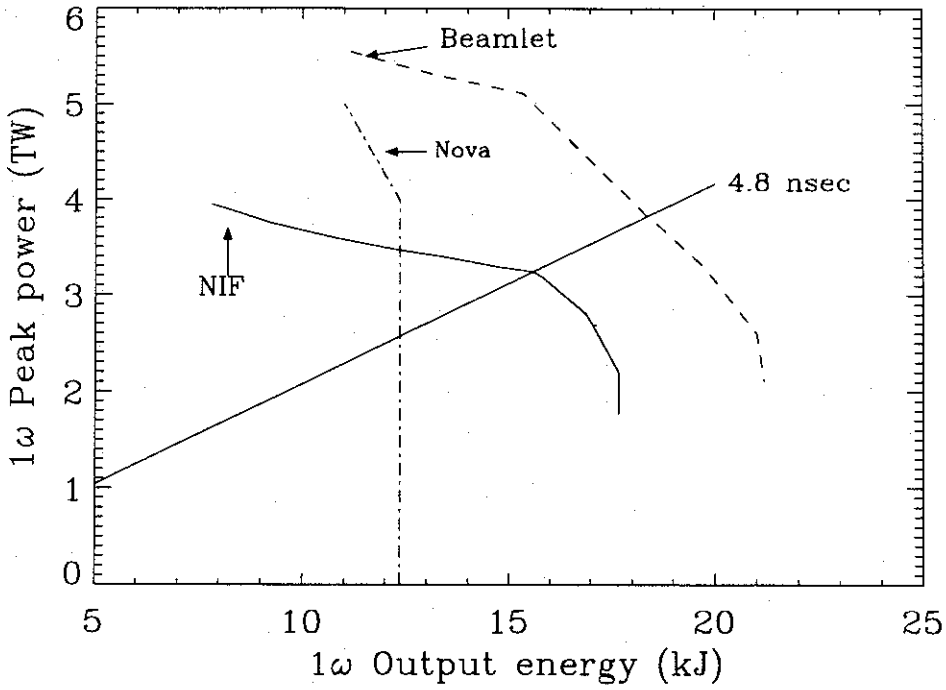

Figure 6-2 Power versus energy for three systems—Beamlet, a single Nova beamline, and an NIF beamlet. (See Table 5-1 for design assumptions.

Chapter 7

AMPLIFIER

The designs for NIF are based on multisegment amplifier architectures that achieve substantial cost savings by building the smallest number of large modules. The amplifier assembly, shown in Figure 7-1, consists of hardware required to provide laser gain—the laser medium itself, the mechanical assembly to hold it and the pumping lamp arrays, the flashlamps, the pulse power needed to drive the lamps, and any covers or shrouds required for protection.

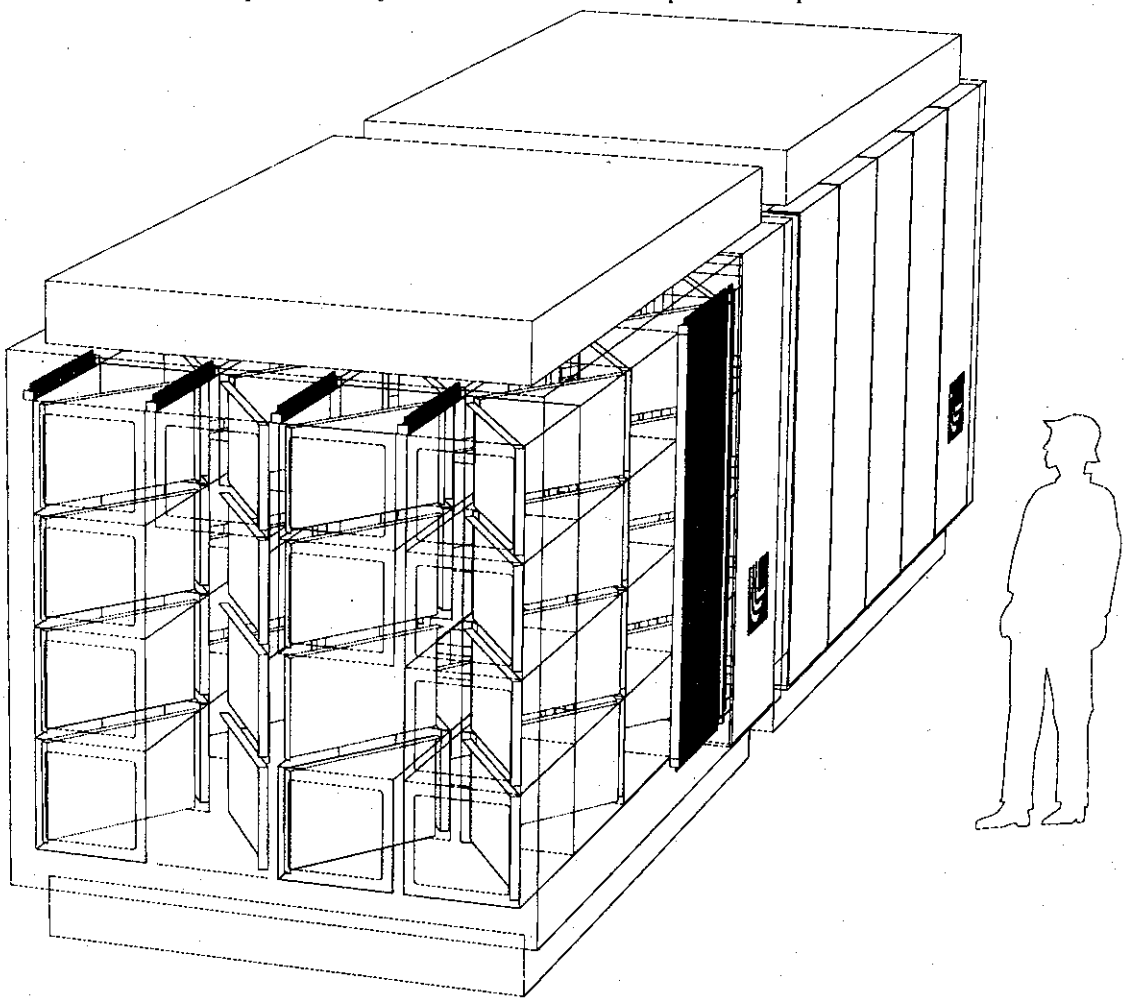

Figure 7-1 NIF amplifier.

In the following sections, we will be creating a cost basis for the NIF amplifier derived from the Beamlet Demonstration Project—a difficult procedure since we must somehow scale Beamlet's performance to NIF, and then make some assumptions on how the cost would scale as well. Table 7-1 compares the design features of the Beamlet amplifier to those of the NIF amplifier. Note that the two amplifiers are different in their specifications. Beamlet is a technology testbed for the NIF design—the latter may change because of experimental results obtained from Beamlet. For example, the deliberately-chosen large aperture for Beamlet will provide needed information on likely aperture sizes for NIF devices.

Table 7-1 Design parameters: Beamlet amplifier vs NIF amplifier.

	Beamlet	NIF
Pulse		
Energy	18.5 kJ (red)	4.5 MJ (red)
length	4.8 nsec	4.8 nsec
Slab Count	$11 + 0 + 5$	$11 + 5 + 3$
optical channels	1	288
total slab count	16	5472
Lamp pulse power	106 kJ/slab	53 kJ/slab
pulselength, τ	500 μsecs	360 μsecs
Flashlamps		
count	9 per slab	3 per slab
length	91 cm	162 cm
bore	2.5 cm	2.5 cm
explosion fraction	20%	20%
Glass		
volume	14.7 liters/slab	8.4 liters/slab
thickness	4 cm	3.2 cm
doping density	3.5×10^{20} Nd ions/cc	5.15×10^{20} Nd ions/cc
Mechanical		
Array	2×2	4×4
reflectors	flat side, no wedge between slabs	optimized side, wedge shape between slabs
vertical separation	6 cm	5 cm
other	energy between slabs is lost	reduced loss between slabs
Aperture	38.3 cm $\times$ 38.3 cm	35 cm $\times$ 35 cm
beam area	1168 cm^2	940 cm^2

The overall Beamlet amplifier hardware cost (labor not included) is \$77 per joule. Scaled to 4.5 MJ, this implies that the NIF amplifier could cost \$346M—more than the total NIF laser hardware budget allocation. Based on Beamlet, we've identified a cost reduction path for the NIF amplifier that should result in a projected hardware cost of \$153M.

7.1 *Glass Slab Cost*

The flexible design margin purposely built into Beamlet accounts for much of the difference in slab parameters between NIF and Beamlet. For example, Beamlet is using an amplifier slab with the largest clear aperture and pump volume that would be contemplated for any NIF design thereby allowing us to interpolate between data points for cost and performance projections for

the NIF amplifiers. Such an aperture permits relaxed alignment tolerances with greater vignetting losses during the activation phase, and can accommodate the wider beam offset caused by thicker disks. The thicker disks in Beamlet result from lower slab doping, and the pulse power system design is sized to produce 20% higher output energy at nominal tolerances.

Figure 7-2 compares particular system design parameters for Beamlet and NIF. A shorter pump pulse is used in the NIF design, which allows higher doping with Nd and decreased slab thickness. Thus, we obtain an equal energy/cm^2 for less glass. There is always the possibility that the lowered cost of less glass will be offset by the potential increase in cost of the pulsed power system; however, our current projections favor shorter pump pulses.

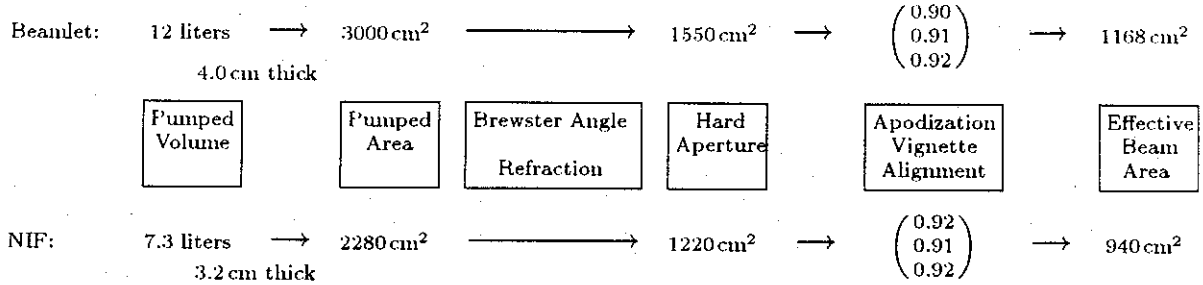

Figure 7-2 Glass considerations.

One must do more than change the cavity and slab design to meet NIF's cost goal for the amplifier slab. A Beamlet slab costs \$49K, but at sizes required for NIF, the current price is \$37K. If the same pouring and finishing technology were used for the 5472 slabs in NIF, the total slab cost would amount to \$202M. A cost reduction program for the slabs has been proposed that will reduce the cost per slab from \$37,000 to \$11,300. Development of new fabrication technologies and the capitalization of two manufacturers to produce the slabs would reduce the project cost by \$141M: i.e., the cost charged against the NIF project would be \$62M, not \$203M. Figure 7-3 summarizes the cost reduction path for the NIF amplifier slabs and the cost reduction monies needed to achieve it.

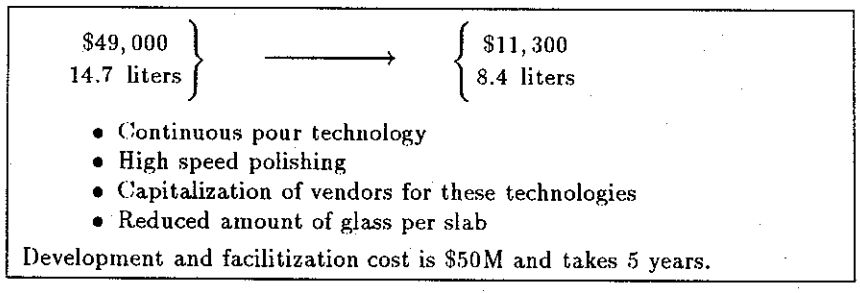

Figure 7-3 Cost reduction path for the NIF amplifier slabs and cost reduction program needed to implement it.

Based on this reduction path, we can compare the cost per joule for Beamlet amplifier slabs and NIF slabs:

Slab Comparison

$$\textbf{Beamlet}: \quad \frac{16\,\text{slabs} \times \$49,000\ \text{per slab}}{18,500\,\text{J}} \approx \$42\ \text{per joule}$$

$$\textbf{NIF}: \quad \frac{5472\,\text{slabs} \times \$11,300\ \text{per slab}}{4.5\,\text{MJ}} \approx \$14\ \text{per joule}$$

7.2 *Pulse Power System Cost*

The pulse power hardware for the Beamlet amplifier costs \$18 per red joule. Scaled to the 4.5 MJ design for NIF results in \$81M. However, simple scaling is not appropriate since the NIF amplifier has been optimized at a different optical pulse length and contains different size amplifier slabs. Optimization of the pump cavity for smaller slabs and longer laser pulses changes the slab count per optical channel from 16 to 19, raises the one micron fluence from 15.8 J/cm^2 to 16.7 J/cm^2 (See Figure 6-2) and decreases the pump energy per slab from 106 kJ to 53 kJ. These actions represent a 1.42 reduction factor in cost per red optical joule for the pulse power system. Improvements in the amplifier efficiency for NIF depend on clarifying the gain uniformity/efficiency trade off—a task expected to require additional development effort.

The electrical bank design for Beamlet is flexible, but conservative. Flexibility was incorporated to accommodate any changes to the amplifier for testing a wide range of operating conditions. For example, it will allow testing flashlamps above 20% of their explosion fraction for achieving higher gain; or additional lamps may be added to improve gain uniformity.

An aggressive development program for the NIF amplifier will quantify performance risks—permitting an aggressive bank design and reducing any need for flexibility. For example, NIF uses monolithic bank modules, switches larger amounts of electrical energy and operates flashlamps in parallel, not series. Estimates show that this new bank design can reduce the cost per electrical joule delivered to the flashlamps from \$0.20 to \$0.125—a multiplicative cost reduction factor of 1.6.

Such cost reduction provides us with the following comparison for pulse power systems:

Pulse Power Comparison

$$\textbf{Beamlet} : \quad \frac{16\,\text{slabs} \times 106\,\text{kJ/slab} \times \$0.20/\text{J}}{18,500\,\text{J}} \approx \$18 \text{ per joule}$$

$$\textbf{NIF} : \quad \frac{5472\,\text{slabs} \times 53\,\text{kJ/slab} \times \$0.125/\text{J}}{4.5\,\text{MJ}} \approx \$8 \text{ per joule}$$

The last equation provides an overall estimate of \$36M for NIF's pulse power system.

7.3 *Flashlamp Costs*

The cost of flashlamps for Beamlet's pumping is \$5 per joule. Reducing the design margin in NIF means that fewer lamps are used in the new pump cavity design. Currently, there is only a single vendor for flashlamps—we will need to qualify another vendor to ensure competition in the market and keep the fixed costs per lamp from increasing.

Past experience shows that the primary issue for the lamps is their reliability. New concepts for flashlamp cassettes have been suggested and we need proactive consultation with all potential vendors to seek low cost solutions. We will need an inexpensive quality assurance program to guarantee the reliability of all the flashlamps.

With only moderate improvement, the following equations are the basis for projecting flashlamp cost for the NIF amplifier:

Flashlamp Comparison

$$\textbf{Beamlet} : \quad \frac{16\,\text{slabs} \times 9\,\text{lamps/slab} \times \$700/\text{lamp}}{18,500\,\text{J}} \approx \$5 \text{ per joule}$$

$$\textbf{NIF} : \quad \frac{5472\,\text{slabs} \times 3\,\text{lamps/slab} \times \$800/\text{lamp}}{4.5\,\text{MJ}} \approx \$3 \text{ per joule}$$

(Note: We've used comparable length lamps for Beamlet's cavity to simplify the cost comparison.) The reduced cost per red joule is mostly the result of optimizing the pump cavity for shorter pump pulses and using smaller slabs and longer lamps.

7.4 *Mechanical Assembly Cost*

The cost of Beamlet's mechanical hardware per slab is \$13,500. Figure 7-4 shows cost parameterization of the mechanical hardware per slab for the NIF amplifier as a function of the slab grouping. This figure shows how the cost decreases as the number of slabs in the group increases; i.e., the larger groupings require less hardware.

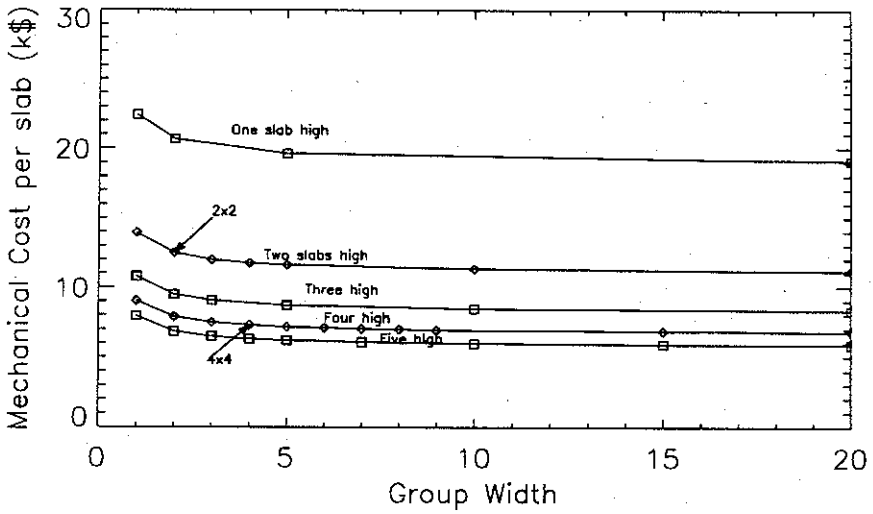

Figure 7-4 Cost parameterization of the mechanical hardware per slab for the NIF amplifier as a function of slab grouping. Assumptions: No flashlamps, No slabs, Includes connectors, does not include side losses, Jan/93 dollars.

According to Figure 7-4 , the mechanical cost for a 4×4 grouping of slabs for the NIF amplifier is \$7300 per slab Comparing mechanical costs against Beamlet:

Mechanical Comparison

$$\textbf{Beamlet} : \quad \frac{16\,\text{slabs} \times \$13,500\ \text{per slab}}{18,500\,\text{J}} \approx \$12\ \text{per joule}$$

$$\textbf{NIF} : \quad \frac{5472\,\text{slabs} \times \$7300\ \text{per slab}}{4.5\,\text{MJ}} \approx \$9\ \text{per joule}$$

7.5 *Amplifier Cost Summary*

By adding the costs for glass, pulse power, flashlamp, and mechanical projected in the preceeding analysis, a reasonable cost goal for the amplifier hardare is \$34 per red joule delivered to the tripler. Achieving this goal will require aggressive cost reduction and component development programs. We've traded-off the amplifier's gain uniformity for improved efficiency and higher energy storage. This will require pre-apodizing the beam to compensate for the gain nonuniformity. Indeed, a cost penalty was paid in the pulse power and flashlamps to obtain the desired gain uniformity in the Beamlet amplifier. We simply cannot afford this added cost for the NIF amplifier—a tradeoff requiring careful analysis which we are still studying.

The amplifier hardware cost goals for NIF are summarized in Table 7-2, which also shows amplifier costs for Nova[1] and Beamlet. The laser hardware cost divided by the number of red joules delivered to the tripler is the figure of merit used to compare systems.

[1] G. J. Suski, *Nova as-built cost analysis,* LLNL ICF internal memorandum, 31 July 1985.

Table 7-2 Cost comparison of the Amplifier hardware for Nova, Beamlet, and NIF. Units are $ per red joule delivered to tripler.

System	1982 Nova Cost	Actual Beamlet Cost	Projected Beamlet after reducing glass and pulse power costs	Projected NIF Cost
Pulse Power	$87	$18	$12	$8
Glass	$76	$42	$21	$14
Flashlamps	—	$5	$5	$3
Mechanical Assembly	$41	$12	$12	$9
Total:	$204	$77	$50	$34

Most of the cost reduction can be attributed to cheaper amplifier slabs and cheaper pulse power. The remaining reduction comes from an improved, but more risky, amplifier design and a larger number of beamlets per grouping.

Given a successful component development effort, the amplifier cost is estimated at $4.5\,\mathrm{MJ} \times 34\,\$/J \approx \$153\,\mathrm{M}$. Note, this does not include labor costs to assemble.

7.6 *Component development strategy*

We estimate that the development of the NIF amplifiers will take a minimum of 3.5 years to complete. This level of effort will be required in order to achieve a more cost-effective design and to ensure that the NIF amplifiers meet all performance requirements. The proposed development program has four major areas, each of which are discussed below: 1) pump cavity design, 2) flashlamps, 3) fixturing for assembly and maintenance, and 4) design, construction, and testing a NIF prototype amplifier. The schedule for the proposed amplifier development program is shown below:

NIF Component Development Schedule—Power Amplifiers

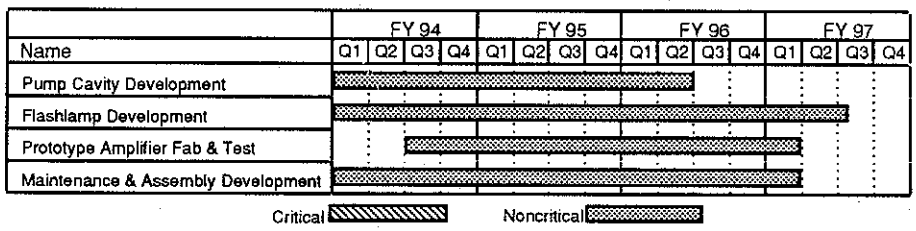

Table 7-3 Amplifier development schedule

7.6.1 *Pump cavity design*

The most cost-effective pump-cavity design for the NIF system will reflect tradeoffs between requirements, some of which conflict—high cavity transfer efficiency, good gain uniformity, low pump-induced wavefront distortion, strength and stability of the mechanical design, improved access to parts to reduce maintenance costs. The balance between these requirements must be determined through a process of optimization that takes into account the cost and performance of the entire laser system.

The parameter having the greatest leverage on system costs is cavity transfer efficiency. Cavity transfer efficiency is used in our amplifier gain model[1] to characterize the transfer of light from the flashlamps to the laser slabs. Cavity transfer efficiency depends on nearly all aspects of pump cavity design—reflector shapes, compactness, number of flashlamps, electrical power delivered to the flashlamps, optical transmission through the flashlamp envelopes, transmission through the blast shields and through slab surfaces. As cavity transfer efficiency increases, stored energy density increases and fewer slabs are needed to provide the necessary gain. CHAINOP modeling predicts that for every 1% increase in cavity transfer efficiency, overall hardware costs for NIF decrease by about 0.67%.[2]

Gain of sufficient spatial uniformity will be required. Gain variations reduce the damage-limited output energy by causing spatial amplitude variations in the beam. However, our previous experience testing multisegment amplifiers has shown a strong tradeoff between good gain uniformity and high cavity transfer efficiency. We anticipate that the NIF laser will use an apodizing filter to convert the input intensity profile into a shape that compensates for the gain variations. With such a filter, it should be possible to relax the gain uniformity requirement so that a higher cavity transfer efficiency can be obtained.

Good mechanical stability and improved access to parts will also be important. These requirements may conflict with high cavity transfer efficiency, especially if the mechanical design affects the reflector shapes or compactness of the pump cavity.

We propose to undertake a three-stage development program to resolve tradeoff issues and to develop a cost-effective pump-cavity design.

In the first stage, new pump cavity designs will be developed and evaluated by modeling. These pump cavity designs must be consistent with the overall amplifier mechanical design. It will be important to evaluate all promising methods for improving cavity transfer efficiency. Some examples are:

- Make the pump cavity design more compact.
- Change the shapes of reflectors in the side and central flashlamp arrays.
- Use wedge-shaped reflectors on the slab holders to reflect more pump light onto the slabs.
- Use anti-reflective coatings on the flashlamps, blast shields, and laser slabs.
- Reduce the lamp packing fraction.

Ray trace models and finite element codes will be used to predict cavity transfer efficiency, gain uniformity, pump-induced wavefront distortions, and pump-induced depolarization. The predictions must be made for all four different types of apertures that occur in multisegment amplifiers with 3×3 or larger groupings. The figure-of-merit for each possible pump cavity design will be the system cost per joule, as determined by the CHAINOP code.

In the second stage, the most cost-effective pump cavity designs will be tested in the Beamlet prototype amplifier, a one-slab-long 2×2 multisegment amplifier. Testing will consist of gain and beam-steering measurements, made with flat silver reflectors placed over the ends of the amplifier to simulate adjacent one-slab-long modules. Both flashlamp energy and pulselengths will be varied.

In the third stage, the results of the second-stage experiments will be used to update the models. New pump cavity designs will be developed and evaluated with the updated models. Again, the most promising pump cavity designs will be tested in the Beamlet prototype amplifier. Two or three iterations between modeling and experiments should be sufficient for developing a cost-effective pump cavity design that meets all performance requirements.

---

[1] H. T. Powell, A. C. Erlandson, K. S. Jancaitis, and J. E. Murray, *Flashlamp Pumping of Nd:Glass Disk Amplifiers*, SPIE Proceedings Vol. 1277, High-Power Solid State Lasers and Applications, pp. 103-120 (1990).

[2] J. B. Trenholme, *What are the best laser glass parameters?*, LLNL ICF internal memorandum LT-014, June 2, 1993.

7.6.2 *Flashlamps*

The NIF flashlamps must operate reliably. Both catastrophic failures (explosions) and non-catastrophic failures (failure to trigger) and their effects on maintenance cost and downtime are of concern. Every catastrophic failure has the potential to cause thousands of dollars of damage. Unreplaced lamps that fail non-catastrophically will reduce gain, increase gain variations, and increase pump-induced wavefront distortions. To ensure that the NIF flashlamps operate reliably, we plan to perform a series of flashlamp lifetime tests. Depending on the test results, the flashlamp design will be modified, the quality controls will be improved, or the operating point will be adjusted. Generally, flashlamp failure rates increase when the electrical input energy is increased, or when flashlamps are operated in pump cavities that return light to the plasma.

In the first series of tests, flashlamp lifetimes will be measured at different electrical input energies. These tests will be performed in a pump cavity at the pulselengths that give the most cost-effective performance for NIF. These tests will determine the maximum electrical input energy for reliable operation over the expected lifetime of NIF. We anticipate that existing Beamlet lamps will be used so that the tests can be performed as soon as possible. The test results could affect the point design for the NIF laser.

The second series of tests concern a small number of prototype NIF flashlamps (five-to-ten) from several vendors. These tests will uncover lamp designs with serious problems and give manufacturers an opportunity to correct deficiencies.

In the third series of tests, lifetime measurements will be performed on larger numbers of prototype NIF flashlamps (20 to 30) from each vendor. This will improve failure statistics. In order to qualify for the next stage of testing, manufacturers must submit to audits of their quality control procedures, and their lamps must meet minimum reliability requirements.

In the fourth and final series of tests, lifetime tests will be performed on 100-200 prototype NIF flashlamps from each vendor. Minimum reliability requirements must be met in order for manufacturers to qualify to bid on the NIF flashlamp contracts.

7.6.3 *Fixturing for assembly and maintenance*

Fixturing needs to be developed for the assembly and maintenance of the NIF amplifiers. The design of this fixturing will depend on the maintenance strategy for the amplifiers, which is being developed. However, for the starting-point NIF design, in which 4×4 amplifiers are assembled in modular units that are 1 slab wide $\times$ 4 slabs high $\times$ n slabs long, where n is 1, 3, or 5, the following hardware will be required: a machine for washing all amplifier parts in detergent and water; fixturing for transporting amplifier parts, such as slabs, blast shields, slab holders, and lamp cassettes, through the washing machine; fixturing for assembling the parts efficiently; and carts for transporting the modular units to the laser bay. We plan to test this fixturing during the assembly and maintenance of the prototype amplifier.

7.6.4 *Design, construct, and test a prototype amplifier*

To ensure that the engineering and physics design of the NIF amplifiers is sound, and that the NIF amplifiers will meet all their performance requirements, it will be necessary to build and test a prototype NIF amplifier.

For the starting-point design, the prototype amplifier will be 4 slabs wide $\times$ 4 slabs high $\times$ 5 slabs long. This is the minimum size that will fully test assembly and maintenance techniques. This size is sufficient to test the physics performance.

To reduce costs, the prototype amplifier will use the Beamlet pulsed power system. The pulsed power system will be modified so that the flashlamp energy and pulselength will have the same

values as will be used on NIF.

Gain and beam steering measurements will be performed in all four different types of apertures in the NIF 4 × 4 prototype amplifier. For the first time, it will be possible to measure gain distributions for slabs that are pumped by central flashlamp arrays on both side.

We expect that after the first round of gain and beam steering tests, the pump cavity of the prototype amplifier will be modified for a second series of tests.

Chapter 8

OPTICAL SWITCH

Laser system design studies carried out at LLNL from the early 80's to the present day have consistently agreed that there is a 20 to 30% savings when using a multi-pass amplifier architecture instead of a simple MOPA.[1] One major advance in the design of the NIF is its use of a multi-pass power amplifier which requires an optical switch to extract the high-energy infrared laser pulse from the multi-pass cavity once the appropriate fluence has been reached.

The optical switch in the baseline NIF design is based on a Plasma-Electrode Pockels Cell, (PEPC). Any Pockels cell relies on the first-order electro-optic effect whereby the refractive index of a transparent material (typically a potassium di-deuterium phosphate or KD*P crystal) is altered by an applied electric field. If this applied field has the correct magnitude and direction, the crystal will exhibit an induced birefringence sufficient to rotate the polarization of an incident light wave by 90°. When used with a linearly polarized input beam and a linear polarizer, the PEPC forms an optical switch capable of diverting large aperture, high-energy laser pulses. The voltage required to rotate the polarization of light transiting the cell by 90° is known as the half-wave voltage, V_π which is approximately 8kV for fully deuterated KDP. In most commercially available Pockels cells, V_π is applied across the crystal by ring electrodes around the crystal's optical aperture or by thin-film conductors of metal deposited directly on the crystal faces. The large beam aperture and high-fluence specified for the switches in NIF make both of these methods impractical.

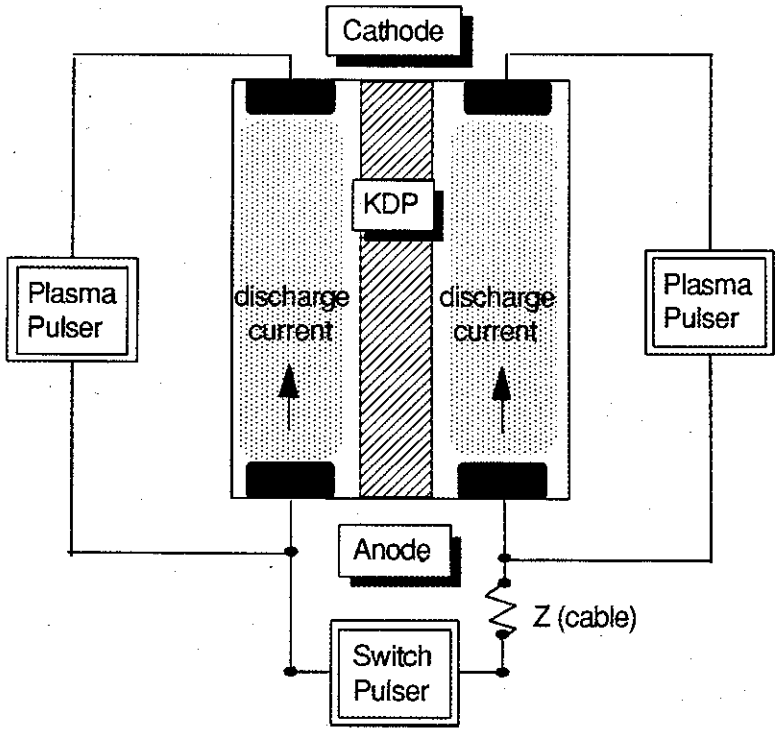

Figure 8-1 Cross sectional view of a PEPC showing the configuration of the external pulse generator circuits.

[1] **Laser Annual Report–1984**, p6-92.

In a Plasma Electrode Pockels Cell, plasma discharges are formed on each side of the crystal. Since these plasmas are highly-conductive ionized gas, they can act as transparent electrodes allowing the uniform application of the half-wave voltage from the switch-pulse generator as shown in Figure 8-1 . The operation of the PEPC is as follows. The interior of the cell is maintained at high-vacuum by a turbo-molecular pumping system. Working gas (typically helium + 1% O_2 at 20-50 mTorr) is bled in by a gas control system. Operating pressure is maintained by balancing the gas input flow against the pump speed. Plasma discharges are initiated between anodes and cathodes on either side of the crystalline plate by capacitor discharge. Just after the peak of this 6 μsec, 2 kA plasma pulse, a rectangular voltage pulse is applied across the two anodes by the switching-pulse generator schematically pictured in Figure 8-2 thus charging the crystal to its half-wave voltage of 8 kV for KD*P.

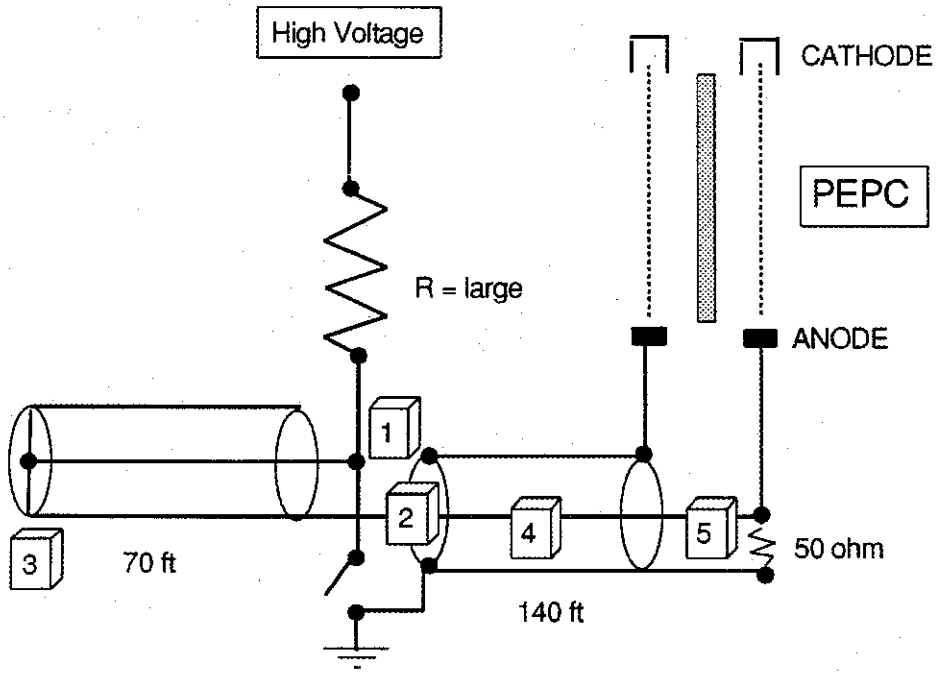

Figure 8-2 Switch-pulse generator for PEPC. At $t = 0^-$, a coaxial pulse forming network (PFN) is charged to $+V$ at ① At $t = 0^+$, ① is pulled to ground by a thyratron closing switch; ② goes to $-V/2$ and a negative going voltage wave of magnitude $-V/2$ is launched back into the PFN towards ③. At $t = 100$ nsec, the leading edge of this negative going wave reaches ③ and doubles and changes polarity as it reflects off the open circuit. At $t = 200$ nsec this wave reaches ② ending the pulse launched into the output line. At $t = 200$ nsec the leading edge of the output pulse reaches ⑤ and starts to charge the capacitance of the KDP crystal to $-V/2$. The 50Ω termination minimizes voltage reflections back down the output line. At $t = 400$ nsec the voltage at ⑤ goes back to 0 (end of pulse) and the crystal starts to discharge into the parallel combination of the output line impedance and the resistive termination. At $t = 600$ nsec the crystal is fully discharge and the switching cycle is completed.

Building on earlier work at LLNL by Goldhar et al., a 32 cm aperture Beamlet Demonstration Project's prototype PEPC was tested during FY'92. This switch exhibits better than 99.9% efficient switching over the full aperture with rise and fall times less than 100 nsec, and an on time of 50 nsec.

FY'93 has seen the start of construction of the Beamlet PEPC which will have a slightly larger aperture, 37 cm, and the same switching characteristics.

8.1 *Specifications*

Between 192 and 288 PEPC-polarizer switch assemblies, one for each beamlet, must be provided for NIF with the following specifications:

- Clear aperture: 36×36 cm
- Crystal surface flatness: $< \lambda/8$ for 99% of area, Ripple spec 1/70 wave
- Switching efficiency: $> 99\%$
- KD*P absorption: < 0.02 per cm
- Voltage induced depolarization: $< 2\%$
- Risetime & duration: < 100 ns rise; 50 ns top
- Repetition rate: 0.2 Hz

8.2 *Basis of Estimate for NIF switch costing*

NIF switch subsystems, exclusive of assembly labor costs, should be obtainable for about \$9.89 per red optical joule at the tripler based on the proposed cost reduction effort outlined in Section 8.5. Table 8-1 compares Beamlet costs to projected NIF PEPC costs.

Table 8-1 Cost comparison between Beamlet and NIF's PEPC. Units are \$ per red joule delivered to the tripler.

System	**Actual Beamlet Cost**	**Projected NIF Cost**
KD*P Plates	3.78	1.77
Polarizer	2.34	1.43
Mechanical Assembly		
Pockels Cell	3.60	1.96
Polarizer mount	0.65	0.54
Windows	1.45	1.00
Pulser		
Plasma driver	1.06	0.65
Switching pulser	1.09	0.71
Controls	4.41	1.83
Total:	\$18.38	\$9.89

The method used to reduce these data to dollars per red optical joule is:

PEPC Comparison

$$\textbf{Beamlet}: \quad \frac{(1 \text{ KD*P cell} + 1 \text{ polarizers}) \text{ @ } \$340,000}{18,500\,\text{J}} \approx \$18.40 \text{ per joule}$$

$$\textbf{NIF}: \quad \frac{(4,\ 1\times 2\text{–KD*P cells} + 8 \text{ polarizers}) \text{ @ } \$1.24\text{M}}{8 \times 15,625\,\text{J}} \approx \$9.89 \text{ per joule}$$

8.3 *Laser System architectural constraints driven by the PEPC Switch*

This section outlines some of the design constraints imposed by PEPC switch assemblies. The PEPC subsystem primarily affects one beamline dimension; e.g., width. If the current 4 cell design is possible, one might orient these cells vertically making this PEPC constraint largely redundant with the limit imposed by flashlamp length. Another space saving alternative is to offset pairs of 2×4 assemblies axially, overlapping anode structures in the gap between beamlets.

The wavefront distortion and scattering specifications to be met by the switch are:

- Polarizers and windows are lap polished and must meet $< \lambda/8$ for 99% of area.
- KD*P is diamond turned and in addition may require a light polish to reduce scatter.

Vertical mounting of the polarizer assembly is possible and may result in cost savings. This choice of polarizer orientation costs additional turning mirrors and makes the pointing of the switch crystal more critical. It must be traded against polarizer sag and the cost/risk associated with thick, potentially damage prone, polarizer substrates.

Figure 8-3 shows how one may nest beamlets and route beams around polarizer assemblies so that the architectural distinction between switching out in reflection (always more desirable from the laser designer's point of view) and switching out in transmission (always more desirable from the facility designer's point of view) may be eliminated; however, such a configuration adds mirrors that must be included in the cost.

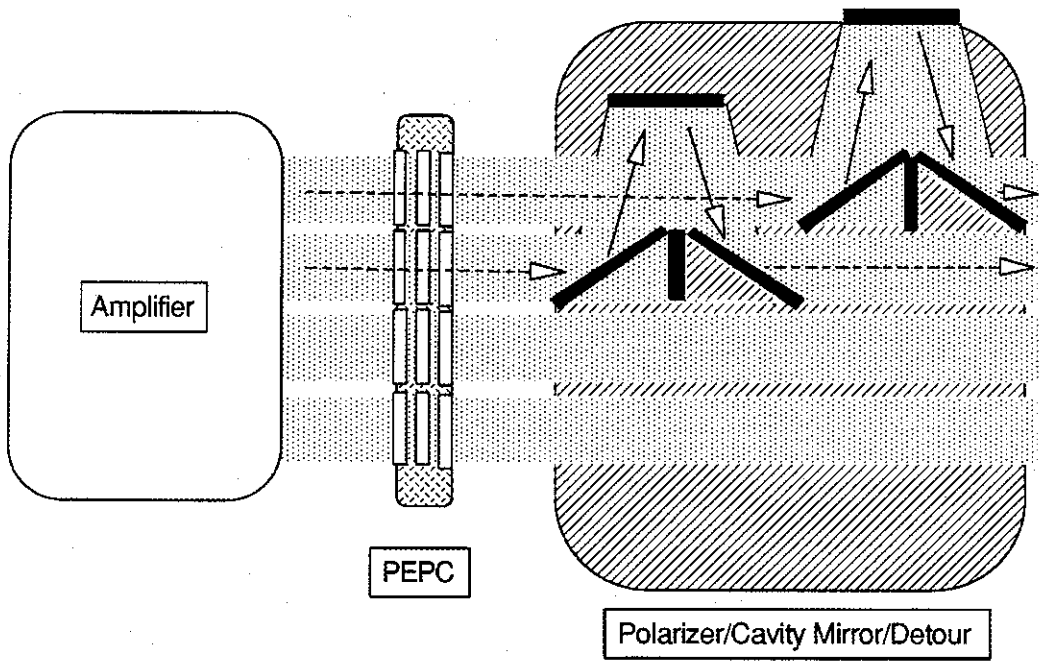

Figure 8-3 Routing beams around polarizer assemblies.

Finally, integration of the switch with the spatial filter would save a window and some mechanical hardware, but restrict the system to two rather than three amplifier blocks.

8.4 *Optical switch design for the NIF*

While much of the optical switch technology developed for Beamlet is directly applicable to the

NIF, the 1×1 switch module used in Beamlet must be extended to 4×4 in order to match the other optical components in the amplifier cavity. A 4×4 switch assembly is shown in Figure 8-4.

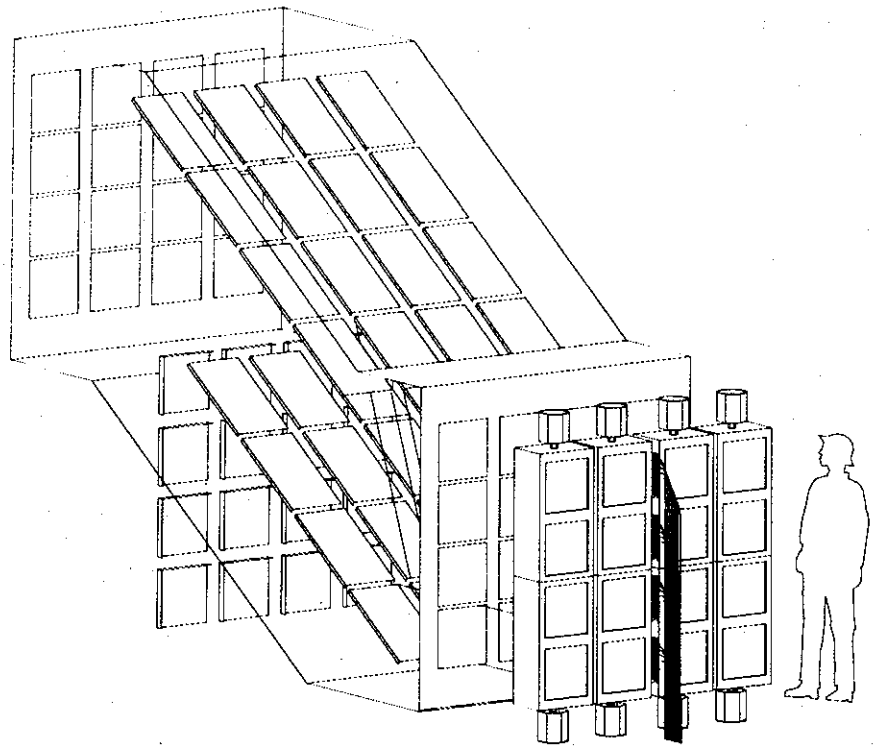

Figure 8-4 NIF Optical switch assembly.

This 4×4 assembly will be made up of 1×2 modules—a significant extension of the Beamlet switch technology. A 1×2 switch module is shown in Figure 8-5.

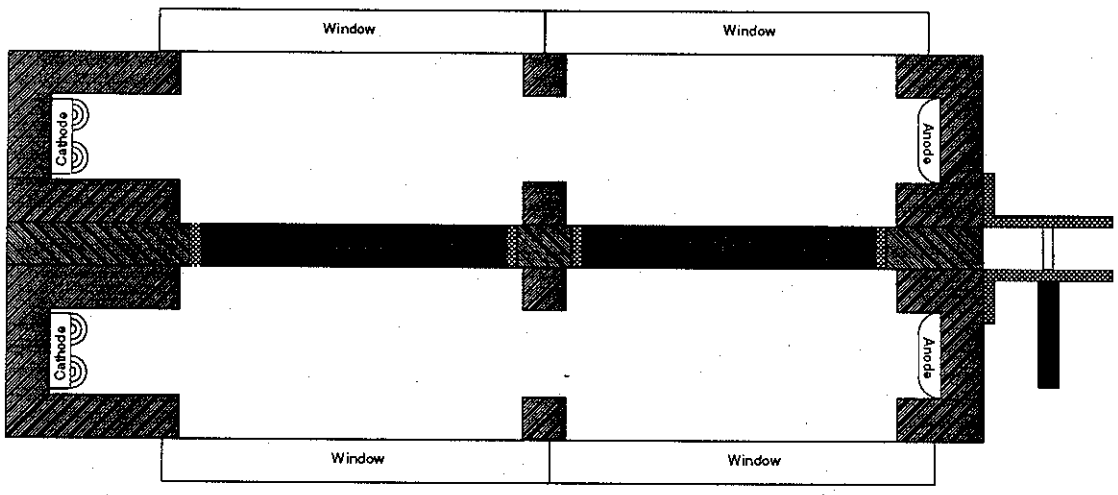

Figure 8-5 PEPC 1×2 sub-assembly.

Details of how the 1×1 Beamlet technology will be developed into 4×4 NIF technology is described in the next section. The pulser technology used for NIF will be essentially the same as

for Beamlet. The plasma discharge will be capacitive, i.e., the temporal shape of the plasma current pulse will be determined by the storage capacitor in the plasma generator and the inductance of the cable that delivers the pulse to the switch. The discharge resistance together with a small resistor inside the discharge supply insure that the current waveform is over damped. The circuit constants in the Beamlet plasma pulser provide a current pulse that reaches its peak value in about 6 microseconds. Since the NIF plasma pulser will have to fill a volume at least twice as large as the Beamlet switch, we may have to modify some of the operating parameters experimentally. These will include operating pressure, simmer current, and time constant of the plasma pulse. The operating pressure and simmer current must be adjusted to provide jitter-free breakdown. If we find that we need a longer duration current pulse to uniformly fill a 1×2 module, we will achieve this by using a larger storage capacitor. A factor of 4 increase in capacitance will yield a factor of 2 increase in pulse duration.

The NIF switch-pulse generator will use the same basic technology as in Beamlet. Pulse forming networks comprised of lengths of charged coaxial cable will be switched with high performance thyratrons into output lines comprised of coaxial cable. The exact length of the PFN and output cables is determined by the optical cavity length and the relative position of the switch within the cavity. The cable lengths will be set after the cavity layout design is finalized

The vacuum system for the NIF switch will be somewhat different than for Beamlet. Since the switch aperture will be arrayed in a 4×4 configuration, it will not be possible to directly pump each cell. Referring to Figure 8-4 we see that it will be possible to mount pumps along the top and bottom of the 4×4 assembly. The interior cell will be pumped by coupling apertures leading to the outer cells. The background pressure in the interior cells will therefore be somewhat higher than the outer cells. The sensitivity of switching performance to base pressure and the exact design of the vacuum system will be determined as part of the component development plan.

8.5 *PEPC component development strategy*

A schedule for NIF switch development is shown in Table 8-2. The major development tasks are: metal housing evaluation, extension to a 1×2 module, extension to a 1×4 module, and finally, construction of a 4×4 prototype. After proper testing, this last could become part of the first NIF beamline. Necessary support tasks include pulser engineering, plasma modeling, and design of a large lens for testing switch modules at full aperture.

8.5.1 *Metal Housing Evaluation*

The switch development program must resolve issues relating to the basic construction of the switch. Previous switches, including those constructed for Beamlet, have used Ultra-High-Molecular-Weight (UHMW) polyethylene as housings for the crystal. This UHMW polyethylene is a low-cost, electrically insulating material, with a low vacuum outgassing rate. Since pairs of electrodes spanning the crystal surface are mounted inside the housing, the plastic insulation guarantees against any electrical short. Though inexpensive, UHMW is difficult to machine to close tolerance and tends to creep under vacuum load. Other plastics that are easier to machine have poor vacuum outgassing rates. Other insulators such as ceramics or cast glass are either expensive, difficult to obtain in large sizes or are difficult to machine. We will continue to explore different low cost insulating materials during the component development program.

We have proposed making housings out of metal (aluminum or stainless steel), such that the entire housing acts as the electrical anode with the cathode mounted inside an insulating bucket. Such a housing would be easy to machine to close tolerances, would have reasonable material cost, and could be made smaller due to material strength. Switching performance may improve since the larger surface area anode surrounds the crystal. The critical technical issue to be assessed is the

uniformity of plasma discharge in this configuration, and the corresponding electric field uniformity across the PEPC optical aperture.

NIF Component Development Schedule—Pockel's Cell

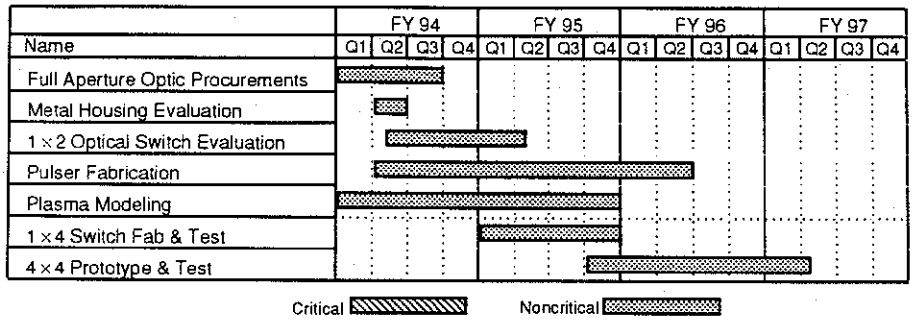

Table 8-2 Switch development schedule.

8.5.2 *Extension to a* 1 × 2 *Module*

Once the type of housing (metal or dielectric) is selected, a prototype 1 × 2 module must be developed. This configuration is the minimum that enables matching the horizontal and vertical inter-beamlet spacing posed by the cavity amplifier. In this module, the plasma discharge will cover two crystals, so the development program must solve any uniformity problems. Also, in the 1 × 2 module, a single switch-pulser is used to charge two crystals which may have slightly different half-wave voltages due to internal strain. The development program must demonstrate that the two crystals are sufficiently matched so they can be switched with a single pulser and meet the specified switching efficiency.

8.5.3 *Extension to a* 1 × 4 *Module*

The next step toward a 4 × 4 switch will be extending the 1 × 2 module to a 1 × 4 module. The 1 × 4 module will actually function electrically as two separate 1 × 2 modules. The design goal will be to design the 1 × 4 as a building block for the 4 × 4 so that we will be able to build the 4 × 4 by adding three more 1 × 4 modules. Demonstration of a 1 × 4 switch will be a good intermediate step since it will require simultaneous operation of separate electrical systems. It will also unearth any problems that must be overcome to achieve 4-way crystal matching.

8.5.4 4 × 4 *Switch Prototype*

The final step in the switch development plan is to demonstrate a 4 × 4 switch array. A full-scale prototype will be designed, fabricated, and tested to confirm performance capabilities and engineering design. Testing will be performed in off-line laboratories and possibly in the Beamlet Demonstration Project.

8.5.5 *Support Activities*

There will be three main support activities in the switch development program. These are pulser engineering, plasma modeling, and design of a large test optic. While we foresee no major changes in the pulser technology for the NIF, the development program will afford the opportunity to further refine the pulser designs with the goal of reducing cost.

Some of the issues concerning the uniformity of the plasma discharge can be answered more efficiently with modeling than with experiment. While plasma modeling was not explicitly part of the Beamlet switch development program, it will be an important part of the NIF program, and will compliment experimental efforts.

Chapter 9

PULSED POWER

9.1 *System design/requirements*

The pulsed power system includes the capacitor bank and associated hardware and controls to operate the main cavity and booster amplifiers for the NIF. This includes the ac power substation, charging supplies, capacitor bank, switches and power transmission to the flashlamps (Figure 9-1). The flashlamps themselves are covered in Amplifier, Chapter 7. Low-level controls for the individual bank modules are also included. Control hardware and software to integrate the modules is reported in Integrated Controls, Chapter 14.

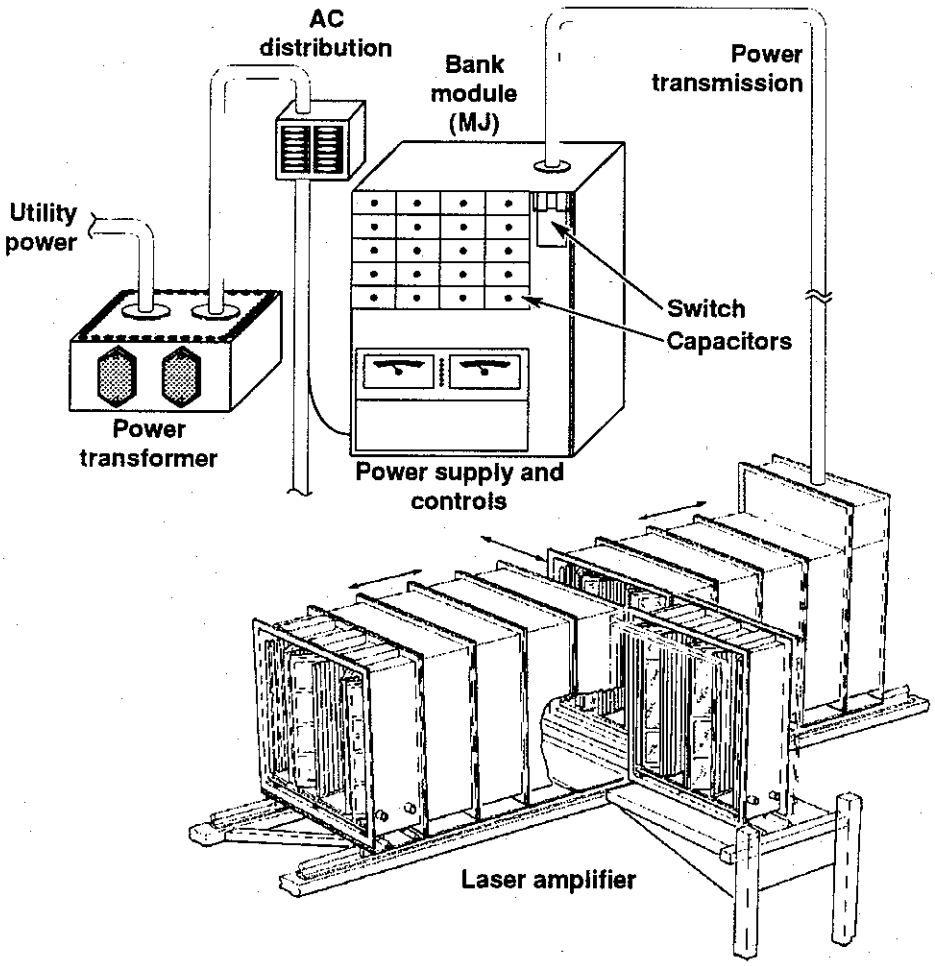

Figure 9-1 Pulsed power system architecture block diagram.

Table 9-1 Top level System Requirements (WBS 3.4).

Item	Requirement	Reason	Comment
Max. Delivered energy per cm^2 of lamp bore	14 J	To drive lamps at 0.20 explosion fraction	
current pulse width $(3(LC)^{.5})$	360 μs	optimum amplifier efficiency	
system lifetime	10,000 shots	consistent with 10 years operation at 3 shots/day	# of shots before capacitors degrade by 5%
flashlamp preionization energy	0.3 J/cm^2 of lamp bore area		
preionization pulse-length	100 $\pm$20 μs		
preionization delay	$0 - 400$ μs adjustable		
lamp diagnostics	gated peak current measurement for each flashlamp	to diagnose failed lamps and circuit faults	
current measurement	accuracy: $\pm$2% repeatability: $\pm$1%	to detect failed capacitors	
energy repeatability, shot-to-shot	TBD	amplifier performance	
energy uniformity, lamp-to-lamp	TBD	amplifier performance	

Table 4-1 summarizes the top level pulsed power system requirements for the baseline NIF design. The stored energy is found from $E_p * N * T$, where E_p is the required flashlamp pump energy per slab, from the amplifier cavity model, N is the total number of slabs, and T is the bank-to-lamp transfer efficiency. The values for the 250 MJ minimum credible NIF design are 53 kJ/slab, 3648 slabs (192 beamlets) and 85%. The flashlamp explosion fraction of 20%, compared with 30% for the Beamlet Demonstration Project, reflects an uncertainty with respect to flashlamp reliability above 20%. Tests on flashlamps off line, and results from Beamlet, will determine whether we can benefit from the reduced system cost associated with a higher flashlamp explosion fraction.

The system design is based on a monolithic 2 megajoule, self-contained module. Once this module is designed and tested, we may simply replicate the module to achieve the desired bank size, and integrate the modules with fiber-connected controls and triggers. This approach differs from Nova, in that many Nova modules are charged by a single power supply. In addition, Nova (and Beamlet) use a separate capacitor circuit for each series flashlamp circuit, while the NIF design employs a large parallel capacitor set, switched and connected to the lamps by a single transmission line per module. This approach, illustrated in Figure 9-2, will reduce hardware and labor costs associated with installing and terminating many large high voltage cables. The charging supply for each module will be a high efficiency switching inverter. A resistor and diode network will protect the supply from capacitor voltage reversals in the event of bank faults.

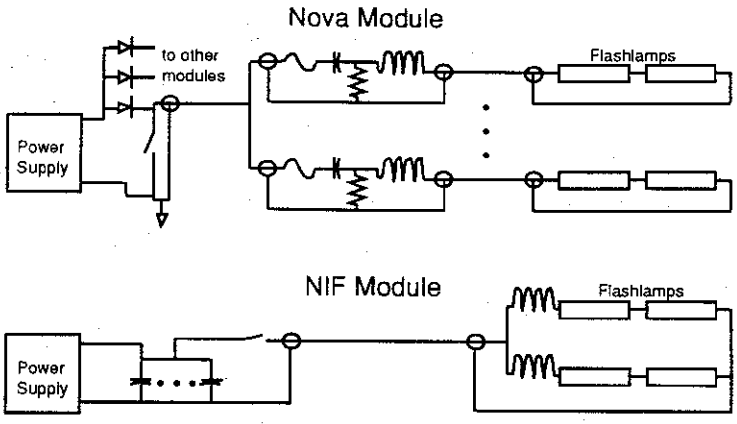

Figure 9-2 NIF and Nova pulsed power architecture.

The capacitors and their mounting will form the main structure of the bank module. The structure will be cast from fiber-reinforced concrete for strength and economy. The charging supply, 42 capacitors, the switch, controls and miscellaneous hardware will mount in appropriate cavities in the cast structure. The capacitors will be high density ($0.9\,J/cm^3$), metallized electrode capacitors with self-healing properties for high reliability. This is four times the energy density of the Nova capacitors. A single, 480 V feed will power the module. All other connections except the output will be via fiber optics.

A single switch will discharge the 2 MJ module. If ignitrons are used, two may be required in series to reliably hold off the bank voltage. The peak current capability of the switch limits the module size for a given pulse length. A coaxial mount will transfer the bank energy from the capacitor buss plates, through the switch to the coaxial transmission line.

A single, rigid transmission line, made from mounting inexpensive aluminum pipes concentrically, will connect each bank module to the junction/fanout box near the amplifier. Pre-fabricated corner sections will allow the line to bend where necessary to fit the facility.

The junction/fanout box will terminate the transmission line near the amplifier. The box will contain a ballast inductor for each flashlamp driven by the module. Flexible, twisted pair cables will connect the junction box to the flashlamp connectors on the amplifier. The current in each lamp will be sensed in the junction box, and the peak value stored by the control system for use as a lamp diagnostic.

9.2 *System costs*

The pulsed power system hardware and labor costs are summarized by subsystem in Table 9-2. The total corresponds to 17 cents/joule (including supplies and expenses and Material Procurement Charge assessments) compared with 30 cents/joule for Beamlet. The largest reduction, 7 cents/joule, results from increasing the module size to 2 MJ compared with 0.4 MJ on Beamlet. Another significant cost lever is the delivered energy per lamp. Delivering more energy per flashlamp reduces the number of circuits, thus reducing the hardware, assembly and installation costs associated with the junction box. An increase from the baseline 17 kJ per lamp to 34 kJ per lamp reduces the recurring bank cost by 1 cent/joule.

Other factors which affect system cost are circuit topology and output pulse shape. The NIF circuit topology represents a lower cost approach since it simplifies assembly and installation, and reduces the number of parts per module. The estimated savings resulting from this approach compared with the Beamlet approach is 3 cents/joule. Reducing the output pulse length increases

costs due to increased losses. The increased losses are caused by a higher peak current per delivered joule, and larger skin effect losses associated with higher frequency operation. Shortening the pulse from the 500 μs Beamlet value to 360 μs increases bank costs by 0.5 cents per joule, assuming the switch costs for the higher peak current remain constant.

Table 9-2 Pulsed Power System Cost Summary.

Component	Totals($M)
Capacitor Assembly	11.95
Switch Assembly	2.54
Power Transmission	1.99
Junction Box	6.74
Module Controls	3.34
Charging Supplies	2.85
Preionization System	2.30
Substation and Facility Mods	0.40
Test and Assembly Fixtures	0.34
Bank QA Facilities	0.22
Design	6.39
Total($M)	39.07

The above cost is higher than the pulsed power system costs reported in Chapter 7, since labor is accounted for in this table.

9.3 *Component development*

Component and system design development is required to implement the above design for the costs shown. This is especially true in the areas of switching and validating the parallel circuit topology. The critical elements leading to success are the construction and testing of a two megajoule prototype bank module, additional cost reductions in high energy density storage capacitors through cooperative programs with industry, and the development of a switch technology capable of transferring 150 coulombs at over 500 kA while having long, reliable switch life. To reach these objectives, we anticipate a 2.5 year development program. The schedule for the program is shown in Table 9-3:

NIF Component Development Schedule—Pulsed Power

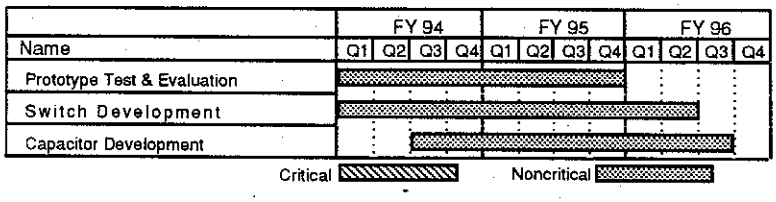

Table 9-3 Pulsed power component development schedule.

The primary technical issues unique to the monolithic circuit approach are related to flashlamp triggering, current sharing among lamps operated in parallel, and fault modes with a tightly bussed capacitor module. In order to resolve these issues, a test bed has been constructed by contract with American Controls Engineering. Results from test bed experiments are being compared with the results of modeling performed at LLNL. Once validated by experiment, computer modeling programs will be used to explore a greater parameter space than is possible with the test bed alone.

Operation during system faults (arcs) is a concern because of the large stored energy in each module. Damping resistors at each capacitor and distributed inductance in the system reduce fault currents to values near normal operating currents for the capacitors. This will enable us to eliminate fuses in the system design, which is desirable from both cost and reliability standpoints. Measurements and modeling of system fault modes remains a high priority and will continue.

The NIF circuit approach raises questions about reliable flashlamp triggering. The "ring-up" triggering method used on Nova depends on the pulse-shaping inductor and coaxial cable capacitance to form a resonant charge circuit. This produces a fast, high voltage spike across the lamps resulting in reliable triggering. In the NIF approach, this resonant circuit does not exist, so the applied voltage and frequency will be lower. In addition, the first lamp in a parallel set to trigger will cause a reduction in trigger voltage to the remaining lamps. If many of the lamps connected to a module should fail to trigger, the remaining lamps will be stressed since the total module energy is still available. These issues will be addressed using the test-bed. Reliable triggering of parallel lamps by pulsing a reflector or trigger wire in close proximity to the lamp envelope will be demonstrated. Adding small capacitors across the lamps to allow resonant ring-up triggering will also be investigated. A flashlamp array has been shipped to ACE in preparation for these tests.

A related issue is current sharing among parallel lamps. If the lamps powered by a given module share current unevenly, pump uniformity problems and stressed flashlamps may result. Adding inductance in series with each series set of lamps will solve this problem, but we must determine the amount of inductance required for an adequate level of sharing. We will make current sharing measurements on a number of parallel lamp sets using the test bed with various inductance values to resolve this issue.

Work in these areas will gradually convert the test-bed into an adequate prototype module for the NIF. This module would then be rigorously tested to predict performance and reliability of the NIF power conditioning system.

Our approach to capacitor development has been to work with the major capacitor vendors to develop capacitor designs with the appropriate performance, energy density and cost for the NIF. Once a promising design is developed, we purchase and test a small sample of full size capacitors at LLNL to gain data which enables us to predict the performance of a large bank.

Improvements in energy density and reliability have been made by the manufacturers in recent years. A new promising capacitor technology, based on self-healing, metallized dielectric, has the advantage of higher energy density (by about a factor of 2) and very low infant mortality. In addition, the reduced material requirements and high manufacturing yield should result in lower cost for similar performance compared to traditional discrete foil designs. A potential drawback is that low impedance faults in the bank may damage the capacitors by exceeding the peak current capacity of the thin capacitor electrodes.

We have tested both discrete foil and metallized dielectric capacitors over the past year to assess their performance and choose a technology for the Beamlet capacitor bank. Based on the results of this testing, metallized technology was chosen for the Beamlet bank. This will allow us to gain experience operating a large bank (13 MJ) of self-healing capacitors. The Beamlet bank, however, uses a circuit layout similar to Nova, so many issues associated with a monolithic bank module will not be explored.

The ability of these capacitors to survive high-current, high-reversal faults without significantly affecting their lifetime must be demonstrated, or their limitations understood and accounted for in the bank design. In addition, only two capacitor vendors presently make this type of capacitor. The larger companies, such as GE and Westinghouse, are just beginning to develop metallized designs of their own. Encouraging and qualifying these vendors will reduce the overall cost of the NIF capacitors.

We have maintained a low-level switch development effort for the past four years. The NIF

design requires a switch capable of about 500 kA, 150 C, per shot. Existing ignitron designs (such as those used on Nova) can operate reliably at 200 kA, 100 C, per shot. Our early development effort yielded design changes to the ignitrons which should substantially improve the current and charge capacity, but have not been completely tested. In addition, it is desirable to improve the voltage hold-off capability of these tubes so that a single tube can switch a 22 kV bank module, instead of two in series as on Nova and Beamlet.

A contract placed with Texas Tech University (TTU) will evaluate the new ignitron designs. The improved designs from each vendor (Richardson Electronics and English Electric Valve) will be tested. Two iterations of tube designs and testing are included in the contract to address these problems. After the design iterations, a tube will be purchased for integration into the test-bed. Other switch candidates such as commercially available air and vacuum spark gaps will also be tested.

Chapter 10

PULSE GENERATION

10.1 *System Design Requirements and Architecture*

The front-end systems generate temporally and spatially shaped pulses with the correct energy, contrast ratio, and wavelength for each of the beamlines of the NIF. Table 10-1 lists the top level system parameters.

Table 10-1 Top level front-end system requirements.

Nominal wavelength	1.053μm
Number of wavelengths	4 separated by 10–20 cm^{-1}
Output energy	3 J
Repetition rate	
Oscillator	100 Hz
Regen	0.2 Hz
Preamp	0.05 Hz
Temporal Shaping	
Number of shapes	2
Dynamic range	500:1
S/N	> 1000 (foot)
Accuracy	±5% match to programmed shape
Spatial Shaping	
Profile	Flat to 15% center to edge
roll off	1 mm on 10 mm square beam
Isolation from main cavity	$> 250,000 : 1$

The two most important requirements of the front-end are: 1) its energy delivered to the injection mirror at the transport spatial filter, and 2) the accuracy for temporally shaping the pulse (including the dynamic range needed to realize the shape of the pulse). The on-going Beamlet Demonstration Project developed modern fiber and integrated optical devices that replace many functions of the Nova front-end system. It is the goal of the designers of the NIF front-end to use as much low-level optical signal processing as possible before power levels force the use of bulk optics for manipulation and transport of the beams. Based on Beamlet experience, a separately shaped, amplitude controlled pulse is supplied to each individual beamlet. This allows for compensation in the characteristic gains, time delays, and amplifier gain saturation effects on an individual beamlet basis. Of the several possible design choices for the amplifier to boost the conditioned fiber signal to the 3 joules needed by the injector we have settled on a high-gain regenerative amplifier followed by a 4-pass rod amplifier similar to the design used in Beamlet. However, the capabilities of the rod amplifier are considerably below the Beamlet amplifier. There is one regenerative amplifier/preamplifier set for each beamlet. An integrated, packaged unit is to be mass produced—a unit that can be assembled and aligned prior to installation in the laser high bay. Each package receives a shaped optical signal via single mode fiber.

Figure 10-1 shows the arrangement of the fiber and integrated optical components for a single channel in the NIF front-end.

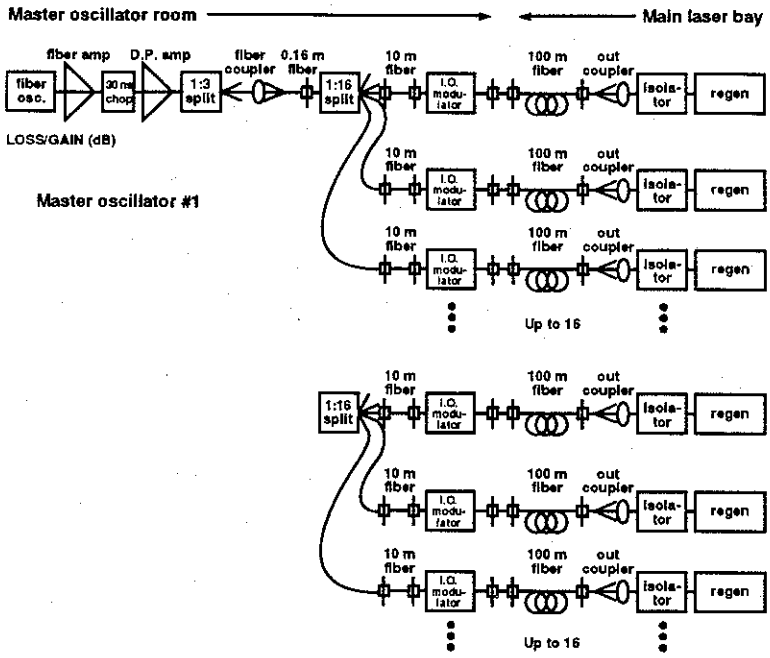

Figure 10-1 Wiring diagram of front-end from the master oscillator to the regenerative amplifier.

Although a fiber oscillator and fiber amplifier, followed by a diode-pumped amplifier are shown, the Beamlet bulk optical oscillator design can also be used. The primary issue in the design of the oscillator is the ability to produce the required four wavelengths. The development program outlined in Section 10.3 addresses this issue. Within the oscillator the optical signals are frequency modulated to provide side bands spaced at least 1 GHz apart to prevent Stimulated Brillouin Scattering (SBS) in the beamlet optical train. After splitting 3 times and then another 16 times, the resulting 48 signals are modulated in amplitude and distributed to the regen/preamp packages. The oscillators and modulators are housed in the Master Oscillator Room (MOR) with the central control area for the entire pulse generation system.

Shown in Figure 10-2 is the peak power of the optical signal as it propagates.

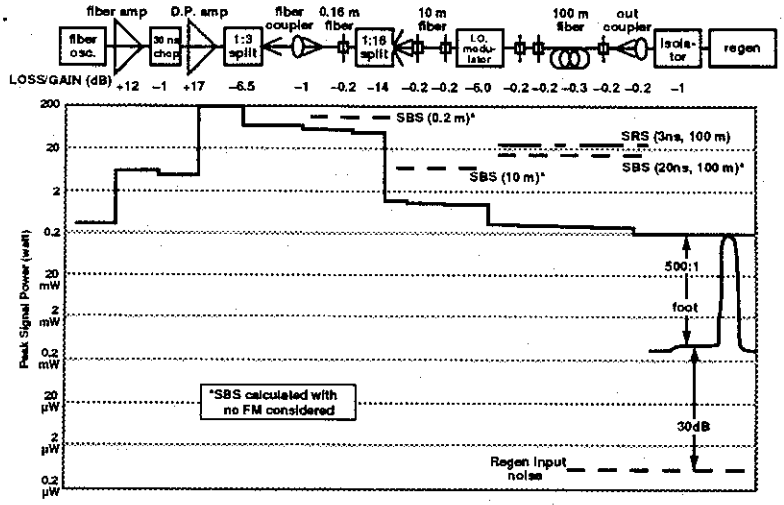

Figure 10-2 Power flow through fiber optic front-end components.

Fiber length and peak powers are chosen to always operate well away from the thresholds of non-linear optical effects, SBS, and Stimulated Raman Scattering (SRS). The lower end of the peak power window is determined by the equivalent ASE input noise of the regenerative amplifier. Measurements on Beamlet and calculations[1] show this to be about 0.5 microwatt peak. We have chosen to maintain the (much lower) foot of the shaped pulse at 1000 times this value. The location of the regen/preamp packages on the transport spatial filter assembly is shown in Figure 10-3. The time of flight compensation for each injected beam is shown in concept.

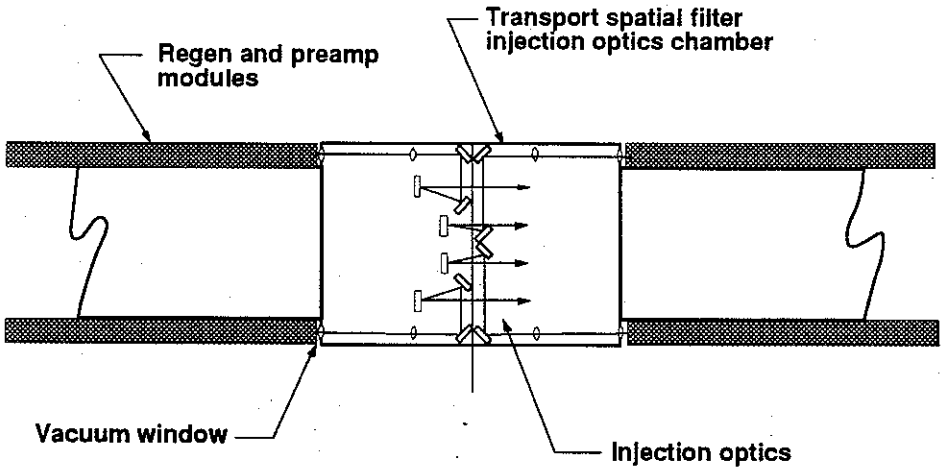

Figure 10-3 Schematic of Regen/Preamp packages on transport filter assembly.

The integrated control system, see Chapter 14, provides configuration and timing data to the Pulse Generation System in the form of messages and timing fiducials passed between the control system and the low level dedicated local controllers associated with each of the front end subsystems.

[1] Jack Campbell, *Notes from May 6th Beamlet Technical Meeting*, LLNL ICF internal memorandum, May 24, 1992.

Slow or time insensitive data is sent over the control system network. For example, configuration files specifying the individual beamlet pulse shapes, fixed delays, type of shot, etc., are sent to the pulse generators and delay generators in the MOR based on the shot directors choices.

Real time synchronization is accomplished with timing fiducials that provide the GO signals to the layered subsystems in the entire NIF. The master clock resides in the MOR. The most challenging task is to provide the 192 signals needed to synchronize the modulators to a standard deviation of ± 10 psec after compensating for the fixed delays. This requirement is probably state of the art. Fiber optics will be the most appropriate technology for the distribution of these signals. Development will be required here. From this clock increasingly coarser delays are developed to control the Pockels cells in the regen and preamplifiers. Also, signals are derived to notify the other time sensitive NIF subsystems including the main cavity Pockels cells and diagnostic packages.

The single largest cost center in the pulse generation system is the regen/preamp package. This self-contained, compact package is to be engineered for reliability, ease of maintenance, and cost. We expect to take full advantage of the inherent modularity and production methodology to lower cost by detailed value engineering of a prototype and quantity buys of similar components. Figure 10-4 shows a plan view of our initial packaging concept.

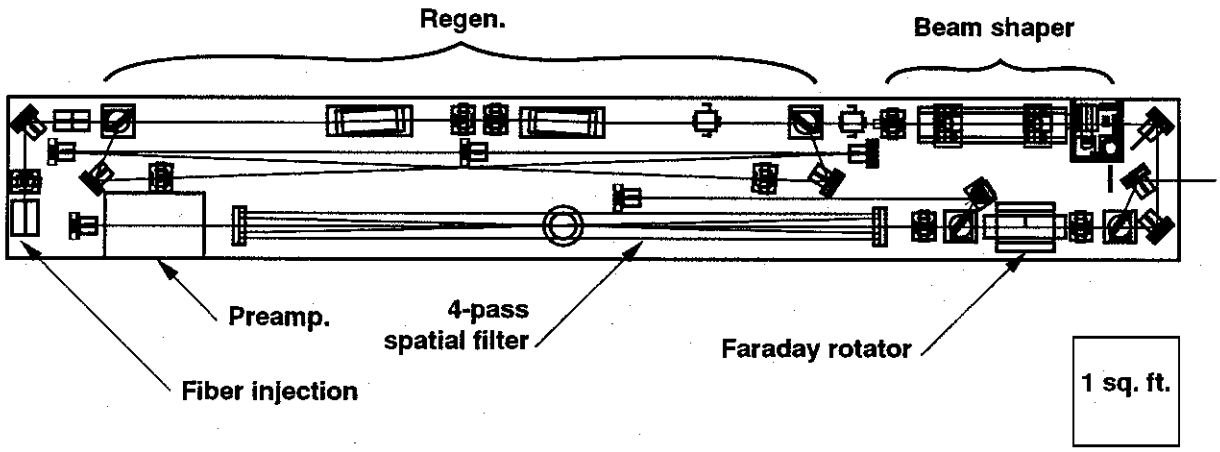

Figure 10-4 Front-end package layout.

The design size of the front-end package is 4 m by 0.5 m—much smaller than the front-end prototype for Beamlet. A major goal of the development program is to build such a packaged prototype. Space is provided for cameras and motorized alignment controls and for the inclusion of additional optical elements in case they are needed for beam smoothing by spectral dispersion. Ideally, the regenerative amplifier and preamplifier heads would be pumped by laser diodes rather than lamps; however, the high cost of the diode arrays is presently a limiting consideration. Gain stability, compactness, and reduced maintenance are the payoffs if this technology can be brought to the package. Two Faraday rotators are likely to be needed at the output of the preamplifier to isolate it from back reflection of ghost images returning from the main amplifier cavity.[2] Finally, an on-board processor is provided to minimize the number of individual control channels needed to operate and diagnose the package. Communication between the supervisory system and this local controller establishes the operating modes (regenerative amplifier shot, rod amplifier shot, etc.), handling routine house keeping functions, and reporting failures within the package.

[2] B. Van Wonterghem, *Front-End Isolation Requirements - Action Item 27*, LLNL ICF internal memorandum, 4 June 93.

10.2 *Projected Costs*

Summarized in Table 10-2 are the NIF project labor and material costs developed for the design described above. Escalation and contingency are not included here.

Table 10-2 NIF construction cost summary.

WBS No.	Title	Labor ($K)	Material ($K)	Total ($K)
3.1.1	Multi frequency Oscillator	174	298	472
3.1.2	Modulators	985	4213	5198
3.1.3	Fiber Distribution System	159	800	959
3.1.4, 3.1.5	Regen/Preamp	7524	17664	25188
3.1.7	Integration/Refurbish facility	1293	850	2143
	Totals	10135	23825	**33959**

10.3 *Component Development*

Several technical areas in the front-end are of sufficient risk or have sufficient cost leverage, that they warrant additional development work. We present a two year plus program to define the design concepts, integrate subsystem components, and finally to build complete prototypes of all elements of the system from the oscillators to the injector. The goal is to develop and verify the front-end systems performance and cost projections prior to conceptual design.

Beginning with the master oscillators, present Beamlet designs will work for a single wavelength centered at the YLF gain-band width curve. NIF, however, requires four wave lengths spaced by nominally $10\,cm^{-1}$ (or possibly even $20\,cm^{-1}$). Also, in the present NIF MOR design, there is a phase modulator in the oscillator cavity to generate the necessary FM sidebands. This removes an extra device from the optical chain, uses the phase modulator most efficiently, and could help the oscillator run single mode, indicating there is considerable leverage in developing an advanced oscillator. For the gain medium, glass has enough bandwidth, but thermal effects have created problems for diode-pumped glass lasers. There are crystal hosts with wide bandwidth and better thermal and optical properties. Besides the options of glass or crystal bulk optic oscillators, and a wide range of diode-pumped monolithic designs, there are fiber based variations that are now being described in the literature. Fiber oscillator designs avoid some of the problems associated with glass lasers while providing flexibility in cavity design and material selection. The options of new fiber optic techniques and an expanded range of low gain materials usable in waveguide lasers can provide for better optimization of the NIF oscillators. Thus far, reported peak powers have been lower than bulk optic oscillators, and a preamplifier would be required. This preamplifier is included in the proposed design and would be part of the oscillator development program. We need to pursue a focused program to select an oscillator system design and engineer it for stable, reliable operation.

In the area of integrated electrooptical modulators, new devices are appearing on the market. Modulator technology has evolved since the designs for Beamlet were decided. Not only has the unit price dropped, but more vendors are in the market. A program to develop advanced electrooptic amplitude modulators will be carried out with industry, resulting in modulators which meet NIF cost and performance goals.

To meet NIF performance requirements, the front-end must generate a precisely shaped 1ω input pulse which, when propagated through the remaining laser chain, produces a specified 3ω shape. To accomplish this, we plan an aggressive effort over two years to develop an electrical pulse generator which can effectively and inexpensively drive the electrooptic modulators. Methods which have been used previously for pulseshape generation have not been adaptable to computer control, whereas the NIF design will require a pulseshape system under direct programmable control. Techniques for doing this primarily revolve around the use of microwave power MESFETS, which are GaAs transistors capable of operating in excess of 10 GHz. Existing devices in both chip and packaged form show switching speeds sufficient to build up a NIF-like pulse. The major challenge for this development project is to utilize these devices in this unusually large signal regime, and to be clever in their usage to keep the cost down on the final developed device. For example, the combination of a chain of MESFETS and some high speed digital to analog converters could form the basis for a relatively inexpensive pulseshape generator. To prove the concept will require significant circuit modeling and electrical circuit prototyping.

The regenerative amplifier is to be based on the existing Beamlet design. There are features of this design that are undesirable in the NIF. An example is the use of lamp pumping. To achieve the necessary gain stability, the lamps are long pulsed. This increases the stored energy pulsed power supply. The answer is to use diode pumping. A significant amount of resources are needed to carry out the development of a diode pumped regen that meets our cost goals. Both industrial development and LLNL programs will be undertaken to accomplish this goal. Another major cost item for the regenerative amplifier is the electrical pulse generator which switches the Pockels cell. The current technology utilizes tubes, which are both expensive and have an unacceptable reliability for such a large system. To reduce the unit cost and obtain reliability, we will develop a solid state electrical Pockels cell driver, capable of switching the pulse into the regen at a triggered time, and switching it out again after the appropriate number of round trips are achieved. Additionally, it is desirable to diode pump the preamp as well. Again cost is the obstacle.

Package design will take several iterations. Not only does the regen/preamp assembly have to perform as expected, it must be serviceable, and have sufficient reliability that virtually all the packages are in specification at shot time with a high degree of confidence. A program as outlined includes the ability to make use of commercial or aerospace resources in the design. Detailed design and subsystem prototyping are the underpinnings of this effort.

Finally, the front-end development program will culminate with the construction and testing of a fully integrated regen/preamp package. Once perfected this prototype will be the basis for commencing the conceptual design and detail specification for the NIF project.

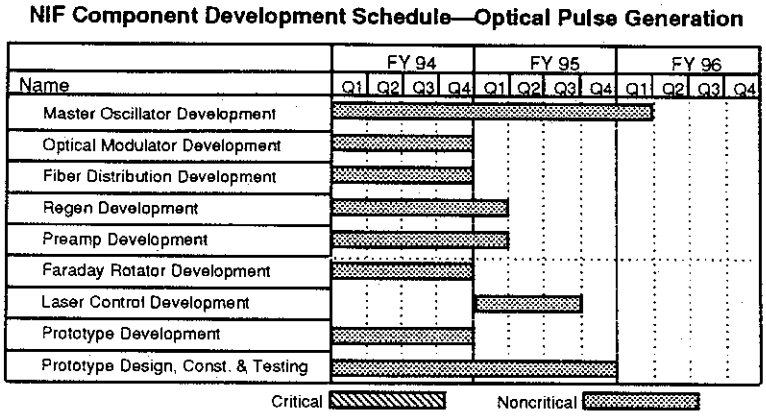

Table 10-3 Optical pulse generation development schedule.

Chapter 11

SPATIAL FILTERS

11.1 *Design concept*

A spatial filter is a confocal lens pair with a pinhole located in their common focal plane. The beam's low frequency spatial modes pass through the pinhole. High frequency modes are removed from the beam by the region exterior to the pinhole

The primary function of these devices in the NIF laser system is to reduce the risk of damage to expensive optics. High fluence that leads to damage can occur by uncontrolled nonlinear growth of beam modulation; or failure of the optical switch, thus trapping the beam in the main cavity. A beam dump in the current spatial filter design limits the number of amplifier passes to four. Pinholes in the spatial filter strip high frequency components from the beam, thus controlling their subsequent nonlinear growth. Proper spatial filter length will cause the beam to repeatedly reimage on itself at various locations in the cavity. This relaying effect is used to control the growth of low frequency beam modulation.

The spatial filters in NIF also provide an inexpensive way for injecting a low energy pulse into the high-gain amplifier cavity. An arrangement of small aperture optics route the input beam from the pulse generation system into the vacuum vessel, through the spatial filter pinhole, and into the cavity.

For each grouping of NIF beamlets (a 4×4 beamlet array in the current baseline design) two spatial filters will be required. One is located in the middle of the main amplifier cavity and the other is between the booster amplifier and the target chamber.

Each filter is a large rectangular vacuum vessel with a lens at each end. Its dimensions are approximately $18\,\mathrm{m} \times 2.5\,\mathrm{m} \times 2.5\,\mathrm{m}$, as shown in Figure 11-1. They will be constructed with thin metal panels that have been reinforced with internal stringers and external ribs to resist vacuum loads. Four vessel materials have been analyzed, aluminum, mild steel, stainless steel and stainless clad mild steel. Mild steel has been chosen as the base line design to minimize material costs. The steel surface will require a surface treatment to meet the low outgassing (10^{-11} Torr – Liter/sec) and surface cleanliness requirements. The vacuum pumping will maintain internal pressures below 10^{-2} Torr.

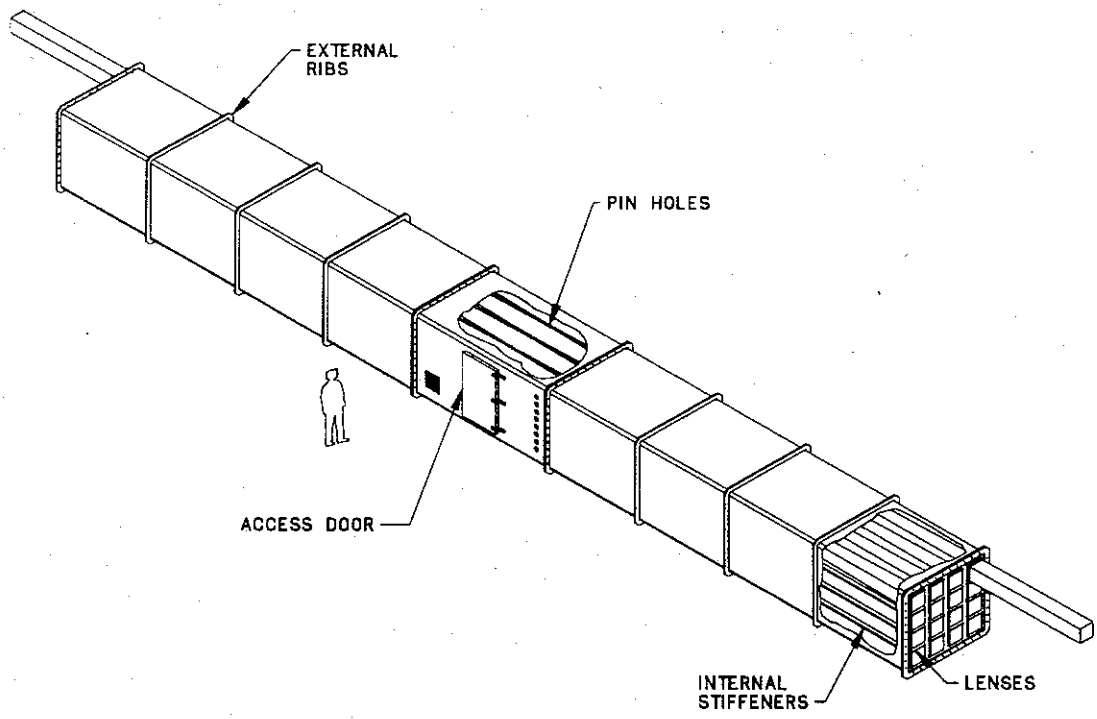

Figure 11-1 Spatial filter structure concept

Doors will be constructed on either side of each vacuum chamber to permit human access to the internal hardware, pinhole assemblies, beam dumps, baffles, diagnostics and injection optics (output spatial filter only). Repair and maintenance of these components will require that the vacuum chamber be periodically brought up to ambient pressure and then evacuated again. During this process the location of all of the pinholes must be maintained to within about 5% of the pinhole diameter. The external walls of the vacuum vessel will be used as a platform for the pulse generation and diagnostic packages. Access to the equipment at these locations will be convenient allowing rapid turnaround for alignment and maintenance activities.

To accommodate multipassing within the laser cavity the spatial filter requires multiple pinholes at the focal plane of each beamlet as shown in Figure 11-2. Pass one is injected into a pinhole located at a lower corner of the pinhole array. One of the cavity mirrors is tilted to cause the beam to then pass through the second pinhole which is in the diametrically opposite corner. Subsequent passes will be directed through the holes in the remaining two corners and finally onto a beam dump which intercepts the fifth pass. The beam dump is necessary to absorb the laser pulse should the optical switch fail, and to absorb the 1-2% of the pulse energy caused by switch imperfection. The pinholes will be mounted on a holder which can index up to 10 pinhole assemblies into the beam path to accommodate different shot and alignment configurations. The pinholes will be approximately 3 mm in diameter and will be shielded with tubes to prevent plasma blow-off from one hole interfering with an adjacent hole.

Pinhole spacing and mirror tilt can cause vignette on the laser slabs. To avoid clipping the beam, space around the nominal beam position in the laser slabs has been allocated. This increases the size of the hard aperture required for a given beam size. Since amplifier aperture is a major cost center the pinhole spacing must be minimized. For a 35 cm hard aperture optimum pinhole

spacing is presently estimated to be about 0.7 cm × 3.4 cm.

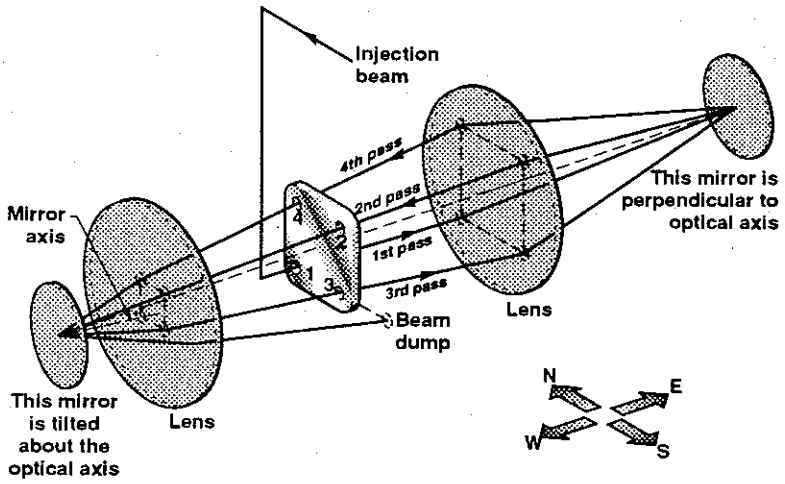

Figure 11-2 Pinhole configuration for a single beamlet

11.2 *Hardware costs*

Costs have been estimated for the spatial filter including the internal hardware discussed above and the supporting vacuum and electronic control systems, Table 11-1.

Table 11-1 Spatial filter labor and material costs

Item	Labor ($K)	Material ($K)	Total ($K)
Cavity spatial filter	2321	8464	10785
Output spatial filter	4093	9253	13346
Total	6414	17717	24131

The single dominant mechanical cost is the vacuum vessel estimated at $245 K. Twenty four vessels are required for the 192 beamlet configuration, and the total cost is just less than $6 M. This is based on material and fabrication rates of $6.00/Lb which is comparable to costs that have been achieved on other large vacuum vessels constructed in the LLNL Laser Program. If the vessel were made of stainless steel the costs would be approximately 40% greater. Costs for the other components are based on hardware that has been purchased for both Beamlet and Nova. The sensitivity of the costs to different design parameters has been examined. Aperture size changes less than 5 cm do not have a significant effect on the overall filter mechanical costs (±1.5%). Focal length changes less than 2 meters have a slightly greater effect (±3%). A more important parameter is the amplifier grouping (2 × 2, 4 × 4 or 4 × n) which is projected to be about a ±6% effect.

11.3 *Component development*

Several engineering evaluations must be performed and prototypes evaluated to meet the cost goals and design criteria. The total effort can be completed in about one year.

The lens mounting assembly requires a prototype to investigate vacuum sealing integrity,

mounting stress and stress induced birefringence in the lens. All previous lenses within ICF have been round; NIF lenses are square. We must ensure that all precision optical requirements can be satisfied in this new configuration.

Using mild steel as the primary vessel material will require evaluation and tests to demonstrate that the material can meet the outgassing and cleanliness requirements. A development program may be required to validate a satisfactory coating or surface treatment. These costs will have to be weighed against using a more costly vessel material.

Cleanliness requirements of the optical surfaces internal to the vacuum demand that nearby mechanisms and motors have low outgassing and particle generation characteristics. Test and evaluations will be performed to identify components and methods for achieving the specified requirements.

The full size beam dump that has been fabricated for Beamlet uses copper doped APG-121 glass. This prototype will be tested and evaluated to determine its suitability for NIF. Other beam dump approaches should also be considered to determine the most compact design to minimize pinhole spacing. Smaller pinhole spacing can be leveraged to reduce laser glass size and cost.

NIF Component Development Schedule—Spatial Filters

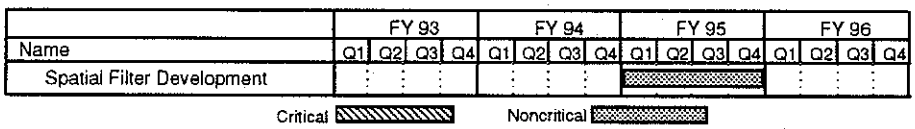

Table 11-2 Spatial filter development schedule.

Chapter 12

BEAM TRANSPORT AND FINAL OPTICS

12.1 *Design concepts*

The beamlet transport from the output spatial filters in the laser bays to the target area is through beamtubes to control temperature induced density gradients. The beamtubes could also be filled with a noble gas to prevent stimulated rotational Raman scattering (SRRS), although this does not appear to be a problem for 1ω transport. The beamlets are grouped into 2×2 groups of 4 for transport to the target chamber. Each of the four beamlets has an independent monolithic BK-7 turning mirror for every turn required. A finite element study of the gravity induced deformations of mirrors with aspect ratios of 8:1 indicates that surface flatness of $\lambda/10$ can be maintained using three-point rear surface mirror mounting. Mirror mounts in groups of four will be mounted on large support plates which will be attached to the supporting spaceframe.

The ideal beam distribution around the target chamber would be two cones of beams in each hemisphere at 27.7° and 52.5° to the target axis. The beam groups are staggered around these ideal angles by ±4.2° with one hemisphere's distribution rotated slightly about the target axis in order to prevent laser light from passing from any beamlet into ports on the opposite side of the chamber. The beam groups are equally spaced around the base of the beam cones with one-third of the beams in the low angle cones and two-thirds in the high angle cones. Beamlets that form the low angle cones require two mirrors per beamlet, both of which have tip and tilt capability for pointing and centering. Beamlets that form the high angle cones require three mirrors for each beamlet, the second mirror being fixed while the first and last mirror control pointing and centering. The transport layout for the 192 beamlet case is shown in Figure 12-1. Similar CADs models have also been developed for up to 288 beamlets.

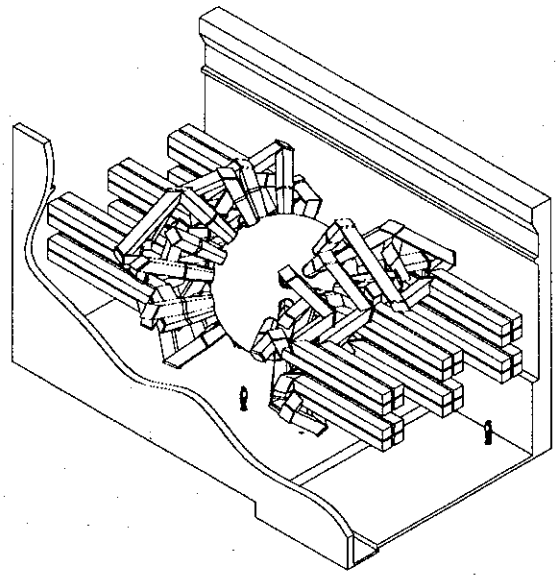

Figure 12-1 NIF conceptual drawing showing beam transport of 4 beamlet groups to the spherical target chamber. This drawing shows how 192 beamlets could be routed to the target chamber.

Path lengths vary from 15 m for the low angle cones to 23 m for the high angle cones. By placing the target chamber on a line between the centerline of the output spatial filters, eight-fold symmetry has been achieved which greatly reduces the layout difficulty and the number of sizes and shapes of turning mirrors.

The 1ω beams are converted to the third harmonic in the KDP/KD*P conversion crystals that are mounted on the final optics tubes attached to the target chamber. After 3ω conversion, each beamlet passes through the vacuum window, the 700 cm focal length lens and the debris shield as shown in Figure 12-2. A kinoform phase plate on the input side of the debris shield smoothes each beamlet. Each of the four beamlets in a transport group are focused to the same location near the target. This enhances smoothing and makes the speckle length much shorter since the beams form f/8.3 focal cones. The center of the support structure for the four beamlets also shadows the 1ω and 2ω residual beams preventing unwanted light from entering the target laser entrance hole. Each lens or lens/window combination is the equivalent of a segment of a larger f/8.3 lens in order to cause the beams to overlap at a common focus. Alternatively, the focus lenses could be made thinner and the beamlets directed toward a common focus by using the final turning mirrors to point toward the center of each beam group by 5.5 degrees. Depending on the detail design of the final optics support structure, beamlets might have to be slightly diverged from each other before the final turning mirror.

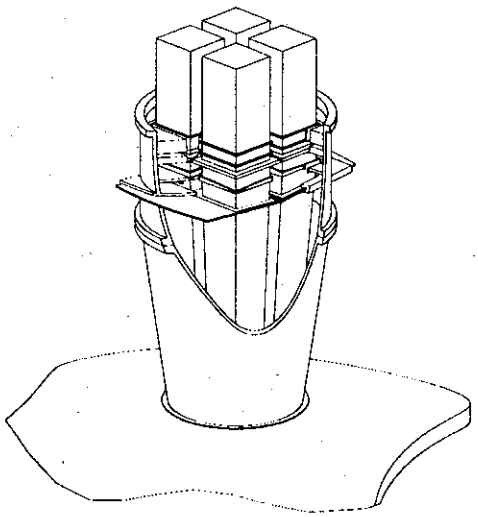

Figure 12-2 NIF conceptual drawing showing beam transport thru a frequency converter, lens, and debris shields.

Convergence of the beam after passing through the focusing lens increases the irradiance downstream at the phase plate/debris shield to damaging levels before other limits are reached. That a debris shield might "fuse", is unacceptable. Fortunately, other system constraints limit NIF's performance at only slightly higher output levels. Using a near normal debris shield orientation, the beam size reduction at the debris shield increases the fluence and damage risk by about 6%. This fluence could be reduced to the level at the focus lens by 3% up-collimation in the output spatial filters. This would increase the aperture of the KDP frequency converter and the output optics by about 1 cm and consequently increase their cost. System tradeoff studies will be used to optimize the selection of reduced output or up-collimation.

Experiments on Nova, used to simulate the X-ray output of NIF targets, indicate that sol-gel anti-reflection coatings fail at $0.25\,J/cm^2$. The expected X-ray fluence at the output face of debris

shields is about 1 J/cm^2. The technical options to solve this problem are:

1) develop a 3ω AR coating that can survive the X-ray fluence;
2) place the debris shield at Brewster's angle to remove the need for a coating but requiring an 8% upcollimation at the spatial filters;
3) or suffer the 4% reflection loss.

A combination of system studies and development efforts will be used to pick the best option.

12.2 *Mechanical system costs*

Costs in Table 12-1 reflect a 192 beamlet laser configuration, and include electro/mechanical components only. This system contains 512 turning mirrors, each with tip/tilt pointing capability controlled by high resolution stepping motors. The final optics system includes all mounting hardware, 2-axis precision positioners with 2 μrad resolution for the KDP crystal, 3-axis translation stages with 1 μm capability in the lateral directions for each lens, 2-axis tip/tilt positioners with 0.5 degree resolution for each debris shield, and all support structure required to maintain high position stability of the optics at the target chamber. Costs for the beam tubes include material, labor and assembly.

Table 12-1 Mechanical System Costs

Item	Material ($K)	Labor ($K)
Mirror assemblies	2,629	340
Final optics system	4,544	547
Beamtube system	1,521	58

12.3 *Kinoform phase plates for spatial beam smoothing on NIF*

High power ICF laser beams exhibit phase distortion resulting from surface finish errors, pump induced non-uniformities, etc. The consequence of such aberration is that the focal spot is many times diffraction limited and can be non-uniform. While the increased spot size may still be within acceptable limits for specified target dimensions, the spatial non-uniformities, particularly the long wavelength components within it, can be detrimental to target performance.

One approach for correcting focal spot characteristics is to insert binary random phase plates (RPP) in the beam. The plates will homogenize the focal irradiance pattern by creating a fine scale speckle with a smooth overall envelope. The RPPs consist of a two-dimensional, closed-packed array of square or hexagonal phase elements that are randomly chosen to introduce a phase delay of either 0 or π. The focal plane irradiance profile of an RPP consists of an overall envelope characteristic of the diffraction pattern of a single phase plate element and a superimposed speckle pattern from the interference between the contributions from various phase plate elements. When beam aberrations are included, the far-field electric field is a convolution of the far-fields of the beam and the RPP separately. Generally, this convolution broadens the far-field spot and increases the inhomogeneities of the beam. If the far-field spot produced by the RPP is bigger than that produced by the beam alone, then the convolution does not significantly alter the overall spot size. Qualitatively, one could characterize the effectiveness of the RPPs in homogenizing the beam by the magnitude of the ratio r/b where r is the effective divergence of the RPP and b is the divergence of the beam. The far-field spot size on Nova using a 310 cm focal length lens (at 2ω) is of the order of 200 μm suggesting a divergence angle of $\sim 70\,\mu$rad. Our experience with sol-gel RPPs on Nova indicates that the RPPs are effective in homogenizing the focal spot for ratios r/b that are about 1.5 or larger.

Although RPPs are easy to produce and are widely used, they have two serious limitations. First, the far-field envelope is fixed (essentially an Airy pattern) and second, as a consequence of the first restriction, $\sim 15\%$ of the energy is lost outside the central spot; i.e., the region beyond the first zero in the far-field pattern. To overcome these limitations of RPPs we have proposed the use of continuous contour phase plates known as kinoform phase plates (KPPs) for tailoring the far field profile and also concentrating the energy. Numerical studies indicate that the focal irradiance profile can be tailored to contain greater than 95% of the incident energy within a desired region. The intensity distribution in the central region resembles a speckle pattern with a smooth overall envelope. Just as in the case of RPPs, real beam aberrations lead to far field pattern which is a convolution of the irradiance profile with KPP phase screens. Our calculations for Nova indicate that the KPP far-field pattern, and especially the energy content within it, is fairly insensitive to laser system aberrations for ratios $r/b >\sim 1.5$, much like the RPPs.

The effectiveness of the KPPs in homogenizing the focal irradiance profile in NIF depends on the ratio r/b for NIF conditions. It is estimated[1] that the aberrations on NIF would lead to a beam divergence of $\sim 70\,\mu$rad which, with the 7 m focal length lens, would produce a $\sim 500\,\mu$m spot at the target. Since the target spot size specifications is also $500\,\mu$m, a KPP design to produce $500\,\mu$m spot would imply $r/b \approx 1$. This implies that the effects of convolution could be quite severe in straightforward KPP designs for NIF. An aberration model for NIF is currently being constructed to quantify the limits on the ratio r/b. Experience on Nova suggests that to improve the robustness of KPPs on NIF a reduction of the laser system induced beam divergence to around $50\,\mu$rad, or about 5/7 of the $70\,\mu$rad full angle permitted by target requirements, may be necessary.[2]

12.4 *KPPs on NIF - component development plan*

At present we are investigating two promising fabrication techniques for producing large aperture KPPs for high power ICF applications. One is lithographic or raster transferring of a computer generated pattern in a photoresist coating layer followed by ion etching directly into fused silica, while simultaneously ablating away the photoresist. The other is UV lithographic or raster transfer of the pattern into PMMA. Either fabrication technique must preserve the high damage threshold specifications, the specifications on the step heights ($\pm 5\%$), and transition region size between pixels ($\sim 20\,\mu$m). We estimate the exploration of the various techniques and identification of a optimum method to take about 1 year followed by fabrication of a prototype KPP for a reasonably large size aperture (probably about 30 cm). After a successful demonstration, we would scale up to the 60 cm Nova size (smaller, insertable debris shields). We expect to fabricate Nova size KPPs by the end of the second year.

Development of the technology to meet the manufacturing goals of the NIF will require several process improvements and modifications. To produce approximately 200 KPPs the process will have to be time efficient, easily reproducible, and inexpensive. The lithographic manufacturing process will require efficient replication techniques. For example, this may require the development or modification of an appropriate pattern writer/mask maker facility as well as an ion etching facility. Rastered writing for each part may turn out to be inefficient.

---

[1] J. R. Murray, *Beam divergence budget (preliminary) with digressions on frequency conversion*, LLNL ICF internal memorandum, June 1, 1993.

[2] D. Eimerl, *Beam divergence requirements for the NIF laser* , LLNL ICF internal memorandum, June 16, 1993.

A development schedule for the kinoform phase plates, as well frequency conversion topics discussed later is provided in Table 12-2.

NIF Component Development Schedule—Beam Transport

Name	FY 94				FY 95				FY 96				FY 97			
	Q1	Q2	Q3	Q4	Q1	Q2	Q3	Q4	Q1	Q2	Q3	Q4	Q1	Q2	Q3	Q4
Frequency Converter																
Kinoform Phase Plate																

Critical Noncritical

Table 12-2 Beam transport development schedule.

12.5 *NIF Baseline Harmonic Generation*

Because of its simplicity, a sequential, or cascaded, application of collinear sum-frequency mixing is usually employed to achieve efficient third harmonic generation, particularly at large apertures. A beam at the fundamental laser frequency is incident upon a nonlinear crystal in which second harmonic generation occurs with degenerate sum-frequency mixing. Two co-propagating beams, one at the fundamental and the other at the second harmonic, emerge from the doubling crystal and are incident upon a second nonlinear crystal in which the fundamental and second harmonic waves interact via the nonlinear polarizability of the crystal to generate a wave at the third harmonic. The harmonic generation efficiency in each crystal is a function of the nonlinear polarizability of the medium, the thickness of the medium, the phase mismatch between the input and generated waves, and the input intensities. The harmonic generation efficiency is particularly sensitive to phase mismatch and to the balance between the intensities of the input waves, which is termed the mix ratio.[1–5]

Phase mismatch, Δk, is the difference between the k-vector of the output wave and the sum of the k-vectors of the input waves. When the sum-frequency generation process is perfectly phase matched, i.e. $\Delta k = 0$, the input and generated waves traverse the nonlinear medium with their phases locked together allowing maximum energy transfer to the wave at the sum frequency. The most common method of achieving phase matching is the use of the birefringence of crystalline media to offset dispersion, particularly for sum-frequency mixing via the second-order nonlinear polarization. This rather naturally leads to two types of phase matching: Type I in which the two input waves have the same polarization inside the nonlinear medium, and Type II in which the two input waves are orthogonally polarized in the nonlinear medium.

Mix ratio is a critical parameter in the third harmonic generation crystal. An imbalance in the photon fluxes of the fundamental and second harmonic beams incident upon the tripling crystal leads to back-conversion of the third harmonic beam even with perfect phase matching. Craxton[1,2] has proposed two simple methods for controlling the mix ratio incident upon the tripler: (1) adjusting the phase mismatch in the doubling crystal by angularly detuning it from perfect phase matching; or (2) adjusting the polarization of the fundamental wave incident upon the doubling crystal. The second of these two mix ratio control methods is termed polarization bypass for a Type I doubler, and polarization mismatch for a Type II doubler. Angle detuning and polarization adjustment are attractive mix ratio control schemes because they can be implemented simply in an inline geometry.

12.5.1 *NIF Harmonic Generation Baseline Design*

With two phase matching methods and two mix-ratio control schemes, there are eight possible

configurations for the cascaded crystal pair used for third harmonic generation. Of these eight schemes, which are listed in Table 12-3, four require special two-color wave plates between the doubling and tripling crystals to produce the correct polarizations for the tripler. Although such wave plates can be fabricated, they are expensive and contribute to the B-integral budget, and are therefore rejected as possible configurations for the baseline harmonic generation design.

Table 12-3 Third Harmonic Generation Phase-matching Configurations.

Phase matching Configuration Configuration	Mix Ratio Control	
	Polarization	Angle Detuning
SHG I / THG I	input polarization 35.26° *	input polarization 0° * WAVEPLATES REQUIRED
SHG I / THG II	input polarization 35.26° * WAVEPLATES REQUIRED	input polarization 0° *
SHG II / THG II	input polarization 35.26° *	input polarization 45° * WAVEPLATES REQUIRED
SHG II / THG I	input polarization 54.74° *	input polarization 45° * WAVEPLATES REQUIRED

* Measured from the ordinary axis of the doubling crystal.

The remaining four configurations are evaluated on the basis of nonlinear optical crystal parameters and harmonic-generation computer code calculations. The nonlinear material selected for the baseline design is potassium dihydrogen phosphate (KDP) and its deuterated analog (KD*P). This crystal is presently the only nonlinear optical crystal available in sufficient size and quality. The relevant material parameters of KDP are summarized in Table 12-4. From the entries in Table 12-4, we see that Type I third harmonic generation in KDP has a lower nonlinear susceptibility and significantly higher angular sensitivity than Type II third harmonic generation. As we shall demonstrate shortly, the use of Type II second harmonic generation leads to third harmonic production that is extremely sensitive to depolarization. Consequently, we shall discard the Type II SHG/Type I THG scheme because of the combination of extreme angular and polarization sensitivities. Because of the high angular sensitivity of the Type I/Type I design when implemented with KDP and our lack of operational experience with such a design, we have not explored this design in depth nor considered it for the NIF baseline design. There are, however, aspects of this design that merit further study; please see the section on development efforts below.

Table 12-4 KDP Parameters Relevant to Harmonic Generation

Phase matching Type	Phase matching Angle*	Angular Rate of Change of Phase Mismatch (cm^{-1} $mrad^{-1}$)*	Effective Nonlinear Susceptibility (picometers/Volt)
Type I SHG	41.188°	-4.9987	0.26
Type II SHG	59.229°	-2.5615	0.34
Type I THG	47.735°	-8.0658	0.29
Type II THG	59.070°	-5.2596	0.34

* Calculated from Sellmeier relation given by Zernike.[6]

We are thus left with two harmonic generation schemes for the NIF baseline design: Type I SHG/Type II THG with mix ratio control by angular detuning of the SHG crystal, and Type II SHG/Type II THG with mix ratio control by polarization mismatch. These designs are shown schematically in Figure 12-3. Both of these harmonic generation schemes have produced third harmonic conversion efficiencies of 70% on Nova; however, the Type II/Type II scheme required repolarization of the beam to achieve high conversion efficiencies.[7] Third harmonic conversion efficiencies in excess of 75% have also been demonstrated on the Optical Sciences Laser.[10]

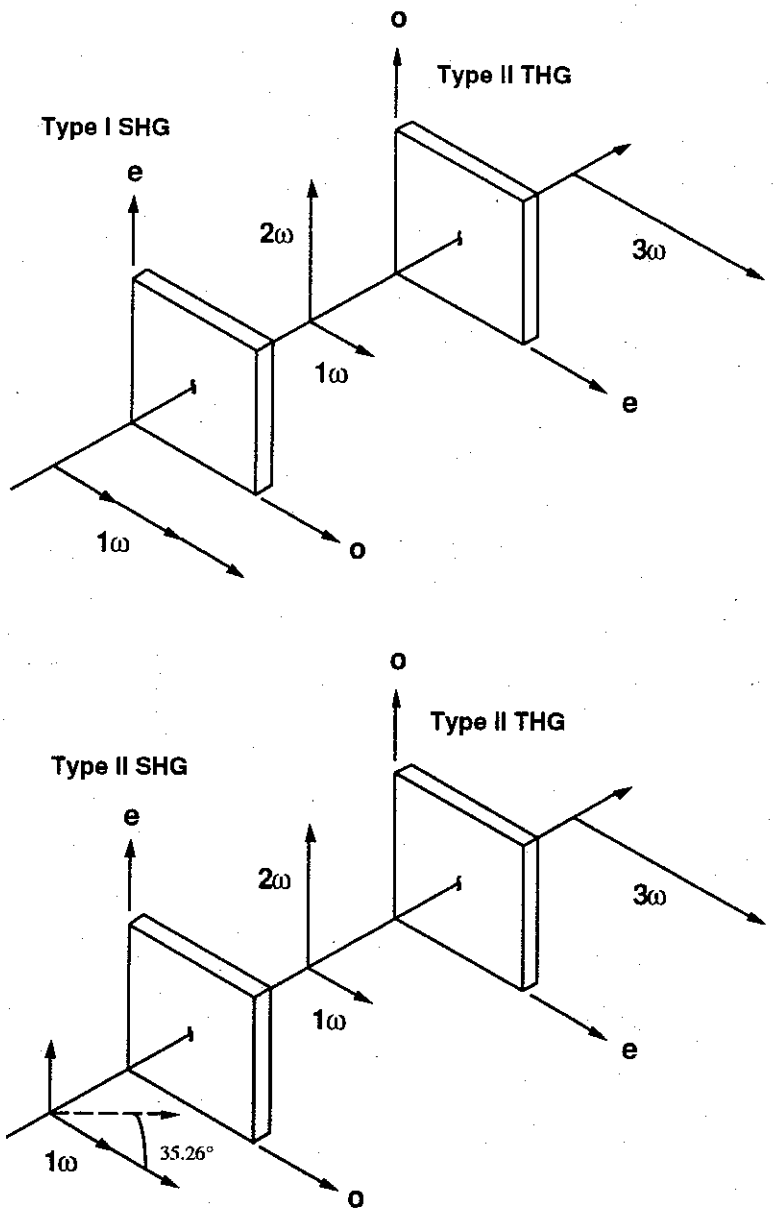

Figure 12-3 Schematic diagram for Type I/Type II and Type II/Type II third harmonic generation schemes.

Figure 12-4 shows the optimum theoretical plane wave performance of both Type I/Type II and Type II/Type II third harmonic generation schemes. These two schemes offer extremely similar performance up to input intensities of 6 GW/cm^2. The Type I/Type II scheme provides better performance at intensities above 6 GW/cm^2, while Type II/Type II gives slightly higher efficiency from 1 to 3 GW/cm^2.

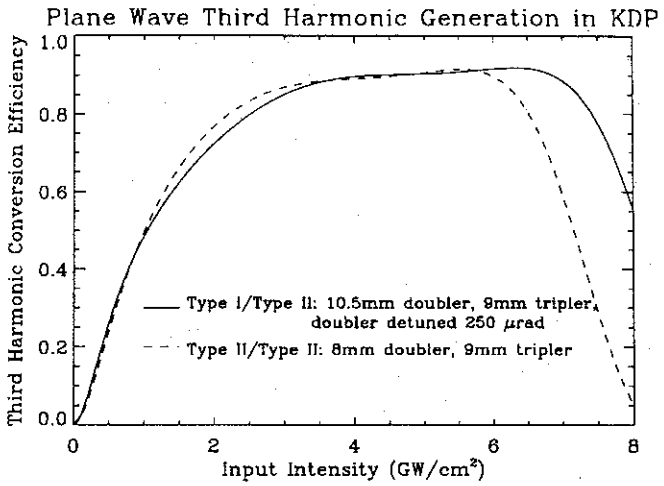

Figure 12-4 Third harmonic conversion efficiency versus input intensity for Type I/Type II and Type II/Type II schemes. These curves were calculated using ideal plane waves. Perfect phase matching is assumed for all crystals except the Type I doubler, which is detuned 250 μrad to provide near optimal mix ratio to the tripling crystal.

Although the angular rate of change of phase mismatch of Type I SHG is less than that of Type II THG (see Table 12-3), the angular sensitivity of the Type I/Type II scheme is dominated by detuning of the doubler—this is a consequence of using doubler detuning as the mix ratio control. Figure 12-5 shows a plot of the angular sensitivity of the third harmonic generation efficiency for a 10.5 mm Type I doubler, which dominates the angular sensitivity of the Type I/Type II scheme, and a 9 mm Type II tripler, which dominates the angular sensitivity of the Type II/Type II scheme. Although the Type I/Type II scheme is significantly more angularly sensitive, the focal spot requirement of ± 35 μrad divergence[9] places a stronger constraint on beam quality than either of the harmonic generation schemes. Consequently, angular sensitivity is not a primary factor in the selection of the baseline harmonic generation design.

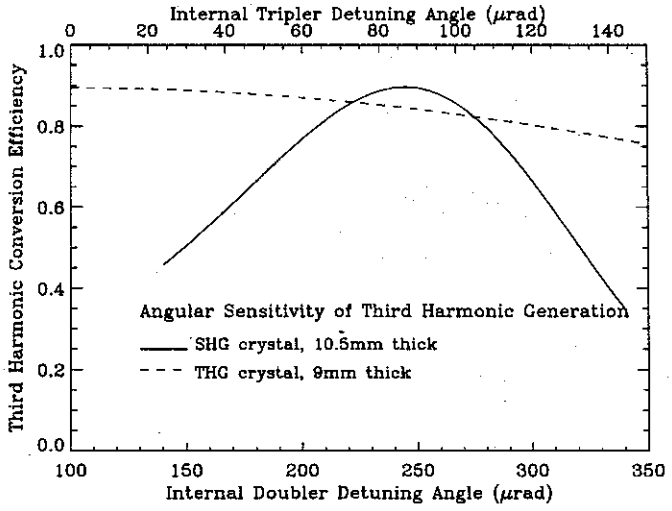

Figure 12-5 Third harmonic conversion efficiency as a function of internal angle relative to exact phase matching for a 10.5 mm Type I SHG crystal and a 9 mm THG crystal. These curves are calculated assuming an ideal plane wave input of 4 GW/cm^2.

One of the two primary reasons for the choice of Type I/Type II as the baseline design for NIF harmonic generation is depolarization sensitivity. Figure 12-6 presents a plot of third harmonic generation efficiency versus depolarization of the incident fundamental beam. The dotted vertical lines in the figure indicate the deviations of the input polarization angle that correspond to 0.2%, 0.5%, and 1.0% of the incident energy being carried in the "wrong" polarization. In the Type I/Type II third harmonic generation scheme, the incident energy carried in the wrong polarization does not participate in the sum frequency mixing process in either crystal. Consequently, as the solid curve in Figure 12-6 indicates, Type I/Type II is very insensitive to depolarization. On the other hand, depolarization of the fundamental beam incident upon a Type II/Type II design significantly affects the efficiency of the doubling crystal, which in turn strongly impacts the energy mix ratio delivered to the tripler. As the dashed curve in Figure 12-6 shows, Type II/Type II third harmonic generation is extremely sensitive to depolarization. Harmonic generation experiments on Nova show that repolarization of the beam is necessary to achieve high efficiency with a Type II/Type II scheme. This, in turn, requires high damage threshold polarizers, which add B-integral and cost to the overall system.

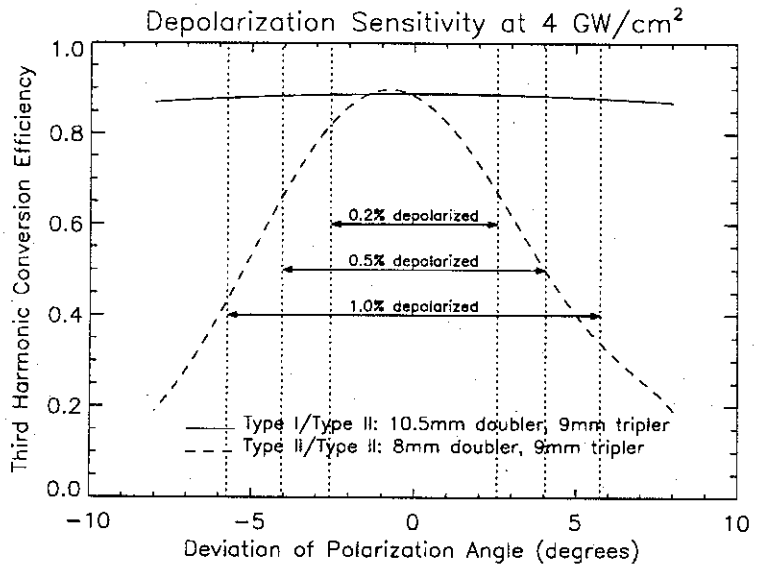

Figure 12-6 **Sensitivity of third harmonic generation to depolarization of incident fundamental beam at input intensity of 4 GW/cm². Dotted vertical lines indicate 0.2%, 0.5%, and 1.0% of the incident energy in the wrong polarization.**

The other primary reason for selecting Type I/Type II over Type II/Type II is the size of the crystal boules required to produce harmonic generator plates. Figure 12-7,12-8 and 12-9 depict the oriented crystal plates for Type I SHG, Type II THG (Type I/Type II), and Type II SHG/THG (Type II/Type II). The polarization mismatch scheme that is used for mix ratio control in a Type II/Type II third harmonic generator is implemented most simply by rotating the harmonic generation crystals by 35.26° relative to the polarization of the incident beam. Together with a square beam cross section, this increases the size of the boule required to produce harmonic generation plates of the required size for Type II/Type II. If, instead of rotating the crystals, the incident beam polarization was rotated 35.26°, the boules required to produce crystals for the Type II/Type II scheme would be the same as for the Type I/Type II scheme. Rotating the beam polarization, however, requires a full aperture, high-fluence waveplate. Adding such a component increases the B-integral of the system as well as increasing the cost due to the additional substrate material and finishing.

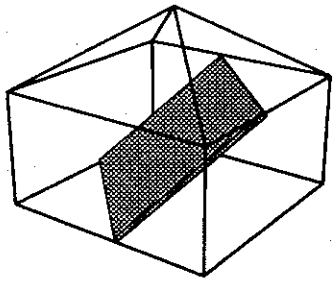

Figure 12-7 37 cm square Type I second harmonic generation crystals require a 46 cm square KDP boule

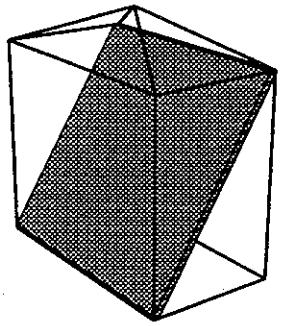

Figure 12-8 37 cm square Type II third harmonic generation crystals for Type I/Type II require a 37 cm by 21 cm KDP boule

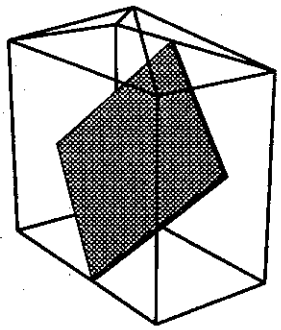

Figure 12-9 37 cm square Type II second and third harmonic generation crystals for Type II/Type II require a 28 cm by 52 cm KDP boule

12.6 *Harmonic Generation Development*

The proposed harmonic generation development program for NIF consists of two parts: 1) investigating alternate converter designs that show the promise of a larger dynamic range and a higher peak power conversion efficiency and, 2) validation of the performance of the baseline Type I/Type II converter design.

We intend to invest development funds to develop and test converter schemes that show the promise of having a larger dynamic range and a higher peak tripling efficiency than the baseline Type I/Type II scheme. For example, Henessian[12] and Eimerl[13] have proposed four crystal tripling designs based on quadrature or alternating z arrangements that show the promise of increasing the dynamic range of the converter by a factor of more than two relative to the baseline design. Eimerl[14] has suggested that improved performance can also be achieved with non collinear phase matching schemes by carefully controlling the energy of the two pump beams in the mixer crystal. It is also believed that improved performance can be achieved by using different crystal materials such as rubidium dihydrogen phosphate (RDP) instead of KDP, albeit it at higher schedule risk and development cost.

These alternate designs would be ranked in terms of improved conversion efficiency, development cost and schedule risk. The ranking by performance would be done using plane wave computer models to calculate the tripling efficiency as a function of the phase matching variables and the mix ratio. The priorities of the experimental program necessary to validate the performance would be determined by this ranking.

Validation of the baseline Type I/Type II design would be accomplished by doing more detailed calculations of its performance and confirming the code predictions with experiments. For example, the deformation and stress of the crystals caused by gravity loading would be calculated using a finite element code. The data produced in this analysis would then be used to assess the effect that the crystal's gravity sag had on phase matching. If these calculations showed that gravity sag caused an unacceptable degradation in the performance, we would determine by calculation and experiment which of several potential solutions to this problem would be implemented. Possible solutions are the use of continuous or semi-continuous supports instead of point supports for the crystals, bonding the doubling and mixing crystals together to provide a stiffer monolithic structure, applying a small pressure differential across each crystal to compensate for the gravity sag, or developing a UV reflective coating for the beam transport mirrors that would eliminate the gravity sag of the crystals because they could now be installed at the end of the laser with their large surfaces perpendicular to the force of gravity.

REFERENCES for Section 12.5–12.6

[1] R. S. Craxton, *Theory of High Efficiency Third Harmonic Generation of High Power Nd-Glass Laser Radiation,* Optics Communications, 34, 474 (1980).

[2] R. S. Craxton, *High Efficiency Frequency Tripling Schemes for High-Power Nd:Glass Lasers,* IEEE J. Quantum Electron, QE-17, 1771 (1981).

[3] R. C. Eckardt and J. Reintjes, *Phase Matching Limitations of High Efficiency Second Harmonic Generation,* IEEE J. Quantum Electron, QE-20, 1178 (1984)

[4] D. Eimerl, *High Average Power Harmonic Generation,* IEEE J. Quantum Electron, QE-23, 575 (1987).

[5] M. A. Henesian, P. J. Wegner, D. R. Speck, C. Bibeau, R. B. Ehrlich, C. W. Laumann, J. K. Lawson, and T. L. Weiland, *Modeling of Large Aperture Third Harmonic Frequency Conversion of High Power Nd:Glass Laser Systems,* Modeling and Simulation of Laser Systems II, SPIE Proceedings 1415 (1991); Lawrence Livermore National Laboratory, Livermore, CA, UCRL-JC-104439 (1991).

[6] F. Zernike, *Refractive Indices of Ammonium Dihydrogen Phosphate and Potassium Dihydrogen Phosphate between 2000 A and 1.5 m,* J. Opt. Soc. Amer., 54, 1215 (1964).

[7] P. J. Wegner, M. A. Henesian, D. R. Speck, C. Bibeau, R. B. Ehrlich, C. W. Laumann, J. K. Lawson, and T. L. Weiland, *Harmonic Conversion of Large Aperture 1.05-mm Laser Beams for Inertial Confinement Fusion Research,* Applied Optics, 31, 6414 (1992).

[8] C. E. Barker, D. Milam, and R. Boyd, *High Fluence Third Harmonic Generation,* scheduled for publication in ICF Quarterly vol. 3, no. 2, January - March 1993 93-2; also distributed as LLNL internal memorandum BLT-FC-93-01, April 29, 1993.

[9] J. R. Murray, *Beam divergence budget (preliminary) with digressions on frequency conversion,* LLNL internal memorandum M30526-1, June 1, 1993.

[10] Bob Ehrlich, *Issues Involved with Specifying KDP Crystals for Frequency Tripling Noncircular Beams,* LLNL internal memorandum, September 20, 1990.

[11] D. Eimerl, *Electro-Optic, Linear, and Nonlinear Optical Properties of KDP and Its Isomorphs,* Ferroelectrics, 72, 95 (1987).

[12] M. Henesian,*Four Crystal Third Harmonic Generation: A Dynamic Range and Polarization Bandwidth Extender for the the Third Harmonic*, LLNL internal memorandum 9037R, December 11, 1984.

[13] D. Eimerl, M. A. Summers, B. C. Johnson, J. D. Williams, and G. J. Linford, *Harmonic Conversion*, 1981 Laser Program Annual Report, LLNL UCRL-50021-81, pp7-1 to 7-12; August, 1982. D. Eimerl, *High-Dynamic-Range Frequency Conversion*, 1983 Laser Program Annual Report, LLNL UCRL-50021-83, pp6-69 to 6-74; June 1984. D. Eimerl, *Quadrature Frequency Conversion*, IEEE J. Quantum Electron, QE-23, 1361 (1987).

[14] D. Eimerl, *High-Dynamic-Range Frequency Conversion*, 1983 Laser Program Annual Report, LLNL UCRl-50021-83, pp6-74 to 6-77; June 1984. K. R. Manes & D. Eimerl,*Non-collinear phase matched tripling for the NOVA Upgrade*, LLNL internal memorandum, April 27, 1992.

Chapter 13

ALIGNMENT / SYSTEM DIAGNOSTICS

13.1 *Subsystem requirements and design concepts*

13.1.1 *General*

Preliminary designs suppose that NIF will use a non-rigid space frame which requires typical beam alignment functions for centering, pointing, and collimating. The large number of beams dictates automation of these functions. However, Nova experience shows operator verification and over-ride capability for all functions is highly desirable. To reduce alignment time, tasks should be performed in parallel. For example, independent target and laser alignment systems should allow those systems to be aligned in parallel. Multiplexing hardware/software over several beams is necessary to keep costs low; one sensor at the target location should sense pointing for all the beams. And within a single beam, hardware should be used for several functions. For example, one camera in the output spatial filter can view all the pinholes in the multipass amplifier. Since power balance and beam quality on target are critical, accurate measurements of beam energy ($\pm 5\%$), high resolution power monitors (30 ps), and near-field beam imaging are needed at several locations on each beamlet. For those instruments requiring calibration, automated procedures are important for consistency and archival.

13.1.2 *Modular hardware*

Certain basic functional capabilities are required at multiple locations in each beamlet, and some are common to the alignment and diagnostic tasks. A modular development seems appropriate, with the following functional building blocks:

- **Generating a laser alignment beam:** The output from the regenerative amplifier serves as the standard alignment beam. A ~ 10 mJ pulse repeating at more than 0.2 hertz is specified. Portable alignment laser(s) are available for backup.

- **Centering beams through amplifiers:** Fixed cameras located behind mirrors that transmit a fraction of a percent provide images for measuring beam position. We determine centering errors by comparing a signature in the center of the beam with a local position reference. The beam signature is created, for example, by inserting an obscuration in the preamplifier beam (see Figure 13-1). A spatial difference in shadow location on the camera and the pre-established software reference indicates an error in beam centering. Beam centering is required to within $\pm 1\%$ of the beam aperture. Since the beams are square, beam rotation must be controlled to ± 5 mr. Mirror motors are moved to correct a beam translation error, and the beam apodizer in the preamplifier is rotated to correct a beam rotation error.

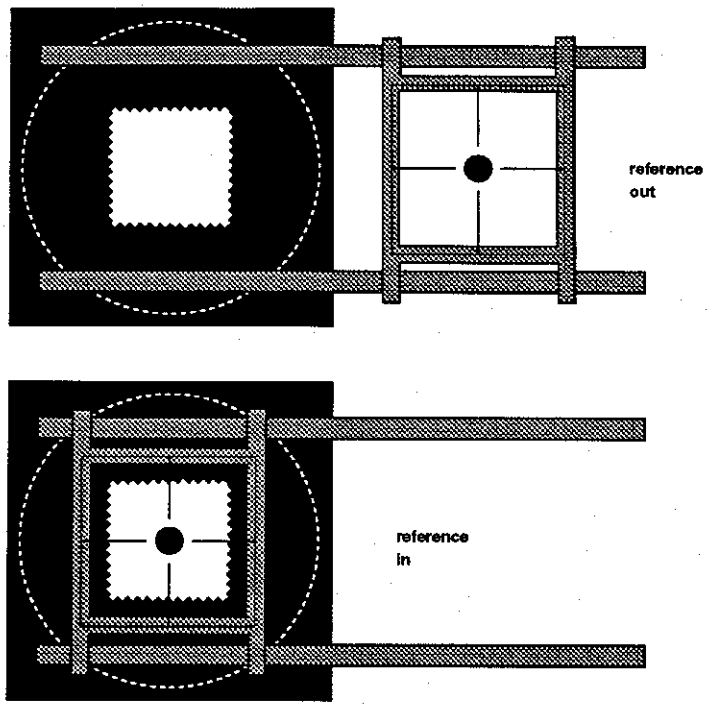

Figure 13-1 Beam center is marked with an insertable reference.

- **Pointing beams through pinholes:** Fixed pinholes in the spatial filters are used as pointing references, and the beam is pointed to pass through the pinhole. The relative location of a beam to a pinhole is sensed with a camera inserted into the beam path (see Figure 13-2).

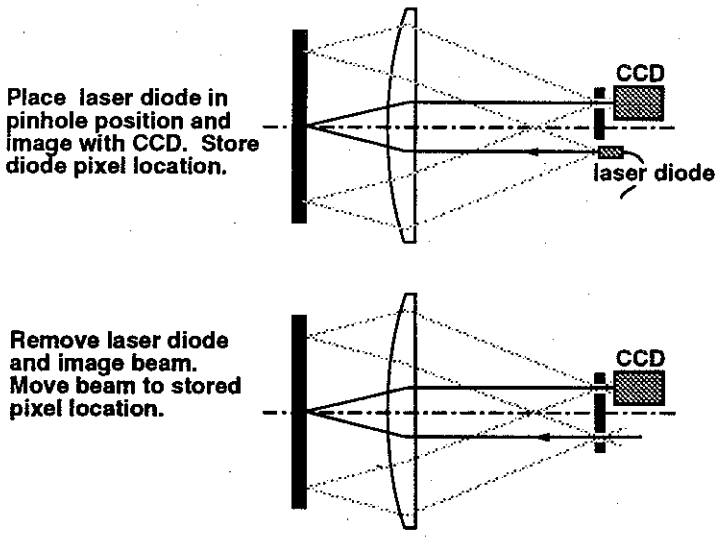

Figure 13-2 A camera senses the beam pointing through fixed pinholes.

An inserted laser diode first identifies the pinhole location in the camera field of view. Then a transparent screen replaces the diode, and the beam position is viewed by imaging light scattered off the screen. Mirrors are adjusted to point the beam through the pinhole to an accuracy $\pm 10\%$ of pinhole diameter.

- **KDP tilting:** To measure KDP tilt relative to the beam, the position of the 1ω beam reflected from each KDP crystal is compared to the location of the incoming beam in the output spatial filter pinhole plane. A reticle referenced to the output pinhole position identifies the correct position for each back-reflected beam, and a camera images the beams on the reticle to determine the tilt error (see Figure 13-3).

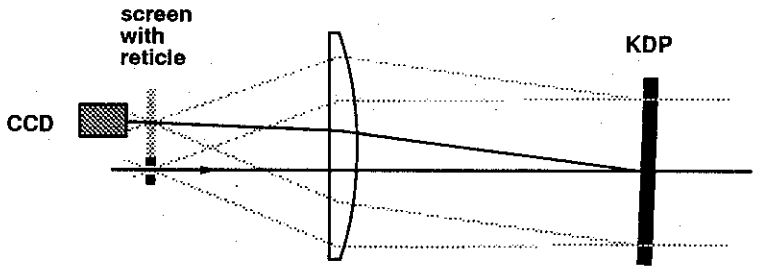

Figure 13-3 Separation of incoming and reflected beams sets KDP tilt.

- **Injecting target alignment beams:** A laser beam fiber accurately offset from the 1ω output pinhole position in the output-spatial filter pinhole plane introduces the target alignment beam (see Figure 13-4). This beam has a wavelength intermediate between 1054 and 351 nm. The specific wavelength is chosen such that the dispersion of the 1ω spatial filter lens and the dispersion of the 3ω target chamber focusing lens cancel for the intermediate wavelength. The alignment beam originating in the pinhole plane therefore comes to focus at the correct distance from the chamber focus lens. When introduced at the correct offset position, it also comes to focus at the correct transverse position in the chamber. Since the laser and target areas are aligned independently, optical registration of the two parts of the system must be accomplished to better than the accuracy required by the tolerance for beam position on target, i.e. less than $7\,\mu$r. Therefore, the fiber offset position and the positioning of the 1ω output beam in its pinhole must be accurate to $< 100\,\mu$m.

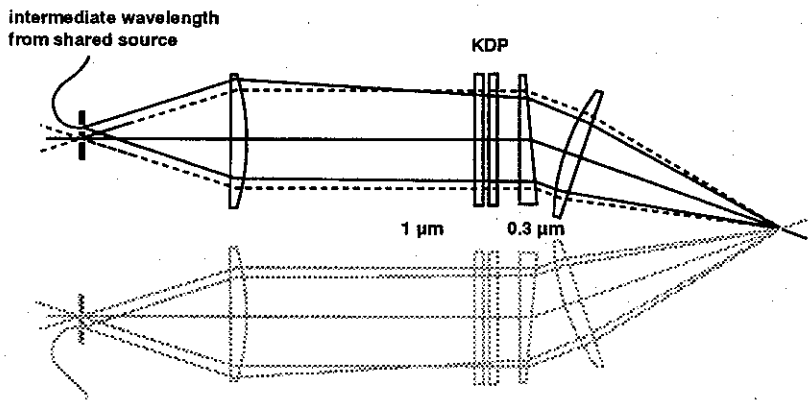

Figure 13-4 The wavelength of the target alignment beam is selected so that its focus is reimaged in the target plane.

- **Target alignment:** The Beam And Target Sensor (BATS) is inserted into the target chamber center as a single reference and sensor for target alignment. It provides images for target and beam positioning and serves as a common reference for target diagnostics alignment. The BATS is about 15 cm in diameter and views the target with three cameras. The beams, which reflect off mirrors onto these cameras, are aligned onto an image of the target without actually illuminating it (see Figure 13-5).

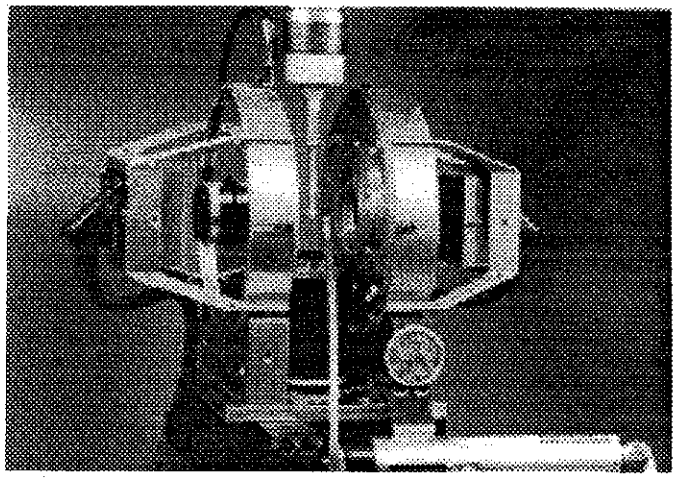

Figure 13-5 The Beam And Target Sensor is the reference and sensor for beam pointing and target alignment.

- **Beam sampling:** Reliable samples of beam energy and spatial profiles are required at several locations in the beam path. At small apertures, small angle of incidence beam splitters (leaky mirrors) with provision for insertable calorimeter calibration serve this purpose. At large apertures, low efficiency diffraction gratings incorporated in the surface of existing large aperture substrates direct low energy samples of the beam to measurement locations. For example, 1ω energy is sampled using a diffraction grating on the last lens of the output spatial filter and measured by a small calorimeter (see Figure 13-6). The expectation is that the fraction extracted from the beam by these gratings is measured off-line and remains stable for long periods of time. Fabrication techniques and performance characteristics of diffraction gratings will be investigated as part of the component development program.
- **Measuring integrated energy:** For evaluating relative performance and troubleshooting, integrated energy measurements are taken throughout the system. The detectors (probably photo diodes) require an accuracy of $\pm 5\%$.

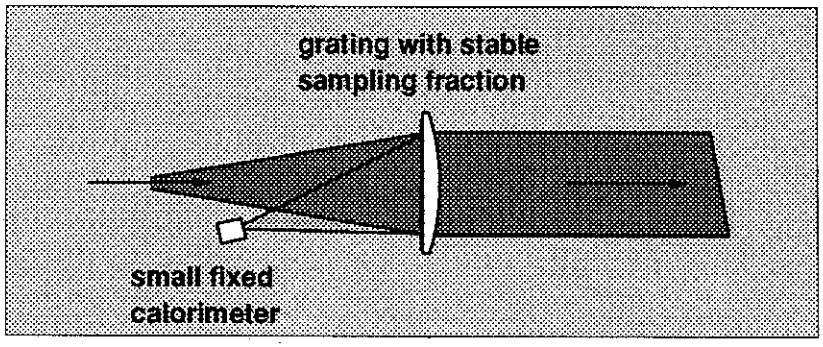

Figure 13-6 Holographic gratings are used to collect large-aperture energy samples.

- **Measuring power of the pulse:** Energy measurements over many short time intervals (30 to 100 ps) are needed to compare the power incident on target from all the 3ω beams. The allowable deviations from exact power balance dictate a sensing device which can take 200 to 400 samples per pulse with a dynamic range of 1000. It is desirable to measure the time resolved power in at least two 1ω beam locations in each beamlet as well. These measurements ultimately provide input for closed-loop front-end adjustments in pulse shape and amplitude.

- **Alignment controls:** The Optical Device Controller (ODC) is the primary element for distributing control to standard alignment stepping motors and binary devices. The alignment control system has approximately 12,000 interfaces. A 90% loaded 21-slot ODC can accommodate 128 motor channels, i.e. one ODC for every two beamlets, or 96 total. An additional ODC unit interfaces target chamber positioning systems including high power motors. Incremental procurement cost for a single motor control channel is approximately $520.
- **Diagnostic controls:** The Beam Diagnostic Processor (BDP) is the primary element for distributing controls for temporal diagnostic digitizers, energy diodes, calorimeters, and power meters. The number of energy sensors is estimated at 2400, and one BDP unit can support up to 200. Therefore, there is approximately one BDP unit per beamline. Incremental procurement cost for a single integrating diode or calorimeter channel is approximately $400. Temporal diagnostic and power meter channels are much more expensive.

13.1.3 *Alignment and diagnostic subsystems*

Each beamlet is conceptually divided into three subsystems: (1) preamplifier, (2) multipass injection and propagation, and (3) output transport and target chamber. We are anticipating that each beamlet will require nine cameras, five integrating energy sensors, and three power sensors. More elaborate designs may be able to reduce the number of cameras, but well-defined sensor modules with predictable costs were used for the current conceptual design.

- **Preamplifier:** Alignment tasks begin where the beam exits the fiber from the master oscillator (see Figure 13-7). The regenerative amplifier is assumed to be stable, requiring infrequent alignment maintenance. However, the position of the beam-shaper/apodizer relative to the regen output is under automatic alignment control. The centering reference is located adjacent to the shaper. The beam is centered at the entrance to the multipass rod amplifier using camera 1 and the centering techniques described above. Pulse energy is also measured in this location. The beam is pointed through the rod spatial filter using camera 2 and the pointing techniques described above. A power measurement is taken at the rod output.

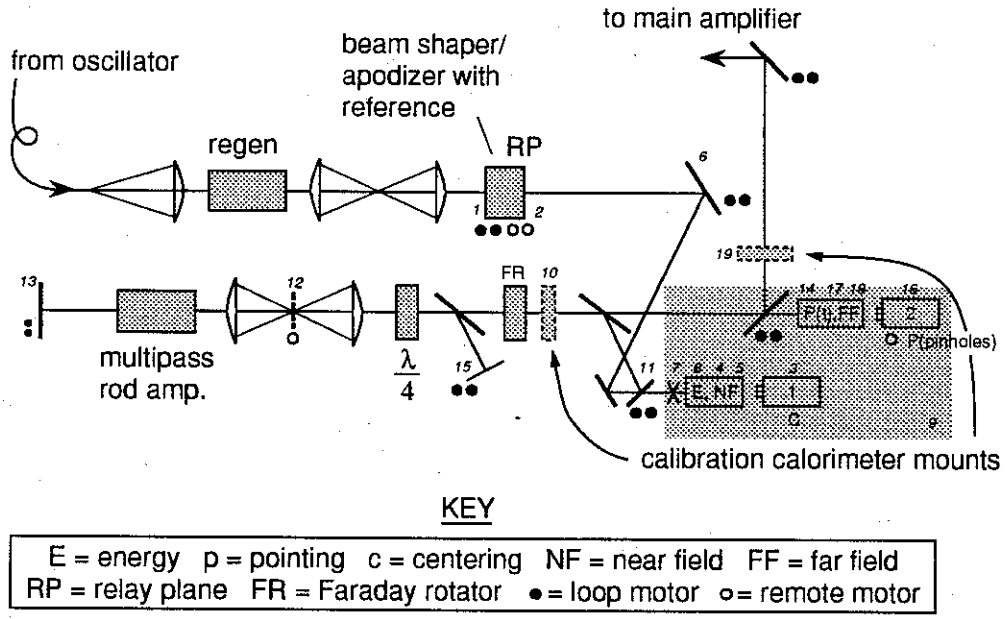

Figure 13-7 Alignment and diagnostic hardware in the preamplifier subsystem

- **Multipass injection and propagation:** The beam is injected into the multipass amplifier by reflecting it off a small mirror in the output spatial filter (see Figure 13-8). Camera 3 monitors pointing of the alignment beam through pinhole 1, and camera 4 views beam centering in the booster amplifier. Mirrors in the injection system are adjusted to correct the pointing and centering of the injected beam. Since the Pockels cell switch is off, the alignment beam reflects off the polarizer, passes through the cavity, and again reflects off the polarizer to focus at pinhole 2 in the output spatial filter. Thus, camera 3 can be positioned to also sense the pointing through pinholes 1 and 2 in the cavity spatial filter. Camera 5 senses the centering through the laser cavity. To simulate pass three and four, the polarization of the alignment beam is changed to pass through the polarizer. This polarization change is accomplished by tilting the switch crystal by about 27 mr, i.e. the switch becomes a passive quarter wave plate. Since the beam is attenuated by a factor of two for each pass through the tilted switch, one sixteenth of the alignment beam energy goes through all four passes of the amplifier. A grating on the mirror at the Pockels cell end of the cavity directs a near-field beam sample to camera 6 and to an integrated energy sensor. The other cavity mirror is deformable to correct for pump induced wavefront distortion in the beam. The beam exits the multipass on pass four, and focuses at pinhole 4 in the output spatial filter. Again camera 3 images the beam in the pinhole plane. Pointing accurately through the pinhole also co-aligns the laser and target alignment beams since the target alignment beam injection fiber is attached to the pinhole mechanism (see Figure 13-9).

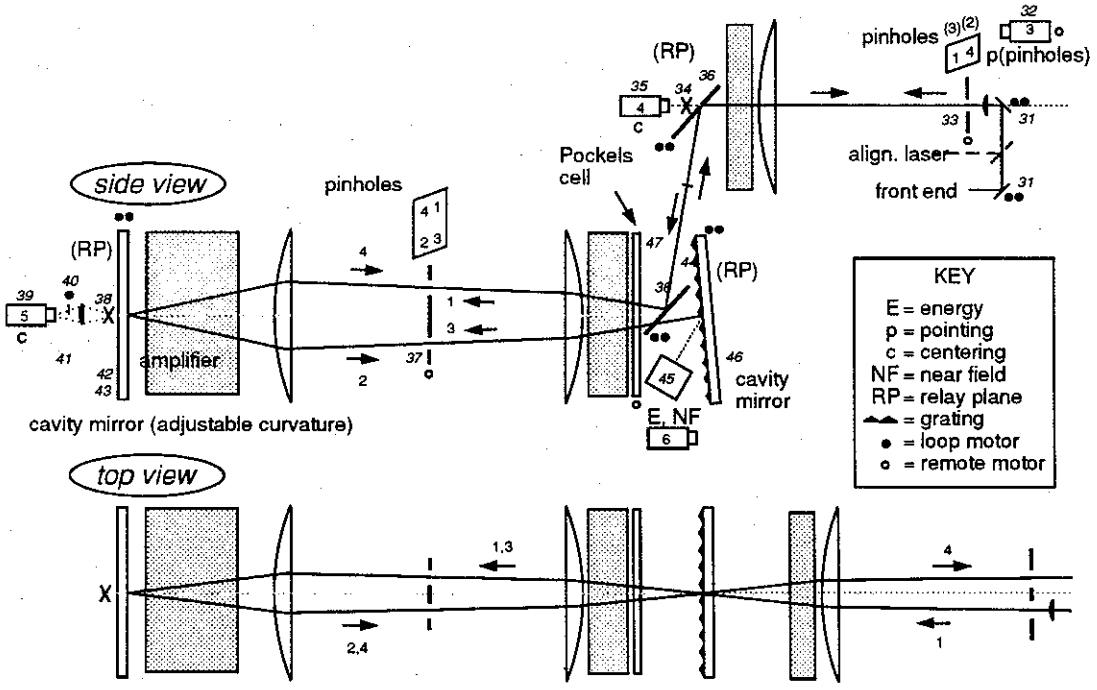

Figure 13-8 Alignment and diagnostic hardware in the multipass amplifier subsystem.

- **Output transport and target chamber:** The turning mirror after the output spatial filter tilts to center the 1ω alignment beam on the KDP crystals (see Figure 13-9). Camera 8 views an image of the beam in the KDP plane using light reflected from the first crystal. To obtain the precise KDP tilt angles relative to the beam, the crystals are tilted until their focused reflections are positioned at the proper reticle location as seen by camera 3 in the output

spatial filter. In preparation for aligning beams into the target chamber, the BATS is inserted at chamber center with $\pm 100\,\mu$m repeatability, and target diagnostics are aligned to it. By moving the final focusing lenses and viewing with the BATS, the target alignment beams from the output spatial filters are pointed onto the proper location with respect to the target, which is also positioned using the BATS cameras.

During a shot, beam diagnostic information at all three wavelengths is collected in the output spatial filter. A grating on the last lens of the spatial filter directs a 1ω beam sample to camera 7 for near field imaging and to diodes for pulse energy and power measurements. The output wavefront is also monitored here. Reflections from the KDP crystals are collected near the pinhole plane to obtain energy information on 2ω and 3ω conversion. The 3ω signal is time resolved for monitoring the power delivered to the target. Camera 9 images the 3ω near-field as reflected off the KDP tripler. At the target chamber a grating on the vacuum window directs a 3ω sample into a calorimeter. This energy reading is used to calibrate the 3ω power data in the spatial filter.

Visible damage to the debris shield and other final optics is inspected by inserting a light source at chamber center and viewing the components with camera 8 in the output spatial filter. Changes in transmission of these optics are periodically checked by inserting an array of diodes in the target chamber to measure the alignment laser power reaching chamber center.

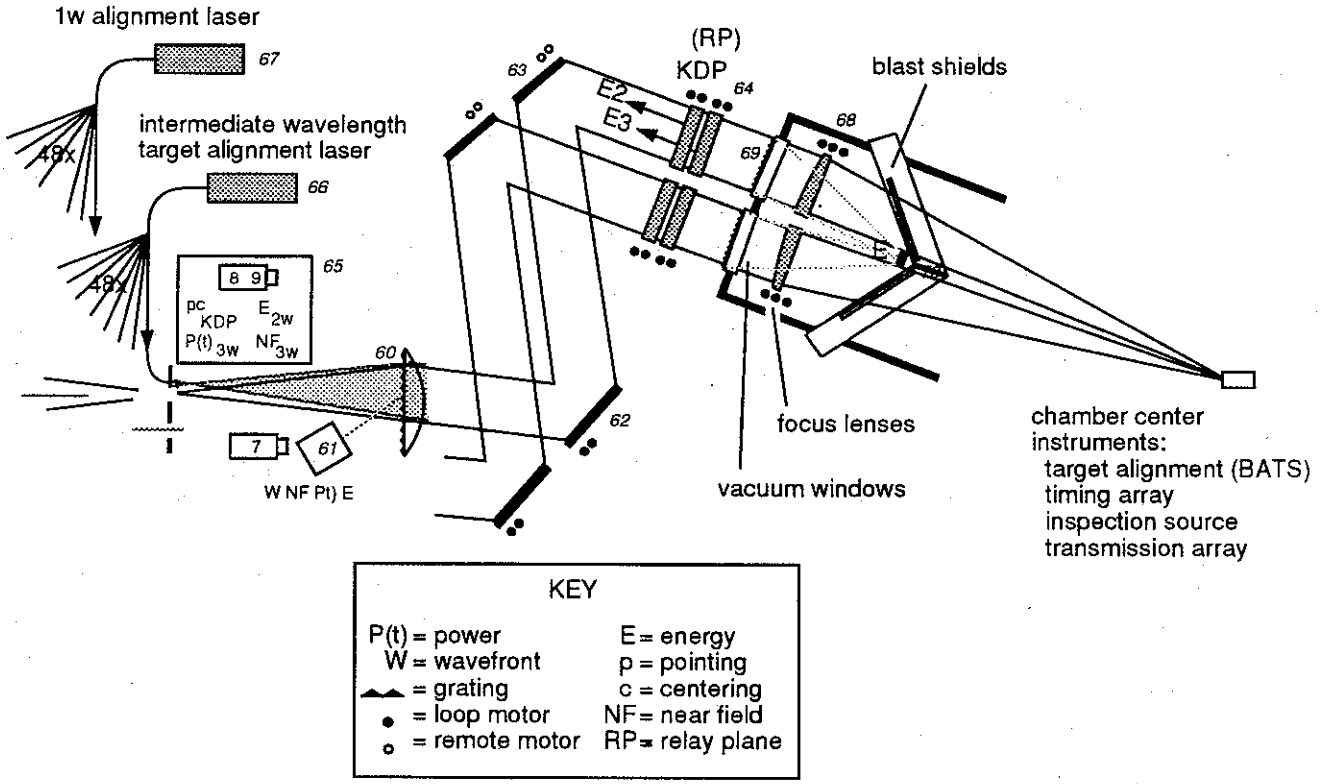

Figure 13-9 Alignment and diagnostic hardware in the output transport and target chamber.

13.2 *Fixed and marginal costs*

The total estimated cost for the alignment and diagnostic system is $45.2 M. That portion associated with the center of the target chamber is a fixed cost since it doesn't depend on the number of beamlines. The rest of the cost does scale directly with the number of beamlines. Costs are summarized by subsystem in Table 13-1.

Table 13-1 Cost summary for alignment and diagnostics.

	Labor ($K)	Material ($K)	Total ($K)
Preamp	2562	3993	6556
Main Amp & beam transport	6622	7097	13719
Target Systems	11758	3434	15192
Alignment Control	1002	6267	7269
Diagnostic Control	788	1685	2473
Total	22733	22476	**45208**

13.3 *Component development strategy*

Nine components have been identified for a development program in order to achieve the cost breakdown in Table 13-10 . We anticipate using the facilities and operations staff of the Beamlet Demonstration Project for testing.

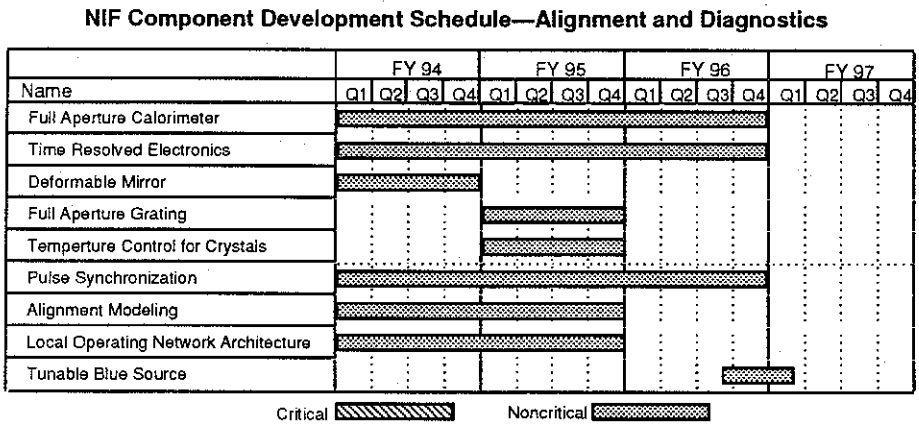

Table 13-2 Alignment and Diagnostics component development schedule.

13.3.1 *Full aperture calorimeter for frequency converted beam*

A full energy calorimeter is required to measure target chamber energy directly during shots or to calibrate reflected sample measurements. Feasibility analysis for each of several proposals is needed with proof of concept testing. This has been suggested to be a Los Alamos task.

13.3.2 *Time resolved power and data processing/power balancing electronics*

Specifications for beam power balance dictate about 200 to 400 samples per pulse with a dynamic range of 1000 and a timing accuracy of 30 psec. Several approaches have been recommended; however, all need more development. One solution for sampling is use of fast photo-diodes and

solid-state digitizers. The photo-diodes are available, but digitizers are prohibitively expensive. Digitizer development plans may reduce system cost to $3 M for one pulse shape measurement per beamlet, but several measurement locations per beamlet are likely. To obtain and verify power balance for all beams on target requires time resolved measurements of the frequency converted outputs. As a practical matter, it would be desirable to accomplish power balance at the laser output first without sending light to the target chamber. If the pulses are also monitored in the front-end, the system cost of measuring at these three locations approaches $10M. Because of the large amounts of data, analysis must be automated and corrections to the front-end pulse shapes must be accomplished by a closed-loop system.

13.3.3 *Cavity deformable mirror for astigmatism*

Wavefront correction is required in the laser cavity to cancel pump induced aberrations. A fixed correction is probably not sufficient because it would degrade the alignment beam when the amplifiers are not pumped.

13.3.4 *Full aperture grating for beam sampling*

A reliable means of obtaining full aperture beam samples is needed for energy measurements and beam imaging. A grating beam sample may be inherently stable with respect to temperature, humidity, and age eliminating the need for an on-line system to calibrate these devices. Activities should be coordinated with AVLIS work in this area.

13.3.5 *Temperature control for KDP frequency conversion crystals*

Peak conversion angle varies at approximately 200μrad/°K. The most direct way to insure high conversion efficiency is to control temperature. Room temperature control is not adequate because of local heat sources.

13.3.6 *Pulse synchronization*

The components described in 13.3.2 will acquire data with sufficient temporal resolution to balance power between beamlets. However, absolute temporal registration of these high resolution data must also be achieved. This requires a very short pulse source, chamber center detector system, a time marker generator with better than 30 psec accuracy incorporated in the facility timing system, and software to combine the chamber center, beamlet power balance, and time marker data.

13.3.7 *Alignment modeling and validation on Beamlet or other NIF simulator*

Proof of concept for alignment and diagnostic hardware is needed, i.e. field of view, signal levels, image quality etc.. Algorithm development for video processing should be pursued in parallel.

13.3.8 *Local operating network architecture for diagnostics data processing*

This is the present preferred choice for low cost handling of diagnostic data. Alternative approaches should also be considered.

13.3.9 *Tunable blue source for intermediate wavelength alignment beam*

It is expected that commercial frequency doubled diode lasers will be on the market in a year

or so. Purchase and testing of at least one of those lasers is recommended.

13.3.10 *Antireflection coated laser slabs*

This would allow the use of small diameter polarization rotators in the spatial filter plane to pass and align an alignment beam through all four passes of the multipass amplifier with negligible loss and without tilting the Pockels cell switch. It could also improve amplifier pump efficiency. This item is included in the optic components development plan.

Chapter 14

INTEGRATED CONTROLS

The NIF Integrated Computer Control System is responsible for consolidating all laser and target area distributed subsystems using networks, work stations, file servers, graphics displays, and considerable software. In addition to the computer system, this WBS area includes a large television distribution network and the automatic alignment system. As a general requirement, the control system must provide coordinated operation of the facility from a central control room utilizing a staff of 6 technicians and a shot director.

Software for the four major subsystems of power conditioning, laser alignment, laser diagnostics, and target diagnostics was sufficiently designed to identify processes and interfaces. This was used to estimate software engineering labor and to propose a strategy for achieving improved design commonality as discussed in the components development section.

Two subsystems were moved into Integrated Controls from other areas. Elements of the fiber-optic distributed master timing and trigger system were combined from three separate subsystems. The facility safety interlock system and the personnel access control system were transferred from WBS 2.

This design draws from relevant work performed at several laser laboratories. The Nova Controls Upgrade Project gave fresh application-domain experience using modern tools such as Ada, Motif graphical user interface (GUI) design, and message-based client-server software architecture. The Omega Upgrade is providing large scale experience in modern embedded controller networks based on the Echelon LONWorks^{TM} system. The AVLIS project has amassed similar tools experience and real-time VME-bus processors such as the reusable Optical Device Controller (ODC).

14.1 *System architecture*

The NIF control system is constructed from a highly-distributed computer system interconnected by information networks. The system is further characterized by the layered architecture shown in Figure 14-1. In general terms, the control layers ascend from pure hardware to pure software elements, with each layer exhibiting increasing functional complexity and level of integration. The architecture is grouped into an upper- and lower-level computer system. This model is used as the basis for evolving improved top-down and bottom-up assessment of the design. Each subsystem was overlaid on the model and examined for performance bottlenecks.

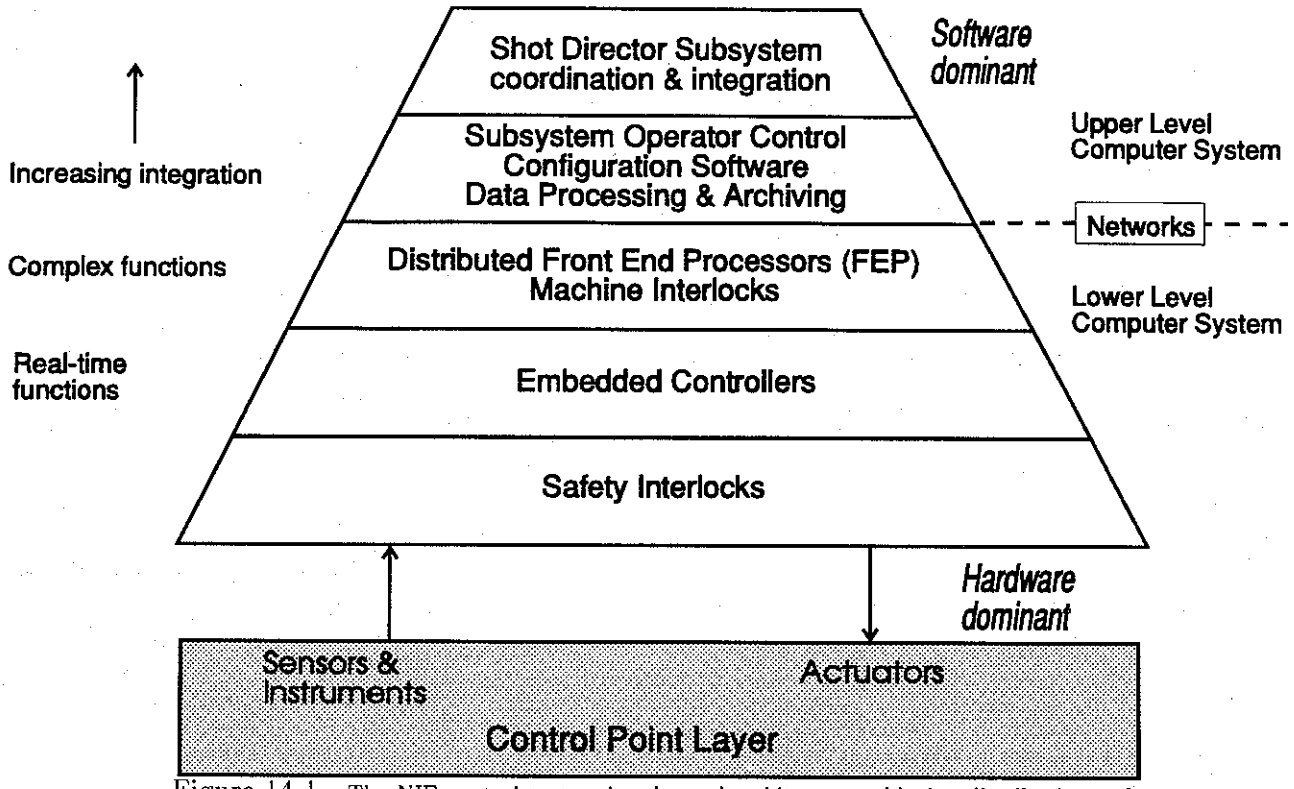

Figure 14-1 The NIF control system is a layered architecture achieving distribution and leveraging commercial technology.

In the lower-level computer system, the bottom layer consists of approximately 35,000 control-points connecting to laser and target subsystem components (Table 14-1). The safety interlock layer is incorporated where needed directly to prevent personnel hazards. The embedded controller layer consists of microprocessor modules performing real-time functions in both commercial and NIF-designed hardware located in the equipment bays. Distributed front end processors (FEP) interface to numerous embedded controllers and provide more complex control functions as well as connection to the upper-level computer system. To prevent equipment damage, machine interlocks are maintained at the FEP level. Several different FEP implementations account for a large fraction of the overall NIF controls capability and budget.

Table 14-1 Approximate number of control points.

NIF Control Subsystem	Typical Type	Control Points
Alignment	motors	13,000
Laser diagnostics	photo diodes	3,000
Power conditioning	current bugs	15000
Video system	TV sensors	2000
Network processor nodes	FEP	150
Interlocks	redundant I/O	3000
Precision triggers	50 ps	40
Fast triggers	1 nS	800
Slow triggers	100 ms	200

The first layer of the upper-level computer system consists of subsystems providing operator controls, machine status, configuration controls, and data reduction and archiving. The top-most

layer implements subsystem integration and experiment configuration.

The computer system architecture shown in Figure 14-2 provides control functions and graphical user interfaces wherever needed in the facility to meet the dual requirements of centralized controls for experiments and remote controls for construction and maintenance. The upper-level computer system is shown attached to the Fiber Distributed Data Interchange (FDDI) high performance network whereas the lower-level system is shown attached to less expensive local Ethernets. Processors located anywhere on the network can access any other using standard communication protocols.

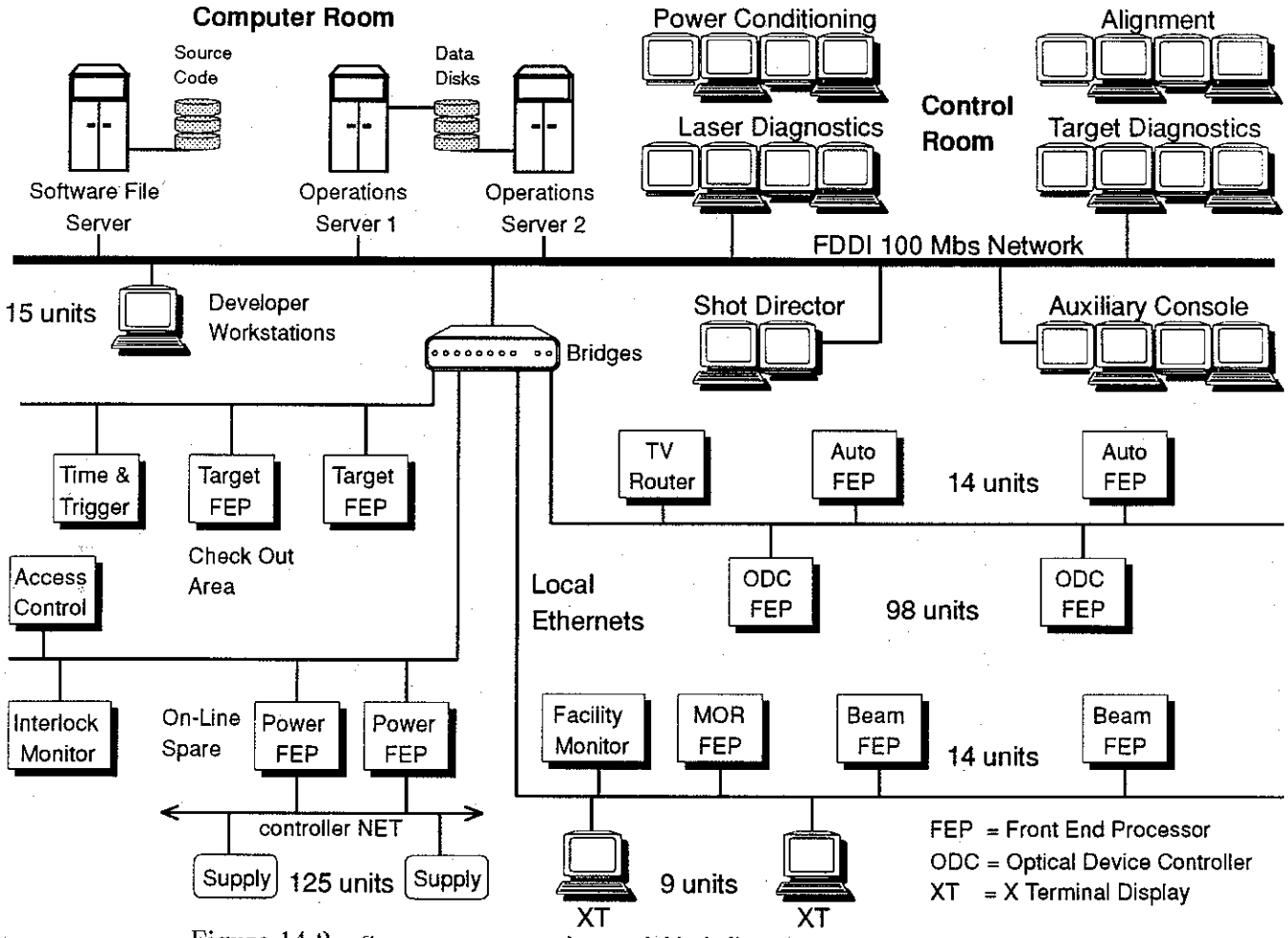

Figure 14-2 Computer system and network block diagram.

Computers on the network access data files from a central operations file server with 10 Gigabytes of disk space. The server is a dual-host configuration that shares the work load and automatically converts to a single server in the event of breakdown. A separate software file server and set of developer workstations segregates software engineering activities from on-line operations until new updates are released.

Operator controls are implemented with graphics workstations adhering to the X-Windows and Motif graphics standards. Four consoles are provided, one for each of the major subsystems. Consoles in the control room offer four display screens and two keyboards along with TV monitors. The fourth screen and keyboard was added in response to requests from Nova operations staff for secondary operator capability. A two screen console serves the shot director. An auxiliary console supplies extra maintenance and calibration support for all subsystems.

The lower-level network attaches to several types of FEP including the TV router, timing

and trigger control, access control, interlocks monitor, and facility monitor. The ODC comprises the largest portion of the network, requiring 98 units. Fourteen Beam FEPs attach to embedded controller networks (see Chapter 13) which collect data from photo diodes and calorimeters. The power conditioning FEP is a gateway to over 100 intelligent power supplies. Local control of FEP systems is achieved by displaying copies of control room GUI software on X terminals placed in the same equipment racks as the processors.

The television distribution system, shown in Figure 14-3, satisfies the primary requirement of routing over 1,700 alignment sensors to the automatic alignment system processors (AAP) and to operator console monitors for manual alignment. Additional capacity is reserved for other facility users. A preemptive switching architecture reduces the total number of cross points without imposing significant constraints. Distribution systems requiring this many inputs are configured using several staged switchers coordinated by routing software.

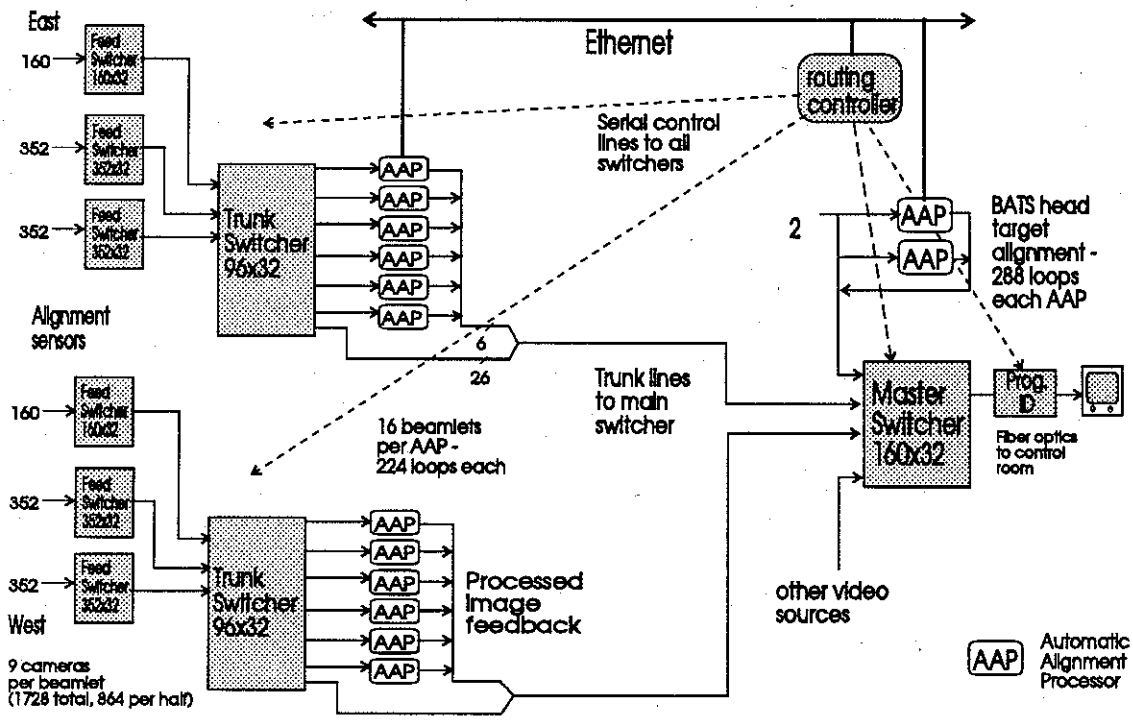

Figure 14-3 Television distribution system

Considerable savings are realized by eliminating hardware-based switcher control panels; GUI controls are easily provided at all operator consoles. The traditional sensor identifier (ID) hardware is placed in series with the (far fewer) monitor output channels and reprogrammed by the routing software. A further improvement is a modular 16-camera sync and power fan-out chassis which greatly reduces sync distribution and sensor installation costs.

The automatic alignment system is required to completely prepare the laser within one hour of the point the laser becomes thermally stable. Image processing is employed to analyze the same sensor images as those observed by operators. Algorithms must be sufficiently robust such that any anomalies are always detected by the software and are few enough in number to be corrected by a minimal crew within an additional 1/2 hour.

The alignment system divides into two parts that are processed in parallel. The first (beam line) portion begins at the point where the beam is air launched from the fiber system and ends at the last spatial filter sensor. The second (target alignment) portion includes pointing and centering for the KDP crystals as well as target pointing and focusing using the target chamber's central

sensor.

Automatic alignment is composed of many iterative loops, each of which is responsible for controlling one active device such as a mirror. These loops have been divided among 14 Automatic Alignment Processor (AAP) units, shown schematically in Figure 14-4. All motorized devices are interfaced to ODC units accessed over the network. Twelve AAP units are assigned to the beam lines, each processing 224 loops covering 16 beamlets. Two more units serve the two target chamber center alignment sensors for an additional 288 loops each. The average time allocated to close each loop is 15 seconds.

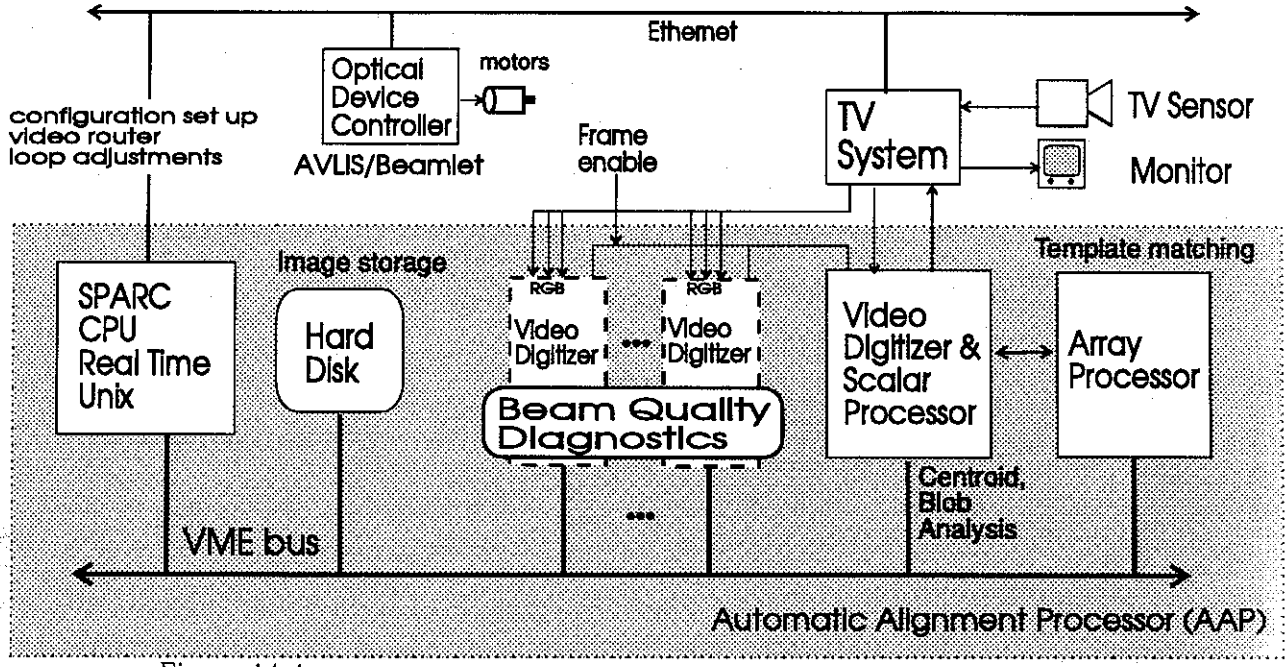

Figure 14-4 Parallel automatic alignment is distributed across multiple image-processing subsystems.

The AAP is a VME-bus system containing a video digitizer equipped with an integral scalar processor capable of analyzing images for location and size of multiple objects (blob analysis). Although most image processing is of this type, a tightly coupled array processor is needed for compute-intensive algorithms such as template matching against reticles or for surface fitting to beam profiles. A real-time UNIX™ CPU controls configuration set up, video switching, algorithm sequencing, and loop adjustment.

Beam quality diagnostics, such as those available with Nova's Big Sky™ system, are conveniently installed in the AAP card cage and share the CPU and hard disk. Large numbers of sensors can be affordably digitized on each system shot by using NTSC digitizers to simultaneously capture 3 monochrome channels in place of color (red, green, and blue). This function does not interfere with automatic alignment.

Upper-level software is organized into five major subsystems, and each is assigned a primary operator console in the control room. All subsystems are centered around elaborate GUI software. Power conditioning, alignment, laser diagnostics, and target diagnostics are directly responsible for operating and maintaining the facility control subsystems, ultimately through messages exchanged with FEPs. Most of the controls functionality and consequently most of the software labor is centered in these areas.

The Shot Director software provides experiment configuration, integration services, and permissives to the four subsystems. Laser shots are initiated by the Shot Director, which also has control over the countdown sequences. This system includes tools for analyzing and displaying

laser performance and for achieving power balance.

The power conditioning software is responsible for power supply configuration, flashlamp performance monitoring, and shot sequence control. It also displays the status of the safety interlock and facility access control subsystems. The alignment software provides manual alignment controls including a virtual joystick, configuration and machine interlocks oversight, and automatic alignment coordination. Laser diagnostics software handles remote diode and calorimeter sensor calibration and configuration, data retrieval, processing, and archival. The target diagnostics software has expanded facilities for flexible instrument integration and configuration, shot data quick-look analysis, and archiving.

The Integrated Timing and Triggering System (ITTS) provides slow, fast, and precision timing and triggering signals via fiber optic cabling to all controls and data acquisition equipment. A Master Timing System (MTS), located adjacent to the laser system master oscillator, is the source of ITTS signals. The computer-controlled MTS contains a precision clock from which all other signals are derived. A signal simulation capability allows most system set-up adjustments to be made without firing the laser. Timing requirements slower than those within a range of ± 1 second are handled by network messages issued by power conditioning sequence software.

The facility monitoring system measures and records temperature, humidity, and fluid flow rate at various locations throughout the facility. These measurements are required because the performance of mirror coatings and frequency conversion crystals is very sensitive to environmental parameters, and laser components can be damaged if they are operated without cooling. Humidity is monitored with thin film capacitive hygrometers. Water flow is checked with simple turbine meters. The sensors are connected to three data acquisition units located in the equipment bays which are attached to the Ethernet via the IEEE-488 instrumentation bus.

The safety interlock system is responsible for monitoring various interlock conditions on doors, hatches, shutters, and other equipment. The design is based on triply redundant fault-tolerant Programmable Logic Controllers (PLC) connected via fiber optic links to remote I/O located in equipment areas. Personal computers (PC) provide operator controls and serve as programming stations for the PLC units. Ethernet connects the PLC and PC units. The cost estimate is derived from an I/O count of 3000 points.

The access control system is similar to equipment successfully installed on Nova. The system tracks entry and egress through monitored doors by sensing special badges carried by all personnel. All transactions are monitored and printed to a log report. A permissive from this system is passed to the safety interlock system to indicate no personnel are present in the bays prior to a laser shot.

NIF control system costs are minimized by strict adherence, where possible, to industry standards in hardware and software. Once in place, these standards form a beneficial environment for future enhancements or upgrades. In addition, design, construction, and maintenance costs are usually lower for equivalent commercial products relative to in-house designed equipment. Part of the initial design process is to identify cost-saving industrial leverage.

14.2 *System costs*

Total system costs for Integrated Controls are summarized in Table 14-2. Costs have been subdivided into marginal and fixed costs to permit scaling for different numbers of beamlets. Marginal costs are, in general, contributed by hardware subsystems with connections extending into the laser bays. Centralized systems such as the computer system and operator consoles are not affected by adding additional beamlets. The cost of adding additional FEP units to Ethernet is included in FEP costs. For software there is only weak coupling to the number of beamlets, and this is attributed to the small amount of installation labor that is expended as beamlets are activated and tested with pre-installed control software.

Table 14-2 Costs for Integrated Control System.

	Labor ($K)	Material ($K)	Total ($K)
Computer	1000	4523	5523
Software	3073	—	3073
Integrated Timing	158	410	568
Integrated Safety	443	404	847
Total	4674	5337	**10011**

The television distribution system cost increases to add 9 cameras per beamlet. Each sensor connection costs about $875 in addition to the camera. Additional cost saving measures are possible given acceptance of more severe operational constraints. The inter-related automatic alignment system requires an additional $40 K AAP unit for every 16 beamlets, or $2.5 K per beamlet.

The timing and triggering system, facility monitor, and safety interlock system contribute smaller amounts to marginal costs, but the access control system cost is fixed.

14.3 *Component development strategy*

The Integrated Control system (WBS 5) consists primarily of commercially available hardware and large amounts of custom software. Design of the remaining hardware elements is considered relatively straightforward. Software engineering accounts for a substantial fraction of the design labor required, and a successful integrated control system is essential to economical operation of such a large facility. For this reason, the following strategy is focused on software development coupled with evaluation of enabling new computer technology.

Evaluation of the upper-level subsystem requirements and software design identified many similar tasks that could benefit from a common engineering approach. Deliverables include software prototypes and proof of performance, reusable software components, and establishment of software frameworks. A framework in this context is a group of code templates and a suite of object-like data definitions intended to be filled out and modified to satisfy unique subsystem requirements. By reducing the prevalence of ad hoc coding styles, design effort and also software quality assurance effort should be reduced.

Figure 14-5 shows generically how NIF subsystem software is organized in a message-based client-server architecture. Client processes in this system are the executive codes that respond to operator inputs from numerous GUI. A few server processes supply services to many requesting clients. Messaging between clients and servers is accomplished over high-speed networks or shared memory depending on where each process resides. Each message is a closed-loop activation, thus each client that initiates an activity subsequently learns whether it has succeeded or failed. Because all processors are interconnected, the entire system's load can be distributed over available processors as needed, and the system can be tuned for effective throughput by reconfiguring processes. Each server process is idle unless acting upon a client request.

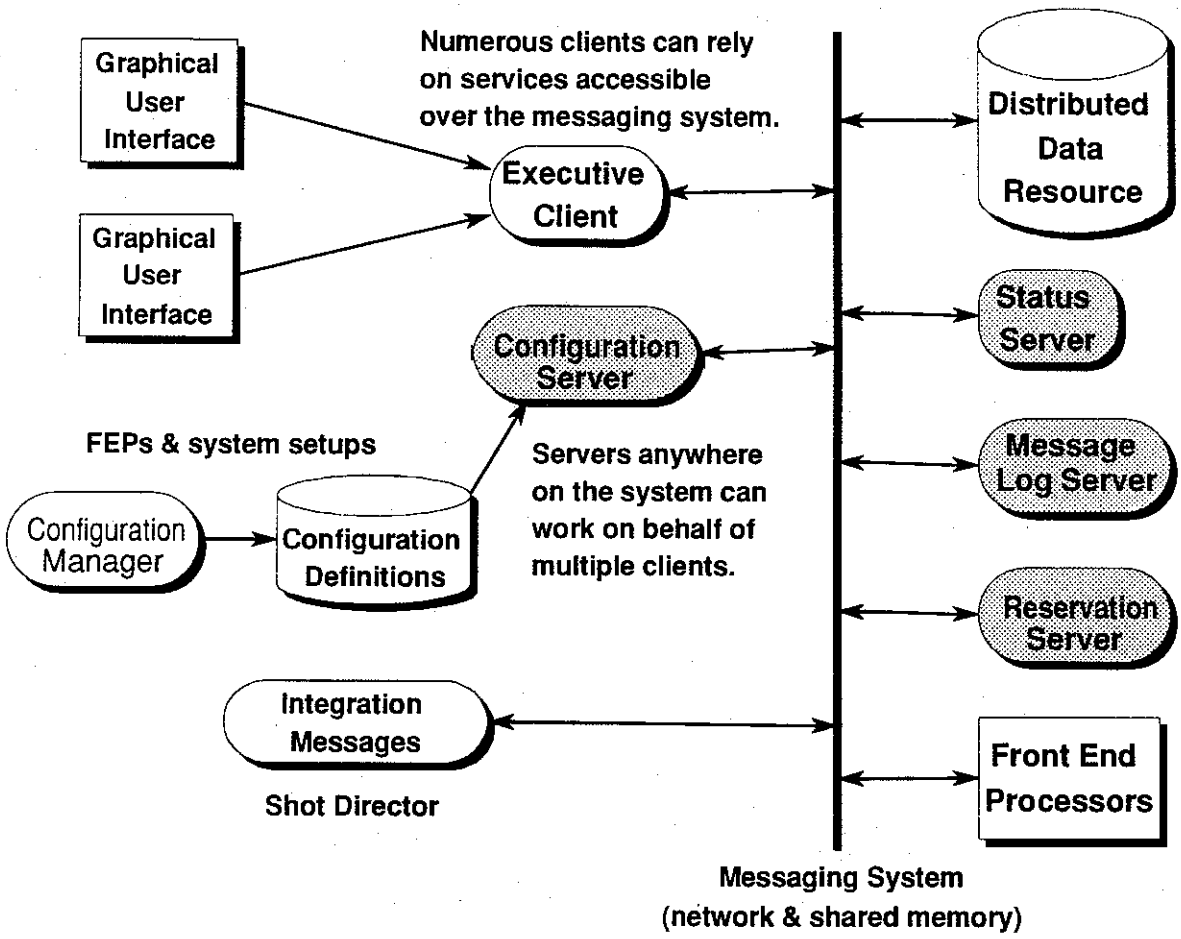

Figure 14-5 Generic upper-level subsystem software block diagram.

The status server, for example, efficiently retrieves and condenses data from FEPs to be viewed on interested GUI displays. The message log server accepts messages from associated clients for a coordinated record of control system activity and alarms. The reservation server implements a scheme for allocating control system devices and services to processes, thus preventing conflicts.

The configuration server acts on client requests to modify the control system in some way. For example, an alignment GUI may request a set of beamlets be set to shot mode. The server retrieves definitions from a simple data base of available configurations. Appropriate commands are sent over the network to ODC units and the results are logged and verified. The data base is edited by operations personnel with help from the configuration manager. The manager is essentially a screen-oriented editor which prevents most operator mistakes.

Another important component of the control system is the distributed data resource. Relatively passive shared data forms an additional coupling between processes. Shared data includes configuration, state, history, and device status. In addition to providing multiple access to common data across multiple processes and computers, the distributed data resource takes care of notifying clients when data has changed. For example, the status server maintains device information using the distributed data resource, which then informs registered clients of changes in the data.

The strategy seeks to develop confidence that the architecture outlined here will support the NIF control system's requirements by executing a program of bench marking on prototype portions of the system. The highest risk lies in the ability of the data resource server to handle the traffic demanded by the status server and GUI processes. The program to resolve this risk involves

building a model, evaluating several potential commercial software components, constructing and testing a prototype, and finally implementing a fully functional data resource server.

The development program will also investigate software available from vendors and other laboratories including software engineering tools, GUI design tools, and operating systems, as well as other software frameworks. In addition, some new hardware is necessary to field prototypes on interesting target computers. These activities begin after the CDR and continue until project funding starts. The program is important to help the design team advance on the requisite learning curve in time to begin detailed design in FY 96.

NIF Component Development Schedule—Integrated Control Systems

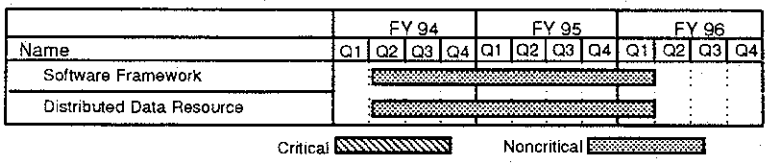

Table 14-3 Integrated controls development schedule.

Chapter 15

OPTIC COMPONENTS

The cost of large optics for the National Ignition Facility (NIF) is expected to reach about $92 M. This cost goal can only be realized after a 4-5 year effort to develop advanced manufacturing technology, to purchase and install the necessary production equipment at vendor sites, and to pilot a production effort (10% of the NIF order) that demonstrates these improved capabilities. The costs for these programs—development, "facilitization", and pilot production—will be detailed in the CDR based on formal vendor estimates. The optics required are of medium size with precision tolerances and high damage thresholds. Although the U.S. optical industry is capable of producing optics to these specifications today (and are, in fact, doing so for the Beamlet Demonstration Project), projected costs for the NIF based upon current production technology would be approximately $276 M, which is deemed to be unacceptably high. Current industrial production capacity is inadequate to meet the project's schedule goals and substantial investments in facilities and training will be required to increase production capacity. About $60 M of the $276 M will be required for this portion of the NIF optics cost.

This situation has been recognized in the ICF program for a number of years. A course of action has evolved over the past several years which has come to be called the Optical Manufacturing Readiness Program. Under this program, detailed analysis and planning have been accomplished with the support and participation of all segments of the U.S. precision laser optics manufacturing industry. This detailed analysis focused on devising credible extrapolations of current manufacturing technology having the potential to reduce production costs by a factor of approximately three, averaged over the full range of optical materials and components required for the NIF. Although the resources for this program have been very limited, key companies in each manufacturing area have been funded to perform their own cost and technical studies. The result has been that in each area these same companies have concurred that the NIF optics manufacturing cost goals could be met with a three year development program.

In parallel with the major vendor contracts to procure the NIF optics, LLNL personnel are required for design, contract management and associated QA activities. This parallel program will cost about $11 M. Oversight is broken down by optical material area rather than by component to take advantage of common issues and vendors. About 2 FTE's are required for each optical materials area which includes scientific, design, and contract oversight. We expect there to be miscellaneous procurement expenses during this period in support of the QA activities. Manpower expenses will be split almost evenly between QA and contract management. The QA expenses include visual inspection and cleaning of 100% of the optics as they arrive at LLNL, and rigorous inspection of 15% of the optics at LLNL, chosen on a statistical basis. This testing includes interferometry, photometry, ellipsometry, stress birefringence, and damage, as appropriate. All of the optics will be source inspected prior to shipment to LLNL. Also included is the cost of laser conditioning of the thin-film coatings and KDP/KD*P crystals.

15.1 *NIF Optics development objectives*

The estimated costs for the NIF optics using current technology and those which make use of advanced technology resulting from a 3 year development effort are summarized in Table 15-1. These costs have been projected using a combination of current prices paid for Beamlet optics and vendor-proprietary cost studies. These costs are for 192 beamlets with 35 cm aperture.

Table 15-1 Comparison of projected NIF optics costs ($M) using current technology and after development.

Area	Projected Cost Using Current Technology	Projected Cost Using Advanced Technology
Laser glass	107	28
KD*P/KDP crystals	42	12
Optics fabrication	63	20
Fused silica	25	8
Polarizer coatings	10	2
High reflectivity coatings	9	4
BK-7 glass	6	5
AR coatings	3	2
LLNL support	11	11
Total	276	92

15.2 *Laser Glass*

All of the cost goals discussed in the remainder of this chapter are for 192 beamlets with 35 cm aperture.

15.2.1 *Cost Impact*

The Nd:phosphate laser glass used in the cavity and booster amplifiers is the largest contributor to optics cost. To meet the NIF schedule goal, the laser glass would need to be produced over a period of three years. The cost of manufacturing facilities and production costs, using current technology, are estimated at $107 M. In addition to this high cost estimate, there is also the problem of not enough adequate trained manpower. Schott Glass Technologies and Hoya are the only two companies in the world currently capable of producing platinum-free laser glass, which is essential for the successful operation of the NIF.

LLNL has worked with both these companies for many years on concepts for reducing the cost of producing high quality, platinum-free laser glass for an advanced multi-megajoule laser. Based on the results of this research, these companies are now in a position to propose to develop an advanced glass manufacturing technique, based on continuous melting and forming of the laser glass, to substantially reduce the cost of manufacturing.

The cost goal is $28 M. For the laser slabs in the current 11-5-3 amplifier configuration, this represents 3648 slabs. Both companies have stated in formal cost studies that this goal can be

attained with the aid of a three year development program.

15.2.2 *Technical issues*

If the production rate is large enough, continuous melting and forming of glass is intrinsically cheaper than the batch processing method currently used for laser glass production. The quantity of laser glass required for the NIF justifies the transition of production method from batch to continuous processing. However, three significant technical hurdles remain, and they will ultimately determine the cost of laser glass.

The first issue is laser damage due to platinum inclusions incorporated in glass. To produce laser glass of high optical quality, all of its components must be thoroughly mixed, or homogenized, during melting. This homogenization of the glass takes place in a platinum-lined furnace. Despite great care given to avoiding the incorporation of platinum particles from the furnace walls or stirring mechanism, inevitably some particles find their way into the melt. These particles lead to damage in the glass when exposed to laser beams with high fluence. The number of platinum particles is determined by a complex interplay of the glass composition, which establishes the platinum solubility, and furnace design, which influences temperature gradients and the transport of platinum. A higher platinum solubility in the glass is desirable because it permits more of the platinum to be dissolved in the glass in its oxidized state rather than in the reduced metallic particulate state which causes damage. Heating techniques which minimize temperature gradients also minimize the quantity of platinum entering the melt from the furnace liner.

The second issue is control of homogeneity and striae. The specifications of the NIF laser require that the refractive index be uniform to within 10^{-6}. This requirement imposes tight restriction on compositional uniformity, since any significant deviation from the nominal glass composition produces large refractive index changes. Homogeneity is controlled by two factors: (1) the glass composition and forming conditions, and (2) control of the initial melting of the raw materials. The forming conditions are established as part of the detailed design of the production system. Initial melting is done in a refractory melter which unavoidably dissolves into the laser glass at a slow rate. The refractory composition and detailed design of this melter can strongly influence the dissolution rate.

The third significant determinant of cost is testing and quality assurance (QA) procedures. Each slab of laser glass must be damage tested to ensure the absence of large platinum particles in the clear aperture. In addition, homogeneity is certified by full aperture interferometry. A well designed manufacturing process can reduce the current requirement for 100% testing to the need for only random statistical testing to ensure that the process is within specification.

15.2.3 *Development activities to achieve NIF cost goals*

Both Schott and Hoya will require about 3 years to complete a development effort to demonstrate the feasibility of advanced melting technology applied to laser glass. The basic technology for continuous melting of glass is well known, and is used, for example, in the production of BK-7. The developments required for laser glass are specific to the phosphate glass composition rather than to an entirely new technology for the melting of glass.

In the first year, the laser glass companies can complete two experiments, the results of which will significantly impact the cost of producing laser glass:

(1) The exact composition of the glass will be identified which impacts laser damage from platinum, homogeneity via the forming conditions, and fracture toughness (not discussed above). The selection will require significant input from LLNL to ensure that the laser properties of the glass remain appropriate for the NIF.

(2) Both companies will build and test an advanced glass melter using improved refractory materials and heating methods to minimize dissolution into the melt and enable the melter to operate for longer periods of time.

In the second and third years, the companies will design, build, and operate prototypes of advanced furnaces. There will also be efforts to improve damage testing methods, raw materials, and other measurement/testing operations.

Following this development program, about 12 months will be required to design and build the NIF production furnaces, and to purchase and install annealing furnaces, fabrication, and inspection equipment. After this facilitization effort is complete, each company will melt about 5% of the total order in a pilot production phase. The purpose of the pilot production is to establish yields so that the vendors and LLNL have a firm basis for scheduling the production orders under firm-fixed-price contracts.

15.3 *KDP/DKDP Crystals*

15.3.1 *Cost Impact*

The nonlinear crystals used in the optical switch and for frequency conversion are a significant source of cost and schedule risk in the NIF project. Without optical manufacturing development, the estimated cost for crystals, before optical finishing, is \$34 M. This cost is dominated by the cost of the deuterated (DKDP) crystals used in the optical switch and the third harmonic generator (THG) plates. Significant schedule risk stems from the very long time required to grow the large crystal boules from which these plates are produced. Approximately two years are required at present to grow the $50 \times 50 \times 80\text{-}100\,\text{cm}^3$, boules necessary to produce the large aperture crystals used in the NIF. Currently, the average yield of plates from one of these boules for the Beamlet Demonstration Project is also low due to the numerous problems that can arise during the growth cycle. These problems include cracking, spurious nucleation, laser damage, and high strain-induced birefringence. The NIF cost goal for unfinished crystals on the NIF is \$8 M. Cleveland Crystal and Inrad are the two major KDP/DKDP crystal growers in the United States. Both companies have indicated that this goal can be accomplished through improved growth rate and increased yield.

Fabrication of the optical surfaces on KDP/DKDP crystals is currently done by single-point diamond turning. The cost to optically finish all the crystals for the NIF using existing diamond turning technology is estimated to be about \$8 M. This finishing cost brings the total cost of the crystals, using existing technology, to \$42 M. Diamond turning is generally more expensive than conventional polishing and is therefore reserved for applications where polishing is particularly difficult or inappropriate. KDP and DKDP crystals are difficult to polish using conventional techniques, which usually leave sleeks. Sleeks appear as fine scratches that can cause laser damage. In addition, precise orientation alignment can be maintained far better with diamond turning than in conventional polishing. The diamond turning proeess currently used at Cleveland Crystals can be improved substantially, and possibly combined with an improved polishing procedure to reduce the crystal finishing cost to the NIF Project cost goal of \$4 M. This reduced finishing cost would bring the total cost of crystals for the NIF, using advanced technology, to \$12 M

15.3.2 *Technical issues*

The cost of KDP/DKDP crystals is largely determined by the growth rate and yield of plates from each boule. These effects compound, so modest improvements in both growth rate and yield are equivalent to large improvements in either individual area.

These crystals grow in a regime in which both the supersaturation of the growth solution and the flow rate past the growing faces influence the growth rate. Hence, the growth rate can be improved by increasing the supersaturation or the flow rate. Each approach has disadvantages, however. Utilizing present growth techniques, raising the supersaturation makes the solution more susceptible to spontaneous nucleation. Increasing the flow rate can produce unwanted turbulence which can induce local growth rate fluctuations and accompanying strain.

Recently, scientists in Russia have demonstrated an improved solution treatment process which enables very high supersaturation to be used without generating spontaneous nuclei. This development has been adapted to crystallizers at LLNL with the aid of the Russian scientist who demonstrated this breakthrough. Incorporating this improvement into the crystallizers at Cleveland Crystals and Inrad can enable them to increase their growth rates from 50% to 250% above present levels.

The crystal yield is defined as the actual number of plates obtained from each boule relative to the maximum number which could be harvested from a perfect boule of the same size and shape. Yields for NIF-sized boules using present capabilities are expected to be very low, perhaps as low as 10 to 20%. Larger boules usually have higher strain and are more likely to crack, especially early in the growth run. Spontaneous nucleation can also occur early in the growth cycle for larger boules. Ultra filtration techniques, which remove small particulates, has been shown to increase damage threshold and reduce scattering sites in the crystal and solution (which can act as nucleation sites) thereby improving yield. These techniques can be optimized for NIF boules in order to improve the yield and therefore reduce the number of boules which must be grown for the project.

Surface damage thresholds at the third harmonic wavelength must be maintained at or above the bulk values. The current diamond turning process produces surfaces which meet this requirement. However, these surfaces induce a slight modulation to the wavefront because of residual errors from the diamond turning machine. This modulation can be reduced by improving the diamond turning process, or by adding light polishing as the final step in the fabrication procedure.

15.3.3 *Development activities to achieve NIF cost goals*

Cleveland Crystals and Inrad both should be funded to begin growing approximately ten large KDP and DKDP boules from which critical information on growth rate and yield can be gained. Toward the end of the first year, an additional 10-15 boules would start growing in crystallizers which have been modified based on initial results. Successful implementation of rapid growth technology could reduce the KDP/KD*P costs below the present estimates.

Although not strictly a development issue, the cost of D_2O contributes substantially to the ultimate cost of KD*P. The DOE has a substantial stockpile of low tritium heavy water, some of which may be utilized for the growth of KD*P during development as well as production. Use of heavy water from the DOE could reduce KD*P costs even further. During the next several months we will do all we can to ensure an adequate amount of D_2O for development activities as well as for NIF production.

This activity must be started as soon as possible because of the long time required to design and build crystallizers, and to complete the growth of these large crystals. Both the crystal growth companies will adapt the high supersaturation approach developed in Russia and demonstrated in large growth tanks at LLNL to their proprietary crystallizer designs. In addition, there will be sufficient time to demonstrate improvement in the ultra filtration process, which is a significant determinant of yield. Cracking of the crystals almost always occurs early in the growth cycle, so this determinant of yield could also be assessed.

The initial development activity in crystal finishing will be to determine the ability to produce diamond turned surfaces which meet the NIF performance requirements. The diamond turning

machine at Cleveland Crystals (which is owned by the Department of Energy) will be modified to improve its performance. These improvements include upgrading the lead screw used to translate the crystal, improving the spindle air pressure regulation which governs the position of the crystal relative to the diamond tool, and investigating the potential contribution of stiction from the slide on which the crystal rests.

In parallel with these activities, polishing of crystals will be pursued to determine the optimum transfer point from diamond turning to polishing if the improvements to the diamond turning process described above are insufficient to meet NIF requirements.

15.4 *Optical Surface Fabrication*

15.4.1 *Cost Impact*

Approximately 85%, of the NIF optical components have flat surfaces. These flat optics are mostly laser glass slabs. Other flat optical components include optical switch windows, target chamber windows, mirror and polarizer substrates, and debris shields. The remaining optics are spatial filter and target focus lenses having mildly curved, aspheric surfaces.

Using current polishing technology, the projected cost of polishing all the flat optical components for the NIF is approximately \$50 M. The NIF cost goal for flat surface finishing is \$17 M. The development necessary to attain this cost goal includes deterministic figuring, medium to high speed grinding and initial polishing, and the use of in-situ metrology to streamline the iterative process of inspection and final polishing. LLNL's two main flats manufacturers, Eastman Kodak and Zygo Corp believe they can achieve this cost goal.

The projected cost of finishing lenses by conventional techniques is \$13 M, excluding the cost of the fused silica blanks. In addition, the NIF design assumes the availability of large-aperture, high precision lenses with square aperture. A manufacturing capability for such lenses that satisfy the required optical tolerances does not exist. LLNL, in conjunction with two optics manufacturers, Tinsley Laboratories and Litton Itek Optical Systems, has suggested the use of rapid spherical grinding and polishing coupled with deterministic figuring methods to reduce the number of man-hours required to meet the figure requirements.

Deterministic finishing processes for lenses would be based on an extension of existing proprietary methods used at Tinsley and Itek. The speed of generating the initial spherical surface can also be increased significantly to reduce the finishing cost. With about three years of pre-production development, the NIF cost goal for finishing square lenses is \$3 M, an estimate that both Tinsley and Itek support.

Thus, we expect this optical manufacturing development program to reduce the total optical finishing costs from \$63 M to \$20 M.

15.4.2 *Technical Issues*

Convergence to the figure tolerance for the flat optics currently requires a large number of iterations (about ten) between interferometric testing and corrective polishing. These steps account for approximately half of the cost of finishing the flats. Therefore, it is essential to develop a deterministic figuring process which converges in only a few steps. In addition, the development of in-situ metrology is highly desirable to reduce the time and risk required for current measurements.

Second, an increase in speed and repeatability of the initial grinding and polishing steps is needed to reduce the time required to prepare the flat optic for the deterministic process needed to achieve final figure. There will be an optimum transfer point from initial grinding and polishing to the final polishing operation. This optimum will involve a trade-off between a rapid, inexpensive

process which leaves larger errors and requires more iterations to converge to final figure, and a slower, more expensive process that delivers more accurate surfaces for final figuring. Repeatability in this initial step may ultimately be more important than speed or absolute accuracy, depending on the convergence rates developed for final figure correction.

The primary concern in finishing square lenses is to maintain tolerances near the edges, and especially in the corners. The deterministic processes must be robust enough to maintain the specifications to within about 1-2 cm of the edge. A second important issue is generating the initial spherical surface rapidly to reduce its cost, while maintaining a low level of sub-surface damage to minimize subsequent polishing and ensure that the laser damage threshold remains high. Note that the NIF lens design requires optics which are only mildly aspheric, having just a few waves of deviation from spherical.

15.4.3 *Development activities to achieve the NIF cost goals*

The main priority of finishing development activities is to reduce the number of production man-hours per optic. With an advanced technology approach, the shape of the optic will be accurately generated by an improved grinding process that leaves much less subsurface damage, about 2-5 μm compared to the current level of 15-30 μm. Because there is less damaged material to remove, less time is required to remove it in the first polishing operation. In addition, this initial polishing operation can be accelerated by using medium to high speed lapping methods that until now have been used only for lower quality optics and semiconductor wafers. In the first year of development, both the flats and lens manufacturers will modify their current capabilities to improve this initial grinding and polishing process. The second and third years will be focused on identifying advanced equipment to demonstrate the feasibility of rapid grinding (low subsurface damage) and polishing for the NIF.

In parallel with the above described work on the initial grinding and polishing, both Kodak and Zygo will begin working on their own proprietary versions of deterministic final figuring. This effort will involve the demonstration of in-situ metrology for more efficient wavefront correction, improved high resolution metrology, and a streamlined process flow. The details regarding deterministic final figuring cannot be discussed here because of their proprietary nature, but each manufacturer is targeted toward a high degree of repeatability and predictability, with a goal of only 1 or 2 metrology iterations. An example of an improved deterministic figuring process which can be discussed is ion beam figuring (IBF) that Eastman Kodak currently uses for the final figuring of the Keck optical segments—convergence rates in excess of 90% have been reported for these types of optics. We demonstrated two years ago that IBF can be used to figure laser glass without fracturing the glass or reducing the surface laser damage threshold.

In the first year of development, experiments will be performed to determine the convergence rate of each vendor's scheme for deterministic figuring, In the second and third years those schemes would be optimized using new or modified equipment for NIF-size quality optics.

Potential manufacturers for the NIF lenses have developed advanced technology for other customers, most notably for large telescope optics. Because of this development effort, the total development cost for reducing lens prices is expected to be much smaller than the development costs for flat optics.

An important near-term development for square lenses is the initial work in the deterministic aspects of producing the aspherical surfaces. Both Tinsley and Itek have suggested detailed proprietary development activities which could produce the initial aspherical surfaces using square blanks within the first year. This work would allow these companies to project NIF lens fabrication costs with much greater confidence. This capability would then be optimized for the large NIF production order during the second and third years of development.

The current NIF lenses are biconvex, with one side only slightly aspheric. Therefore, a second important activity in the initial development of square lens fabrication is to assess the appropriate route to rapid spherical surface generation, including sub-scale experiments and the selection of equipment vendors. This work would be completed during the second year of development, and demonstrated during the third year. At least one lap manufacturer markets high speed grinding and polishing machines that might be directly applicable to NIF lenses. However, the spherical polishing of square lenses carries a reputation for being destructive to the laps with unpredictable results in the corners. It is therefore critical that this spherical polishing development begin immediately to quantify potential problems in order to solve them in a timely manner consistent with the NIF schedule.

15.5 *Fused Silica*

15.5.1 *Cost Impact*

Fused silica is used for most of the transmissive optics in the NIF, including the cavity and transport spatial filter lenses, the final focus lenses, optical switch windows, the target chamber vacuum windows and debris shields. Using current technology, the facilities and manufacturing cost of the fused silica would be about \$25 M. Approximately \$5 M of this amount is due to expensive exhaust gas scrubbers which would be required to meet future federal clean air standards during NIF construction. The LLNL fused silica cost goal is \$8 M, which Corning has supported as an achievable target. This cost would be met in part by qualifying a new process for fused silica manufacture that does not require the pollution abatement equipment. Further, the costs will be reduced by improving this new process to eliminate bubbles and inclusions to increase the overall process yield. Finally, the fused silica boule geometry and process control will be optimized to further enhance yield.

15.5.2 *Technical Issues*

Currently, Corning is the only U.S. manufacturer capable of producing the size and quality of fused silica required for NIF (and presently for the Nova laser). This fused silica, called 7940 is produced by flame hydrolysis of $SiCl_4$, which produces HCl (hydrochloric acid) as a by-product. Federal and New York State Clean Air Standards require Corning either to install expensive pollution abatement equipment during the next few years or to produce fused silica from a nonpolluting source. Corning has recently developed a nonpolluting process which uses a carbonated siloxane starting material instead of $SiCl_4$. The fused silica produced by this patented process is designated 7980.

Specifications for bubbles and inclusions in the NIF transmissive optics are extremely tight to minimize scattering losses and the potential for damage in downstream optics due to holographic reimaging. Early in the development program, the manufacturing process will be characterized to determine sources of these defects. This process will then be suitably modified to reduce the incidence of bubbles and inclusions, thereby increasing the yield and reducing cost.

Corning produces standard sizes of fused silica boules to yield optical blanks for a variety of customer applications. The large volume of fused silica required for the NIF warrants a customized boule geometry to maximize the yield of blanks. The production process will then have to be optimized to accommodate the improved boule geometry.

15.5.3 *Development activities to achieve the NIF cost goals*

During the first year of development, Corning will accomplish the following three tasks, which will make significant technical advances and thereby reduce the required optics contingency.

(1) Corning will fabricate large blanks of the 7980 fused silica which will be optically polished. These blanks will be tested on Nova or Beamlet with large aperture, high fluence, beams.
(2) The production process will be analyzed to determine the origin of defects in the boules. Corning will then engineer the process in the second and third years of development to reduce the number of defects.
(3) Corning will also initiate the boule geometry modification program through the use of appropriate thermal-mechanical modeling and analysis, and identify the appropriate process control variables for optimization.

The second year of development will be directed toward demonstrating the feasibility of process control to incorporate changes to eliminate inclusions as well as to produce boules with a specific geometry consistent with efficient production of NIF fused silica optics. The third year will integrate the new process control parameters into a production facility.

15.6 *Thin-film polarizer coatings*

15.6.1 *Cost Impact*

Although, thin-film polarizer coatings make only a small contribution to the overall cost of NIF optics, they have an impact on potential schedule risk similar to that of the KDP/DKDP crystals resulting from the low yield of high damage threshold coatings. Hence, the estimated cost using present capabilities of $10 M could potentially be much larger without pre-construction development to better understand the source of defects which control the damage threshold and to understand deposition uniformity which controls optical performance. Once this full three year development process is complete, the coating process is expected to be relatively inexpensive. LLNL's cost goal of $2 M has been supported in cost studies by our two prime optical coatings manufacturers, Optical Coatings Laboratories, Inc. (OCLI) and Spectra-Physics.

15.6.2 *Technical issues*

Extensive experimental characterization and theoretical analysis at LLNL has demonstrated that it is the coating defects rather than detailed polarizer coating design that determines the damage threshold. During the last 10 years, polarizer damage thresholds have increased as manufacturers have carefully cleaned their coating chambers to remove contaminants which cause damage under laser irradiation

Nonetheless, the measured damage thresholds remain significantly below theoretical values. Recently, it has been established through quantitative computer modeling that nonabsorbing defects of the coating material itself, in the form of nodules, can produce local electric field enhancements strong enough to damage the coatings. Hence, the development effort will primarily focus on the source of these defects and means to reduce them to acceptable levels.

15.6.3 *Development activities to achieve NIF cost goals*

Improved process control is essential to produce the damage resistant coatings for NIF. Computer modeling and atomic force microscopy results at LLNL have indicated the size and type of defects which must be reduced to improve damage threshold. OCLI and Spectra-Physics can begin to modify their proprietary coating processes to reduce the incidence of these defects. Parameters to be modified include the internal geometrical layout of the coating chamber, coating conditions, and the composition of the coating materials. In addition to this work, OCLI and Spectra-Physics should begin to improve the automation of the coating process to improve reproducibility of coating performance, including damage threshold, spectral and wavefront performance. Work in the first year of development will also focus on potential process modifications which may be required.

15.7 *High reflectivity coatings*

15.7.1 *Cost Impact*

High reflectivity (HR) coatings are required for the cavity mirrors, which reflect the laser pulse back and forth through the amplifier, and the transport mirrors, which direct the pulse to the target chamber. The current technology used to manufacture HR coatings is the same electron beam evaporation process used to produce thin-film polarizer coatings. Such coatings must be laser conditioned (exposed to successively higher laser irradiation) to meet the damage threshold requirements of the NIF. The projected cost of producing the NIF coatings without

further development is approximately \$9 M. Following development, electron-beam HR coatings would still be expected to cost about \$4 M, and require an expensive laser condition process to meet the laser damage requirements for the NIF.

LLNL is developing an alternative coating technique, called the sol-gel process, to produce high quality HR's and a meniscus coater to apply them. This process has been demonstrated using a simple sub-scale meniscus coater. Sol-gel HR's have three significant advantages compared to electron beam coatings. First, they don't require the very expensive step of laser conditioning to achieve the high damage thresholds required for NIF. Second, if the coating doesn't meet specifications, it can be merely wiped off, the substrate cleaned and the process repeated. This feature is important when considering operating costs after the NIF laser is constructed. Electron beam HR's which fail to meet specification or whose performance has degraded must go through the entire optical grinding and polishing procedure; an expensive process. Finally, sol-gel coatings are deposited at room temperature and atmospheric pressure, rather than at elevated temperature in a vacuum chamber, so they are intrinsically less expensive. LLNL projects sol-gel HR costs for the NIF of approximately \$2 M.

15.7.2 *Technical Issues*

The most important technical issue is the development of an appropriate, full-sized meniscus coater. This technology has been used for applying photoresist to high-aspect-ratio substrates which can not be spin coated. It is already compatible with the more demanding application of optical sol-gel multilayer coatings in a sub-scale coater. Nevertheless, it must be demonstrated at full size and to NIF requirements to confidently project a cost for the NIF.

A second important issue relates to the composition of the suspensions. LLNL has demonstrated that the use of a binding agent improves the durability of the coating, increases the damage threshold, and increases the refractive index contrast between the layers, so that fewer layer pairs are required to achieve the required reflectivity. Optimization of the binder composition and the relative amounts of binder and the high-and low-index materials is required in conjunction with development of the meniscus coater.

15.7.3 *Development activities to achieve NIF cost goals*

LLNL will procure a full-size meniscus coater to demonstrate the feasibility of this approach for the NIF. During the first year, a full-size cavity HR will be produced which can be tested on Beamlet. In a parallel effort, LLNL will work to develop an acceptable binder/sol-gel material composition and mix ratio to produce the higher damage threshold materials required for transport mirrors. This work will be demonstrated during the second and third years.

15.8 *BK-7 Glass*

15.8.1 *Cost impact*

A large volume of BK-7 is required for mirror substrates and for the polarizer in the optical switch. BK-7 is a glass produced in large volumes by several companies using a continuous melting process, and is listed on the commodities market. LLNL has a long history using BK-7 for mirror substrates on Nova and earlier ICF lasers. This material costs about \$0.15/cm^3, and will cost about \$3.5 M for the NIF. The current NIF design (as well as Beamlet) also uses BK-7 as the polarizer substrate. The low damage threshold of BK-7 is acceptable for this application because the beam is switched out of the cavity in reflection rather than transmission. Thus, the damage producing

platinum inclusions in BK-7 glass are never exposed to a high fluence laser beam. Because the beam is transmitted through the polarizer in earlier passes, the polarizer substrate must have extremely good refractive index uniformity comparable to the laser slabs and other transmissive optics in the cavity. This requirement substantially increases the cost of BK-7 since it must be selected from a larger volume of already-melted material. The cost of BK-7 for the polarizer without any development would be about \$2.5 M, and there is a legitimate concern about the ability to obtain sufficient quantity of high homogeneity BK-7 in the schedule required for the NIF. A modest development effort would reduce the price of the BK-7 somewhat to about \$2 M, but more importantly would guarantee the availability of high quality BK-7 consistent with the NIF schedule requirements.

15.8.2 *Technical issues*

Very little work has been done to characterize the production process with respect to the control of striae and less severe, but important index variations for requirements such as the NIF polarizer. The primary issue is the availability of acceptably high homogeneity BK-7 for the polarizer given the process as it currently stands.

15.8.3 *Development activities to achieve NIF cost goals*

Development probably wouldn't be started until the second year. We do not yet have any detailed cost estimates or activities. If it is determined that an extensive development effort seems unwarranted, then we can elect to use fused silica as the substrate material at a higher cost for production, but without the expense of a BK-7 development effort and less risk of optical damage.

15.9 *Optic specifications*

Tables in Appendix C contain the specifications of the materials and finished optics, respectively, upon which the NIF cost projections were made. These specifications were derived from Beamlet and Nova specifications, as appropriate. Initial analysis[1] has indicated that some of these specifications may be relaxed without significantly impacting NIF performance. A prime possibility is the booster amplifier, which contains about 30% of the laser slabs. The peak-valley wavefront specification is currently $\lambda/6$ at 6328 Å. This may be relaxed to $\lambda/3$ or $\lambda/2$ for selected optics at 6328 Å. Preliminary discussions with the finishing vendors have supported the notion that relaxing the specification for 30% of the slabs could further reduce the projected finishing cost. In addition, it also reduces the cost risk (contingency) associated with development that is less than completely successful. Once issues such as this are more fully resolved, we will use the appropriately relaxed specifications as the basis for formal vendor cost studies, the results of which will be incorporated into the CDR.

15.10 *Cost summary and comparison with Beamlet*

Appendix C contains a table comparing large optics costs for Beamlet with the cost projections for the NIF. Optics for each beamlet of the NIF are expected to cost about \$425 K versus \$1230 K for Beamlet. Laser glass cost will decrease from about \$3/cm^3 to under \$1.00/cm^3 through the development and application of advanced melting and forming technology using an optimized glass composition. The KD*P cost is currently projected to decrease from \$40/cm^3 to under \$20/cm^3. The improvement in growing these large boules is more significant than indicated by comparing

[1] J. R. Murray, *Beam divergence budget (preliminary) with digressions on frequency conversion*, LLNL ICF internal memorandum, June 1, 1993.

the unit prices, since Beamlet KD*P was grown using borrowed heavy water from DOE. NIF cost projections include leasing the D_2O required for production. Recently, we have secured a commitment from DOE for an additional 12 metric tons of heavy water for development activities. Utilizing this D_2O for KD*P production could reduce the cost by another 30-40%. The formal cost studies for the CDR will properly account for the use of free heavy water, if this is warranted. Note that ordinary KDP costs are expected to drop by a factor of 3. Fused silica is projected to decrease from about $\$1.75/cm^3$ to $\$1.00/cm^3$. The current price of fused silica is this low only because Corning can sell material from Beamlet boules to other customers. The NIF order is large enough that Corning won't be able to easily sell excess material which doesn't meet NIF specifications. Hence, Corning is focused on an improved boule geometry and better process control to meet the NIF target price. BK-7 is a commodity glass, so NIF prices are expected to be comparable to those for Beamlet. Finishing costs are expected to decrease by a factor of 2 to 4 through the use of rapid grinding and polishing and deterministic final figuring. Coating costs for the HR's and polarizers are expected to decrease by a factor of about 3. However, the current damage threshold specification for the NIF polarizers is substantially higher than Beamlet. If the NIF polarizer damage requirement were decreased there would be a corresponding decrease in the cost projection (and development scope, as well).

NIF Component Development Schedule—Optical Components

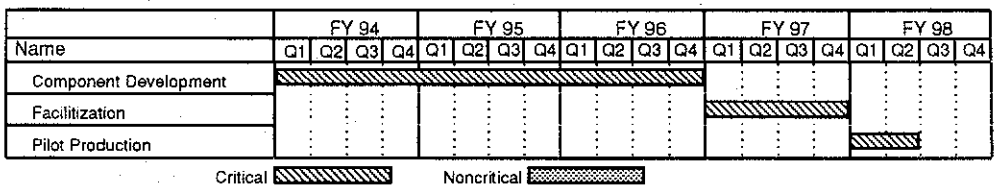

Table 15-2 Optical components development schedule.

Chapter 16

LASER SYSTEM COST AND SCHEDULE SUMMARY

16.1 *Cost estimates*

16.1.1 *NIF construction project cost*

A bottom-up cost estimate for NIF laser system was compiled during the LDB study. These costs provided the basis for the cost scaling that has been summarized in earlier sections. The cost evaluation was based on the following assumptions:

1) estimates include all TEC costs for NIF construction including labor and material for design, engineering, procurement, assembly and installation
2) FY 93 dollars (no escalation considered)
3) standardized labor rates
   a) LLNL rates appropriate for a PACE (Plant and Capital Equipment) project
   b) rates are fully burdened
4) component development program completed before final design review
5) project constructed at LLNL
6) laser systems evaluated
   a) optics
   b) pulse generator
   c) power conditioning
   d) power amplifier
   e) spatial filter
   f) optical switch
   g) beam transport
   h) alignment and diagnostics
   i) integrated computer control
7) systems not evaluated (nominal costs included to permit total project roll-up)
   a) conventional facilities
   b) experiment area(s)
   c) laser support structure
   d) laser auxiliary systems
   e) project office management
8) costs do not include LLNL material procurement charges, supplies and expenses, or contingency

Costs were compiled for the entry point laser configuration defined in Appendix A. Basic system parameters are:

a) 192 beamlets
b) 35 cm hard aperture
c) 11/5/3 laser slab configuration
d) 4×4 amplifier configuration
e) 3.0 J input energy
f) 250 MJ capacitor bank
g) 1.8 MJ delivered (redlined system)

A summary of the labor and material costs for the NIF construction project are provided in Table 16-1. Total TEC costs are about \$413 M, \$301 M (73%) in material and \$111 M (27%) in labor. The distribution of these costs is shown in Figure 16-1. The laser system (WBS 3.0) and the optical components (WBS 6.0) total to about \$327 M which is 79% of the total project.

Figure 16-2 shows the distribution by subsystem of estimated costs for the laser system (WBS 3.0). The main amplification system, which includes the main, boost and switch amplifiers, cavity spatial filter, cavity mirror assemblies, optical switch and interstage hardware, is the dominant cost center at \$82 M. The alignment and diagnostic, power conditioning and pulse generation systems follow in importance with costs of \$45 M, \$39 M and \$34 M respectively.

Table 16-1 NIF construction project costs.

	Labor (\$K)	Material (\$K)	Total (\$K)
1.0 Project Office	13564	2000	15564
2.0 Facilities	1737	16300	18037
3.0 Laser	70929	163729	234658
3.1 Optical pulse generation	10135	23825	33959
3.2 Main amplification system	16402	64771	81173
3.2.1 Main amplifier segments	6350	35386	41736
3.2.2 Spatial filters	2321	8464	10785
3.2.3 Mirror assemblies	377	3116	3493
3.2.4 Polarizer assembly	1304	1609	2913
3.2.5 Pockels cell assembly	6014	15448	21461
3.2.6 Boost amplifier segments	in 3.2.1	in 3.2.1	in 3.2.1
3.2.7 Interstage hardware	36	749	785
3.3 Beam transport	5038	17947	22985
3.3.1 Spatial filter	4093	9253	13346
3.3.2 Mirror assemblies	340	2629	2969
3.3.3 Final optics system	547	4544	5091
3.3.4 Beam tube system	58	1521	1580
3.4 Power conditioning system	13068	25986	39054
3.5 Alignment and diagnostic systems	22733	22476	45208
3.6 Laser structural support	1681	8000	9681
3.7 Laser auxiliary systems	1873	725	2598
4.0 Target area	12303	30050	42353
5.0 Integrated computer control systems	4674	5337	10011
6.0 Optical components	7727	84189	91916
Project totals	110934	301605	412539

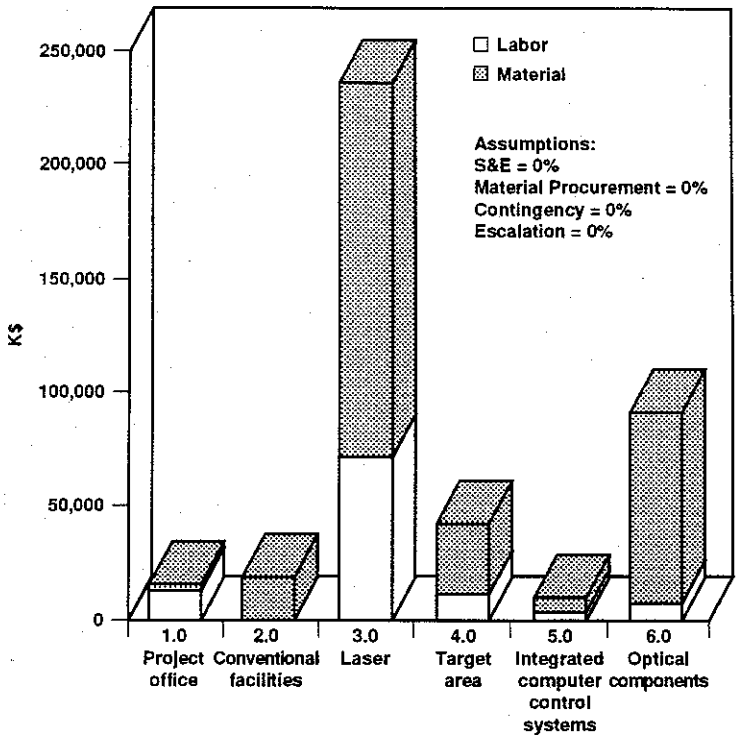

Figure 16-1 NIF WBS distribution of costs

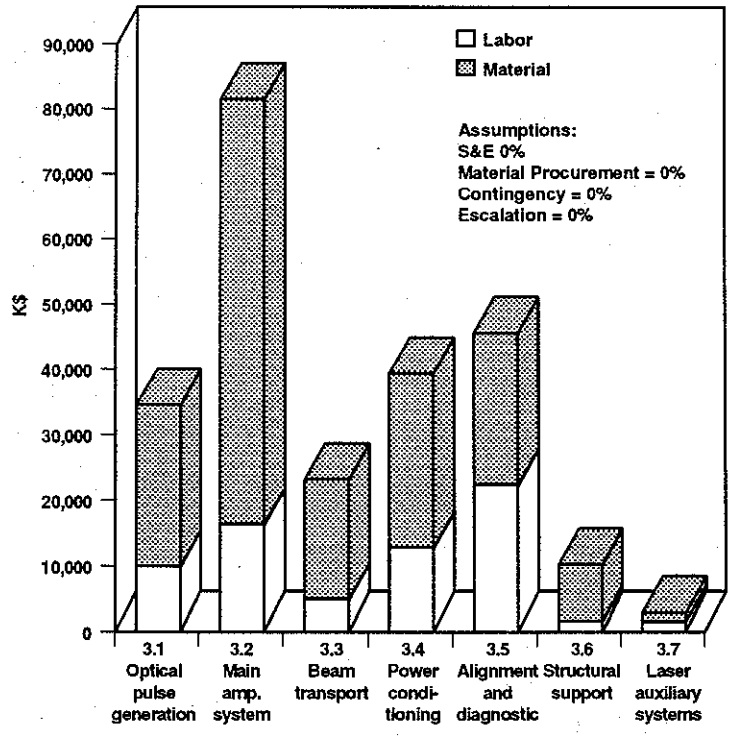

Figure 16-2 Laser system distribution of costs

16.2 *Schedule*

A top level schedule of the NIF construction project and the component development programs has been integrated, Table 16-2. The construction project is a 7 year project that would commence at the beginning of FY 94 with the successful completion of the CDR and the signing of Key Decision-1. This is followed with preliminary and final engineering, culminating in a Final Design Review in 1997. Long lead procurements would begin at this time in preparation for subsystem assembly beginning in mid 1999. Installation and activation of the special equipment into the facility will be a 3 year effort completed in the year 2002.

Component development activities in nine major categories are also shown in Table 16-2. In general all these activities can be completed within 3 years. However, amplifier development is projected to require an additional 9 months which will push the Final Design Review to the third quarter of 1997 and project completion to the end of CY 2002. The critical path in this schedule is the design, fabrication and testing of a full scale amplifier module. This important activity is essential to demonstrating the high efficiency performance that is required of the production units.

Another pacing item in this schedule is the final delivery of the optical components. Present projections indicate that a 3.5 year production run is required. Given the development, facilitization and pilot production activities which must precede this effort, the estimated completion date is at the end of CY 2001. If 6 months is allocated after optic delivery completion for final system integration, then NIF could not be completed sooner than mid-2002. If the amplifier critical path is eliminated then this would become the critical path.

The component development program must be started in FY 94 to complete NIF in 2002. In particular, both the optic and amplifier component development programs are on the critical path of the schedule and should be given highest priority.

Integrated NIF Construction and Component Development Schedule

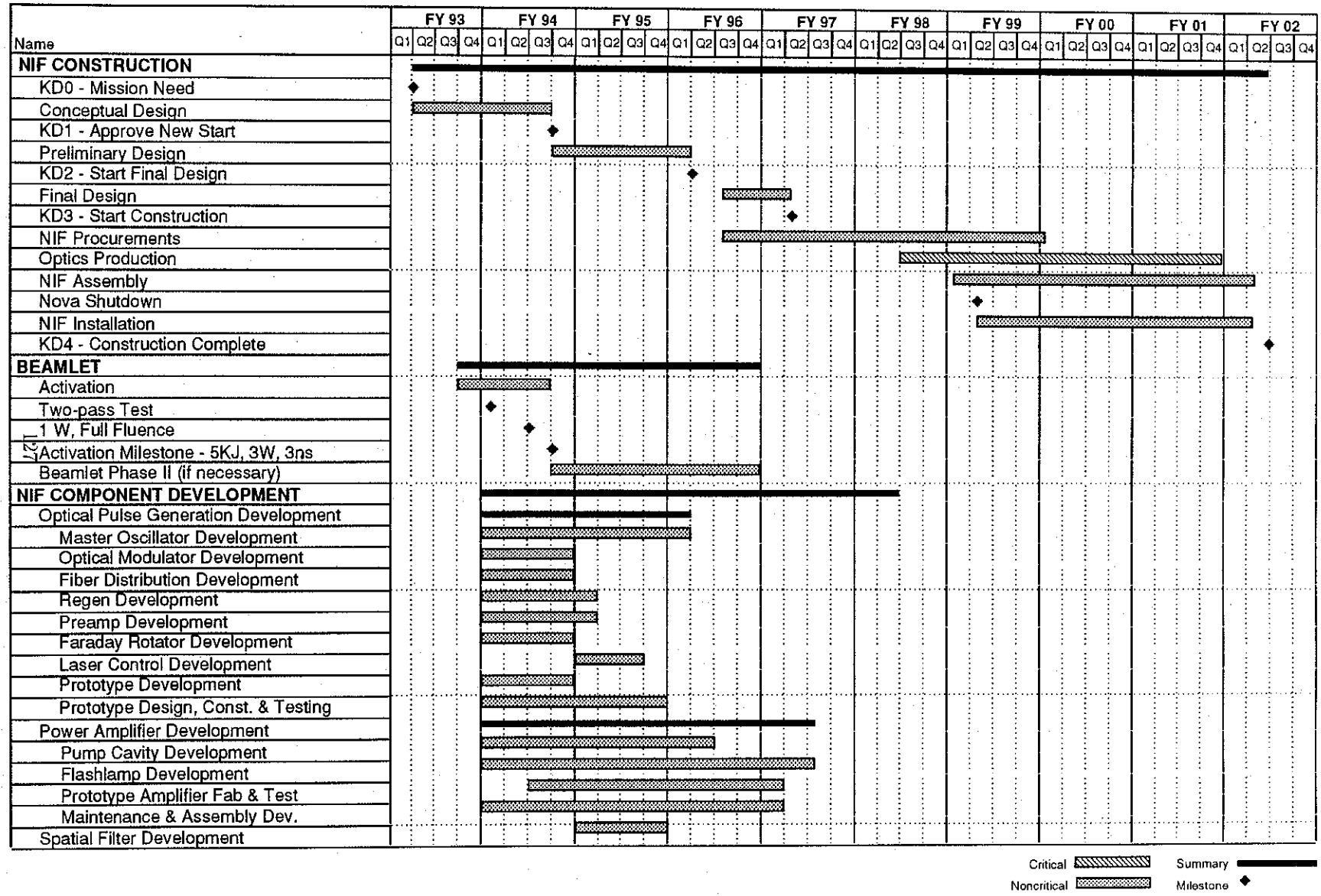

Table 16-2 Integrated NIF construction and component development schedule.

Integrated NIF Construction and Component Development Schedule (con't)

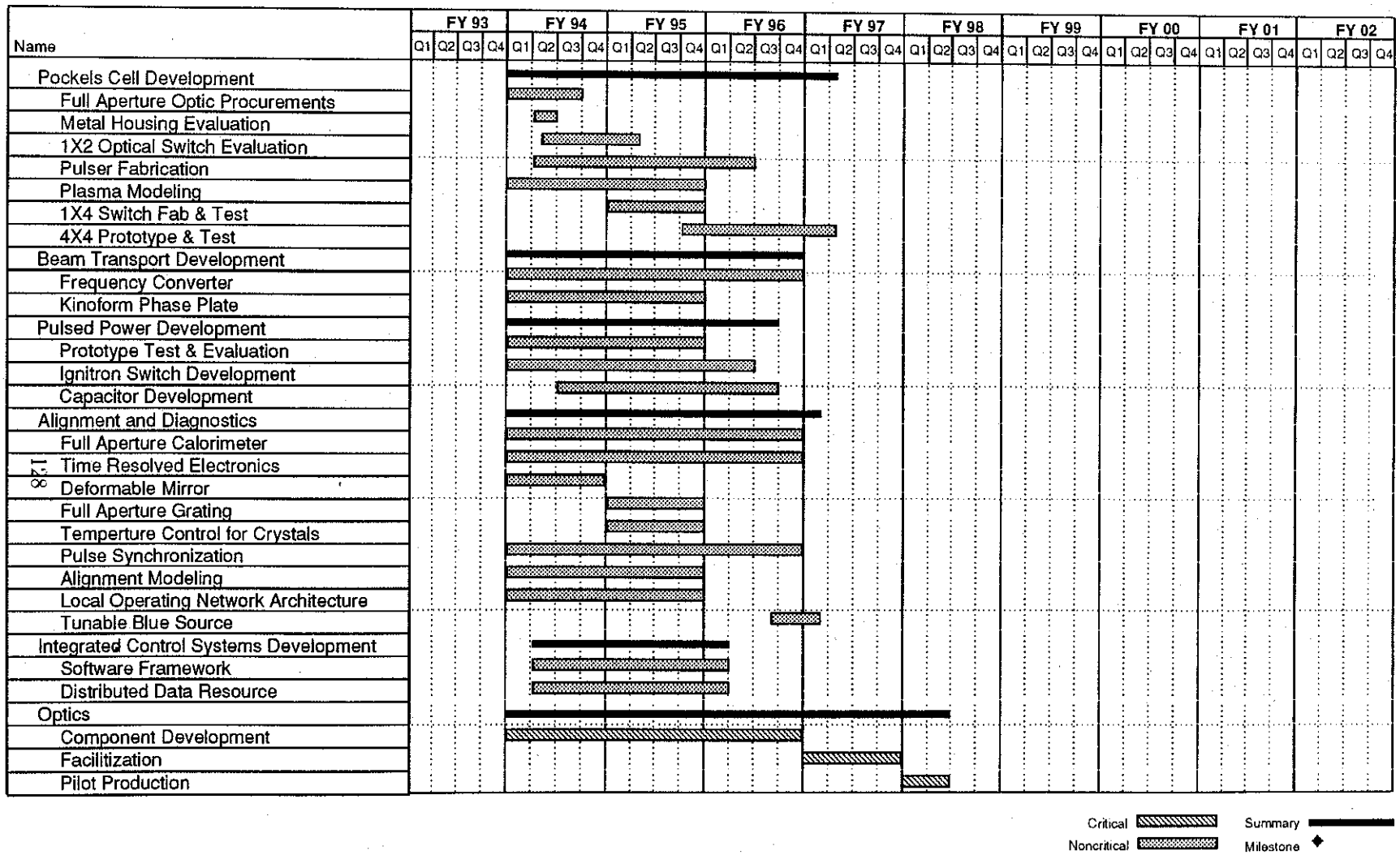

Table 16-3 (continued)

Chapter 17

SUMMARY

In this report a self-consistent data base for cost versus performance of the NIF laser has been developed. Using this data base we estimated the cost of numerous candidate laser systems that satisfied laser target requirements with varying degrees of design margin and technical risk. Where possible, the traceability of these costs to Beamlet and/or Nova has been established. The enabling technologies and component development program required to meet the NIF cost goals is discussed.

A 192 near-optimum beamlet case is used to develop the cost basis for NIF. The NIF beamlet used for the cost basis has a hard aperture of 35 cm and the amplifier contains 19 glass slabs; each slab is 3.2 cm thick. A Nova-style tripler is used in most of the calculations. This tripler is assumed to have a peak tripling efficiency of 70% and a dynamic range of two.

The cost data base has been established by using the Laser Science and Technology (LS&T) engineering staff and supporting organizations to estimate the cost of the 192 beamlet laser. Cost and performance scaling rules have also been developed. For example, the cost scaling versus beamlet aperture for the laser components is provided. The cost estimated for the 192 beamlet laser system was then verified by independent reviewers. This data was then used to update the cost parameters used in the laser optimization code CHAINOP.

Due to time and resource limitations this report did not re-evaluate cost estimates for conventional facilities and the experiment area(s)/target chamber that had been developed in earlier studies. Although these non-laser costs are probably representative, they should be viewed as place holders until they can be independently reviewed.

In Chapter 4 of this study the laser system design requirements for an indirect drive target is developed. A target point design was chosen for which the UV pulse reaching the target is temporally shaped with a contrast ratio of 50:1, has a peak power of 500 terawatts, and an energy of 1.8 megajoules. The pulse must be smooth in the plane of the laser entrance hole when averaged on a spatial scale of 30 microns and a temporal scale of 10 picoseconds. It must also satisfy certain power balance requirements.

The negative impact on the laser's peak power and energy by such effects as gain non-uniformity, beam quality, power balance, damage thresholds, amplifier grouping, etc., were not fully assessed in this study because of time limitations. Instead, we covered these uncertainties by applying laser system design margin.

Several candidate NIF laser systems were analyzed using CHAINOP to study variations in beamlet aperture, amount of design margin, beamlet count and the assumptions about the peak efficiency and dynamic range of the tripler. In all cases the UV pulse reaching the target's LEH has a peak power of 500 terawatts and an energy of 1.8 megajoules. The results of this analysis are shown in Table 17-1.

Table 17-1 Design margin versus cost for several NIF laser designs.

Beamlet count†	Beamlet aperture (cm)	Total aperture area (m^2)	Design margin	Cost*
192	35	23.5	<1.00	\$400M
	37.3	26.7	<1.00	\$426M
	39.0	29.2	1.04	\$437M
	40	30.7	1.11	\$447M
240	31.5	23.8	<1.00	\$442M
	33.7	27.3	<1.00	\$461M
	35.0	29.4	1.04	\$474M
	36.3	31.6	1.11	\$482M
	38.0	34.6	1.23	\$497M
	40	38.4	1.38	\$518M
288	35	35.3	1.23	\$531M
	40	46.1	1.66	\$586M
336	40	53.8	1.93	\$658M

† ±2 beamlets

* LLNL assessments, contingency and escalation not included

All cases in Table 17-1 assume a modification of the final optics from the current design has been implemented to mitigate the ~15% beam area reduction through the debris shield due to the final focus. Since the shield fluence limits laser output, this fluence increase of 15% corresponds to a ~30 M (labor & material) cost increase. The mitigation technique is not defined at this point, but may take the form of an X-ray tolerant AR coating to allow normal orientation of the shield, or beam expansion in the transport spatial filter. Further study is needed on this point.

17.0.1 *Beamlet count of 192*

The least expensive system we investigated is shown in row 1 of Table 17-1. It also has the most risk associated with it because it assumes the maximum operating efficiencies. This 192 beamlet, 35 cm aperture, case will produce the prerequisite 500 TW-1.8 MJ pulse if: 1) we assume we can invent a tripler that has a very large dynamic range, 2) the tripler has a peak efficiency of 75%, 3) we reduce the damage threat to the UV beam transport by either increasing the damage threshold of its optics or we reduce the peak to mean UV beam modulation by reducing the B-integral by eliminating the vacuum window and using the final focusing optic as a vacuum barrier, and 4) we eliminate all of the design margin in optic transport efficiencies. The second row in this table assumes we do items 2 though 4, above, but not item 1. The third row in the table assumes a Nova style tripler with a dynamic range of two, a peak efficiency of 70%, and reduced UV damage thresholds. It has a design margin of 4%. The last row in the 192 beamlet case increases beamlet aperture to 40 cm without changing efficiency assumptions. It has a design margin of ~11%. Note that there is a potential SRS problem in the triplers at 40 cm aperture.

17.0.2 *Beamlet count of 240*

The 240 beamlet designs were considered because they are easily adapted to the direct drive option. In these designs the beamlets are clustered into groups of four and each group, 60 in all, are transported to the target using the direct drive target irradiation scheme. The first four cases represent the same risk scenarios as proposed for the 192 beamlet systems. For example, the design represented by row 5 of the table has the same performance and risk as row 1. All of these 240 beamlet cases are more expensive than their 192 beamlet counterparts. This is our estimate of the price that must be paid for not precluding the direct drive option. Rows 9 and 10 represent designs with increased design margin achieved by increasing the aperture to 40 cm.

17.0.3 *Beamlet count of 288*

Our preliminary analysis of the laser system using CHAINOP showed that if we used a Nova style tripler and assumed a design margin of ~ 1.23, it would take ~ 288, 35 cm aperture, NIF beamlets to satisfy the target requirements. We believe the performance and risk of this design to be reasonable. This same performance and design margin could be achieved with 240, 38 cm aperture, beamlets and it is less expensive. The 288 beamlet, 40 cm aperture, case has more design margin; and therefore less performance risk but it costs more than the smaller aperture designs.

17.0.4 *Beamlet count of 336*

This system has a design margin of 1.93, the largest considered in this study. Therefore, this design has the smallest performance risk but it is the most expensive. At present, LANL believes this much design margin is needed.

Based upon the analysis contained in this report we recommend the 240 beamlet, 38 cm aperture, case for the NIF baseline. Its design margin is modest and it is easily adapted to Rochester's direct drive target irradiation geometry. However, if this design is judged too expensive, design margin will have to be reduced by decreasing beam aperture. If it is still too expensive then we'll have to give up the ability to accommodate direct drive geometry and reduce the number of beamlets below 240.

All of these system designs require an up-front investment for the component development program. This cost is not included in the system cost shown in Table 17-1 . The duration for the various activities in this development program are summarized in Table 17-2.

Table 17-2 Schedule for technology and component development program.

Subsystem	Duration (years)
Pulse Generation	2.25
Amplifier	3.5
Spatial filter	1.0
Pockels cell	3.25
UV beam transport/tripler	3.0
Pulsed power	2.75
Alignment and diagnostics	3.25
Integrated controls	2.0
Optical components	4.5

We used CHAINOP to quantify the sensitivity of the entry point NIF laser design to changes in critical design variables. Table 5-4 in Chapter 5 summarizes these results. This analysis should guide management in setting priorities for the component development program.

During the LDB study numerous documents were generated and many previously written technical references were retrieved from existing files. All of this supporting documentation was compiled into the LDB Quality Assurance file and will be used as a technical data base for the CDR. A listing of the references contained in this file is given in Appendix D.

The results of the LDB study were reported to the DOE NIF Steering Committee on August 11 and 12. The presentation that was given is contained in Appendix E.